Dynamic Model Development and System Study of Ternary Pumped Storage Hydropower

by

Zerui Dong

A dissertation submitted to the Graduate Faculty of
Auburn University
in partial fulfillment of the
requirements for the Degree of
Doctor of Philosophy

Auburn, Alabama
May 4, 2019

Keywords: Ternary pumped storage hydropower, dynamic modeling, frequency response, hydraulic short-circuit, high renewable penetration

Approved by

Robert Mark Nelms, Chair, Professor of Department of Electrical and Computer Engineering
Eduard Muljadi, James J. Danaher Distinguished Professor of Department of Electrical and Computer Engineering
John York Hung, Professor of Department of Electrical and Computer Engineering
Steven Mark Halpin, Alabama Power Company Distinguished Professor of Department of Electrical and Computer Engineering

ABSTRACT

The conventional role of pumped storage hydropower (PSH) is energy storage: it generates power when it operates as a hydro turbine, and store energy from the electric grid when pumping water from the lower reservoir to the upper reservoir. As the deployment of power electronic based renewable energy increases in the United States, PSH will play an important role in future electric power grids to help manage the variability from high penetration levels of renewable generation. However, conventional-PSH (C-PSH) is unable to fit the future needs of a system with high renewable energy penetration as it cannot provide regulation service during the pumping mode. For this reason, advanced-PSH (A-PSH) technology is becoming more popular. There is an industry need for the capability in power system studies to model ternary-PSH (T-PSH), as an A-PSH technology that can provide frequency regulation during generating and pumping by using a hydraulic short-circuit (HSC) mode.

Presented here is a comprehensive dynamic model of a T-PSH in GE's commercial simulation platform positive sequence load flow (PSLF). A new governor model for T-PSH technology is developed with detailed gate valve modeling and shared-penstock function. This model system has the capability to simulate seamless transition among three different modes: generating mode, pumping mode, and HSC mode, and switch between all operation modes with tunable transition time during the simulation. The process of this model implementation in PSLF platform is introduced. The developed T-PSH system has been tested and validated on multiple simulation

platforms and different sizes of systems. A comparison study between T-PSH and C-PSH has also been conducted both on a small test system and the Western Interconnection system. Several sensitivity studies of parameters in the governor model have been performed to illustrate the influence on the frequency response of the T-PSH system. To reveal the dynamic benefit from T-PSH under extremely high renewable penetration condition, the frequency response of the Western Interconnection has been compared with and without T-PSH under different penetration levels of renewable, which are from 20% to 80%.

ACKNOWLEDGMENTS

I would like to express my sincere gratitude to my advisor, Dr. R. Mark Nelms, for his patient motivation, guidance, constant support and encouragement during my study at Auburn University. I am also grateful to his guidance during the research and writing of this thesis. The experience in his lab has gave me a lifelong experience.

Besides my advisor, I would like to thank one of my committee members, Dr. Eduard Muljadi, for his help and suggestions to my research. I would like to thank other committee members, Dr. John Y. Hung, and Dr. S. Mark Halpin, for knowledge I gained from their courses, insightful comments and encouragement during my thesis writing.

My sincere thanks also go to Dr. Jin Tan and Mark Jacobson, who provided me with an opportunity to work with them as a visiting researcher at NREL under a Ternary Pumped Storage Hydro (T-PSH) project sponsored by Water Power Technologies Office of Department of Energy with Contract No. DE-AC36-08GO28308. Without their precious support and professional suggestion, it would not be possible to conduct this research.

In addition, I would like to thank Dham, Rajesh from DOE, USA, Antoine St-Hilaire and Matt Pevarnik from GE Renewable Energy, Eli Bailey from Absaroka Energy, USA, Chris Hodge from GridDynamic, USA, my lab members Jinho Kim and Xingyu Yang from ECE department, Auburn University and anyone who participates in this project for their experimental support, and valuable suggestions in this work.

Last but not least, I would like to thank my family for their love and care all these years. Especially, I would like to thank my parents, Jianlin Dong and Qingjuan Yang for their continuous love, support and encouragement throughout my life.

TABLE OF CONTENTS

LIST OF TABLES

LIST OF FIGURES

LIST OF ABBREVIATIONS

A-PSH	Advanced Pumped Storage Hydropower
AS-PSH	Adjustable-speed Pumped Storage Hydropower
BESS	Battery Energy Storage System
C-PSH	Conventional Pumped Storage Hydropower
CAES	Compressed Air Energy Storage
COI	Center of Inertia
DFIG	Double-fed Induction Generator
EPCL	Engineering Process Control Language
ES	Energy Storage
HSC	Hydraulic Short-circuit
LSP	Light Spring
T-PSH	Ternary Pumped Storage Hydropower
PV	Photovoltaic
PSH	Pumped Storage Hydropower
PSLF	Positive Sequence Load Flow
ROCOF	Rate of Change of Frequency
UFLS	Underfrequency Load Shedding
WECC	Western Electricity Coordinating Council

WI	Western Interconnection

CHAPTER 1 INTRODUCTION

1.1 Background

After entering the 21st century, the renewable energy generation has achieved explosive development. At the same time, the traditional fossil fuel thermal power plants have been retired gradually due to the increasingly serious environmental concerns. Some areas, by adopting a forward-looking renewable energy policy, will usher in extreme high renewable energy penetration in the next decades [1, 2]. For example, California in the USA sets a target of 50 percent renewable energy penetration by 2030 and 100 percent renewable energy penetration by 2045 [3, 4]. Under the extreme high renewable penetration condition, some shortcomings of renewable energy which does not appear in low renewable penetration, will appear in the power grid. Worse system inertia, deteriorating frequency response and variability of renewable generation caused by the power electronic based renewable energy will bring challenges to the system operator to keep the grid stable and reliable. An effective way to deal with these problems is to deploy energy storage (ES) units in the system [5]. The ES units can effectively improve system frequency response performance and make up for the variability of renewable energy. Pumped storage hydropower (PSH) is the most widely used ES technology to provide the ancillary energy service. In the past 90 years, conventional-PSH (C-PSH) provides reliable and effective frequency regulation service. However, a C-PSH unit can only provide frequency regulation in the generating mode, but not in pumping mode. Because of this limitation, C-PSH is not fit to provide ancillary energy service under the increasing penetrations of renewable energy, especially when dealing with a serious

contingency. Advanced-PSH (A-PSH) technology is becoming popular owing to its ability to provide reliable frequency ancillary service both in pumping mode and generating mode. Ternary-PSH (T-PSH), as a type of A-PSH technology, is able to increase system inertia and provide frequency regulation. However, the growth of the T-PSH during the past decade seems to be lagging other renewables like the solar and wind [6]. Only a handful of T-PSH plant have been commissioned all over the world, and there is not any T-PSH project commissioned in the United States. Thus, this is a great opportunity for the T-PSH improvement to leverage the mature technology and increase the penetration level of the hydropower into the power grid. T-PSH can play an important role in managing excess renewable generation and provide essential reliability services.

1.2 Energy Storage Technology

Energy storage technology, as an effective solution to deal with the problems in electric grid caused by the renewable energy generation, is deployed in the power grid [7]. Although the grid can benefit from energy storage technology, the power supplied from energy storage plants is only about 2.5% in the United States, which is far below the percentage of penetration in Japan (15%) and Europe (10%) [8].

Different types of energy storage play different roles in the grid. The practical large-scale energy storage technology connected in the grid can be divided into five types: mechanical, electrical, thermal, hydrogen-related, and electrochemical [9, 10]. These energy storage systems implement three different functions in the grid depending on their system power rating: response

service, grid support, and bulk power management as shown in Figure 1.1. PSH is a kind of mechanical energy storage being used in bulk power management.

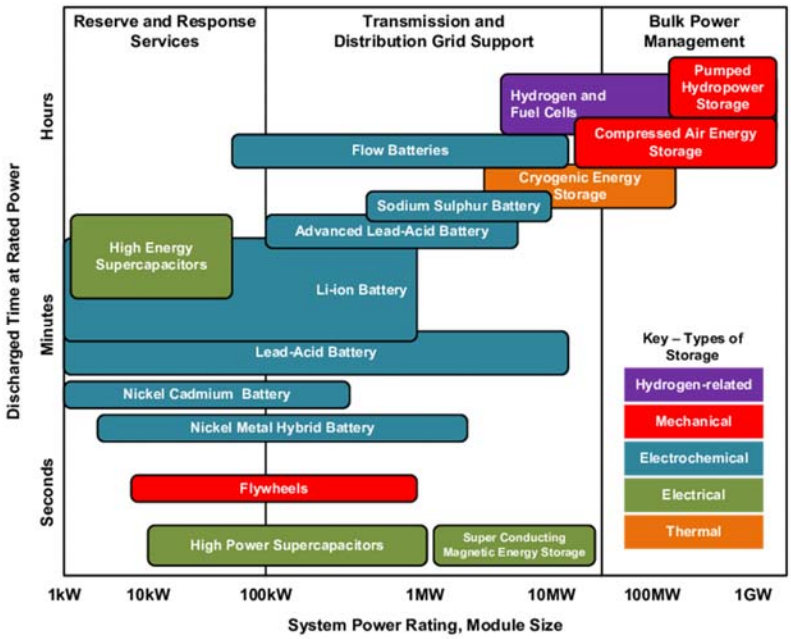

Figure 1.1 Comparison among different energy storage technologies [11]

PSH technology shows some superiorities when compared with battery energy storage system (BESS). T-PSH can easily provide hundreds of megawatts storage capacity, more than a 50-year lifetime and unlimited cycling, while it is hard to find a BESS with one hundred megawatts capacity. Also, an existing BESS using the lithium-ion battery technology has a higher maintenance cost and shorter discharge time than PSH technology. When compared with electrical energy storage like supercapacitors, PSH technology shows its advantages in discharge time and energy storage capacity. Although hydrogen and fuel cells have a great performance of discharge time and energy storage capacity, an obvious problem is durability (always 5-20 years) in comparison to PSH technology [12]. Cryogenic energy storage, as a kind of novel storage method,

is still in the demonstration phase with a low-efficiency problem. In mechanical energy storage technology, the flywheel cannot be used in bulk power management, owing to its limited system capacity. The only technology can compete with that PSH technology is the compressed air energy storage (CAES). Both PSH technology and compressed air energy storage need to choose specific suitable location. PSH technology still shows advantages in lifetime and efficiency [13, 14]. Moreover, owing to the location requirement, only hands of utility-scale CAES plants are commissioned all over the world, whereas PSH technology has been used for nearly 100 years as a mature and iterative technology. In a word, PSH technology is superior in bulk power management deployed in the grid to help a system deal with the severe contingency [15]. The mature technology and high efficiency make PSH technology the most widely used ES technology all over the world.

1.3 Hydropower Generation

Classify by another method, PSH technology belongs to hydropower generation technology. Hydropower is a kind of power generation by using water potential energy to generate. It was used as an energy source in irrigation and operation of mechanical devices in ancient time. In the 19th century, hydropower started to be used for electricity generation. As a power generation technology that produces no emissions to pollute the air, hydroelectricity becomes a competitive power generation technology. Also, the lower average cost of electricity generation makes hydroelectricity more competitive than traditional thermal power generation method. Typically, hydroelectricity is divided into four types which include conventional hydropower, run-of-the-

river, tide and pumped-storage hydroelectricity [16].

1.3.1 Conventional Hydropower Generation

Conventional hydropower generation is always built on a river and uses a dam to store the water in a reservoir. In the chamber, a turbine is connected with a synchronous generator by the shaft in the chamber driven by the flowing water. The potential energy stored in the water is converted into the electrical energy. The flow of water that controls the amount of electricity generated is controlled by the gate in the penstock. The water flows into the penstock affects the turbine's input of hydraulic mechanical power. Conventional hydropower generation has a wide range of installed capacity depending on the river condition. Currently, the largest conventional hydropower plant in the world is the Three Gorges Dam, which is in Hubei Province, China, with 22.4 GW of installed capacity. It is expected to generate 84.7 TWh per year of electricity [17].

1.3.2 Run-of-river Hydropower Generation

Run-of-the-river generation is a kind of hydroelectricity with little or no water storage in the system. This kind of plant is always built along a river and use the kinetic energy in river flows to generate electricity. This technology uses the same kind of turbine and generator as conventional hydropower generation but always has a smaller installed capacity compared with the conventional hydropower generation. The Belo Monte Dam with 11.18 GW installed capacity in Brazil is an example of run-of-the-river generation [18].

1.3.3 Tide Generation

Tide is a new way of generating electricity by using the kinetic energy stored in the ocean's

tide force. Although the tide is easier to predict than the wind and solar, its high cost and difficult site selection always impacts its development and construction and has limited the use of tide generation has not been widely used. The largest tide generation project is in South Korea whose name is Sihwa Lake Tidal plant with a 254 MW installed capacity [19]. In this project, the sea wall defense barriers containing 10 turbines are used to generate electricity. Compared with the two previous methods, tide generation still has some limitations and needs to improve its economy and efficiency.

1.3.4 Pumped Storage Hydropower

Pumped storage hydropower (PSH) is a kind of energy storage technology which comes from conventional hydropower generation. Unlike conventional hydropower generation, it has two reservoirs, the upper one and the lower one, to do the energy conversion between electrical energy and water potential energy. Its two operation modes, generating and pumping, can be switched depending on the grid demand to balance system load or depending on electricity price to make profits. One pumped storage hydro project, Castaic pumped storage plant, is in California, USA. It has six units with total 1507 MW installed capacity to meet the peak requirement of the city of Los Angeles[20].

1.4 Research Objectives

The objectives for the modeling study of T-PSH are as follows:

- T-PSH system modeling and its model programming implementation on the GE PSLF platform.

- T-PSH model performance validation and comparison of characteristics between T-PSH and C-PSH on a small grid system and the U.S Western Interconnection (WI) system.
- Sensitivity study of influence of shared-penstock situation and valve velocity on T-PSH frequency response.
- Effect discussion of T-PSH system in the WECC system with different renewable energy penetration levels- from 20% to 80%.
- Gordon Butte T-PSH project implementation in the U.S. WI system.

1.5 Organization of the Dissertation

This dissertation focuses on the T-PSH system dynamic modeling and implementation on the GE Positive Sequence Load Flow (PSLF) platform. The performance validation and comparison with C-PSH are both performed using a small test system and a large practical system. The effect of T-PSH system in different renewable penetration level situations from 20% to 80% are studied. Each chapter in this dissertation is organized as below:

Chapter 1 introduces the background of this research and the different categories of energy storage technology and hydropower generation.

Chapter 2 gives an overview of different pumped storage hydro technology and briefly compares the differences between each pumped storage hydropower technology.

Chapter 3 presents the detailed dynamic modeling procedure of T-PSH system, especially the development of T-PSH governor model.

Chapter 4 offers an introduction of GE PSLF platform and a detailed programming

implementation of T-PSH system on this platform.

Chapter 5 shows the functional verification simulation of T-PSH system under multi-scenario.

Chapter 6 introduces sensitivity studies of valve velocity and shared-penstock situation.

Chapter 7 presents the study on the influence of T-PSH technology on the high renewable penetrated system and illustrates the potential of T-PSH technology participating in the wide-area control.

Chapter 8 gives a brief introduction of Gordon Butte T-PSH project and its implementation in the GE PSLF platform.

Chapter 9 presents a conclusion of research and a suggestion for future work.

CHAPTER 2 PUMPED STORAGE HYDROPOWER TECHNOLOGY

A PSH plant is a kind of bi-direction hydropower plant which evolves from conventional hydropower generation. This kind of mature hydropower technology works like a battery: it can store potential energy and convert it into electricity by using two reservoirs. During times of low electrical demand when the price of electricity is low, a PSH plant stores potential energy in the upper reservoir by using the pumping mode. During peak electrical demand in the daytime, the plant converts the potential energy by releasing water from the upper reservoir to supply power to the grid and make profits [21].

Classified by structure, there are following classification methods. As the PSH uses the same type of turbine as the conventional hydro plant in the chamber, PSH technology can be classified into three categories-Pelton turbine, Francis turbine and Kaplan turbine according to the different water head and speed of water flow [22, 23]. In addition, the PSH plant can be categorized into two different types of the reservoir-the open-loop system and the closed-loop system. In the open-loop system, at least one reservoir uses a free-flowing water source like a river. On the contrary, the closed-loop system does not include any open-flow water source, so that it can minimize impact to the environment. If we focus on the placement of shaft, there are configurations for the PSH system-vertical shaft placement and horizontal shaft placement. The vertical shaft placement means the shaft is placed vertically in the chamber where the electric machine and turbine are. The horizontal placement is the same way as the vertical one except the shaft is placed horizontally.

Another classification is based on technology. It includes C-PSH and A-PSH as shown in

Figure 2.1. C-PSH evolves from conventional hydropower generation is the most basic and mature form of PSH technology. The A-PSH technology is newly developed technology in recent years which includes adjusted-speed PSH (AS-PSH) and ternary PSH (T-PSH). AS-PSH is power electronic based PSH technology whose main feature is the adjustable operation speed. T-PSH is a great upgrade based on C-PSH that has a new operation mode named hydraulic short-circuit (HSC) mode. These two A-PSH technologies are both developed and improved from C-PSH, but their ways of evolution are totally different. AS-PSH technology still uses the C-PSH's configuration by adding power electronic device to get the ability of speed adjustment. T-PSH technology adopts a new structure to have a new operating mode.

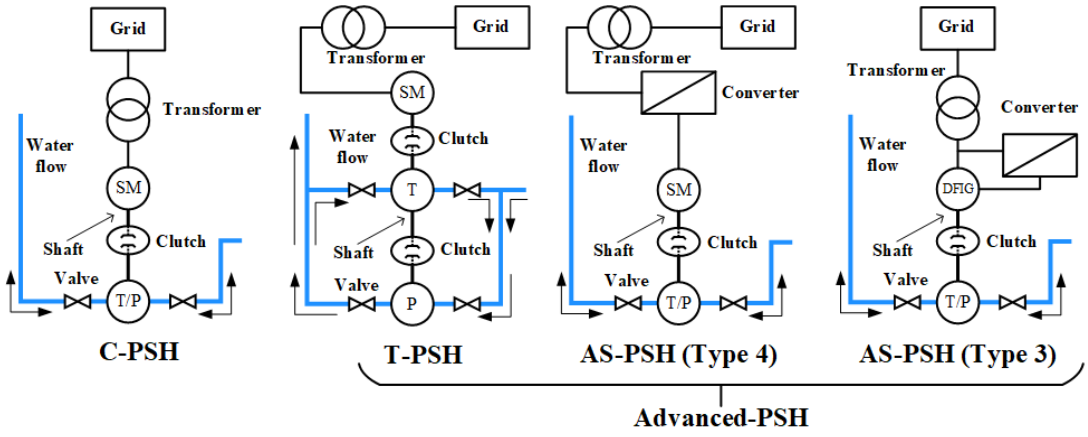

Figure 2.1 Comparison of structures for three types of PSH technology

2.1 Conventional Pumped Storage Hydropower

C-PSH comes from conventional hydropower generation by adding a reverse pumping operation mode. The single reservoir system in the conventional hydropower generation is replaced by a two-reservoir system. An example of C-PSH is the San Luis PSH which is located

in California, United States. It is an open-loop reservoir PSH and has eight Francis turbine units whose total rated power is 424,000 MW [24]. C-PSH in Figure 2.1 uses a synchronous machine with a DC excitation system originating from conventional hydropower generation. In the generating mode, it works at the fixed synchronous speed of 60 Hz in the U.S., which is the same as a conventional hydro generation unit. It can provide frequency regulation by using the controller embedded in the governor system depending on the system demand [25]. However, in pumping mode, frequency regulation cannot be provided by the C-PSH because the governor system is not embedded in the pumping mode; it is always operated at its maximum output in actual operation. Because of this configuration, C-PSH is a kind of reversible PSH technology which means the pumping mode and generating mode have different directions of the shaft. Hence, when C-PSH switches its operation mode, it always must wait for several minutes to stop the shaft owing to large inertia of the shaft system which leads to C-PSH cannot supply a fast-response ancillary service to help system stay balance by switching its operation mode when the system meets a contingency [26].

Nowadays, systems with high renewable energy penetration will be an unavoidable phenomenon. Industry and academia are starting to pay attention to C-PSH again to use existing C-PSH plant to solve the problems caused by the renewable energy generation. Although C-PSH cannot provide frequency regulation in its pumping mode, a large number of existing C-PSH units still play an important role in system operation with high renewable penetration. [8, 27] introduce operation planning and operation optimization of the system with a C-PSH unit, a PV system and

a wind system. In [28, 29], two practical examples of ES with a C-PSH unit to provide energy for two islands are introduced. Although many new methods have been proposed to optimize the operation of C-PSH, it cannot fundamentally solve the shortcomings of C-PSH. Obviously, many new technologies based on C-PSH are constantly appearing, which makes the upgrade of C-PSH possible. Among these new PSH technologies, the most representative one is named advanced pumped storage hydropower technology.

2.2 Advanced Pumped Storage Hydropower

As introduced previously, A-PSH, as a newer PSH technology, evolved from C-PSH in recent decades. Unlike C-PSH which cannot provide the frequency support in the pumping mode, both two main types of A-PSH can provide frequency regulation in the pumping mode by taking different approaches. AS-PSH technology keeps the original configuration from C-PSH technology and adds power electronic devices. Its speed and output power are adjustable in all operation modes. T-PSH technology is developed a new configuration to overcome drawbacks in C-PSH technology.

2.2.1 Adjustable-speed Pumped Storage Hydropower

AS-PSH technology is a combination of wind generation technology and PSH technology. By adopting machine and AC exciter system from wind power, AS-PSH gets a new feature of an adjustable shaft speed [30]. Although AS-PSH uses the traditional structural layout of PSH technology like C-PSH, the electrical machine in AS-PSH works at an adjustable speed depending on water condition in comparison to fixed shaft speed in C-PSH. The power electronic device

adjusts its output voltage at synchronous frequency whatever the water condition is. In addition, the power electronic device can adjust output according to power demand or current operationing mode for the system [31]. Depending on different wind power generation equipment, it can be divided into Type 1, Type 2, Type 3 and Type4 [32]. Since Type 1 is a fixed speed wind power generation technology and Type 2 is a limited variable speed wind turbine generation technology, these two technologies are no longer used. AS-PSH usually uses two wind turbine generation technologies, Type 3 and Type 4, which are shown in Figure 2.1. In Type 3, AS-PSH uses a doubly-fed induction machine (DFIG) with a partial-scale converter-based AC exciter in the electrical machine system. The inverter used in this type is only 25% of system rating capacity, which can reduce the cost of the inverter. Typically, the variable speed range for this technology is ±33.3% around synchronous speed. In Type 4, AS-PSH uses a synchronous machine with a full-size converter in the system. Note that the synchronous machine in Type 4 AS-PSH is not required to operate at synchronous speed. In this type, the operating speed can theoretically be set to any value. However, the full-scale inverter and its output filters must meet the system rating capacity, which will make the design difficult and costly [33, 34]. Owing to one turbine traditional PSH layout, AS-PSH is a reversible direction PSH same as C-PSH. The different direction of rotation for the pumping and generating modes makes AS-PSH spend several minutes to change the operation mode like the C-PSH technology. But the use of power electronic devices allows AS-PSH technology to do quicker power adjustments in all operation modes in comparison to C-PSH technology. An example of AS-PSH is the Okikuyotsu PSH units in Japan. Its No.2 plant has a 300

MW adjustable-speed unit with an open-loop reservoir system [35].

Because of using power electronic device, the generic model of converter-connected generation shown in [36] can be used in an AS-PSH electric machine and exciter model, which simplifies the work of modelling. Also, because AS-PSH technology is similar to wind turbine generation, some modelling methods for AS-PSH technology are based on wind power generation [37, 38]. In [39, 40], control methods used in inverter control and wind generation are also be used in AS-PSH operation. In addition, in order to adapt to the integration of a large amount of renewable energy generation in the future, many methods of using AS-PSH with solar and wind generation were recently proposed in [41-43].

2.2.2 Ternary Pumped Storage Hydropower

T-PSH is a structural innovation based on C-PSH in which the traditional one turbine structure is replaced by two turbines as shown in Figure 2.1 [44]. The pump turbine and generation turbine in the T-PSH are placed in two separate chambers. In order to add the additional pump turbine, an additional set of penstocks is placed to connect the pump turbine into this system. A synchronous machine working at fixed synchronous speed with a DC excitation system is connected to the shaft, which is the same as the C-PSH. On this shaft, both turbines are connected and can be connected or disconnected by clutches according to the operation requirement. Unlike C-PSH and AS-PSH, T-PSH is not a reversible direction PSH because of its two different turbines. The impacts from hydraulic transients are thus significantly reduced which means that a T-PSH does not have to wait for the shaft stop to switch operation mode like C-PSH and AS-PSH. Benefitting from this

innovative structure, a new operation mode named hydraulic short-circuit (HSC) mode is created. In HSC mode, T-PSH system is pumping water (absorbing power from the grid) from the lower reservoir to the upper reservoir. Since the turbine part also participates in operation in HSC mode, a T-PSH unit can adjust its output during pumping water which is an improvement over C-PSH. Compared with AS-PSH, T-PSH can switch operation mode quicker. However, this potential new technology is still in the initial stage and has not been widely investigated.

Even though it has not been widely used yet, a T-PSH plant named Kops II has been deployed in Gaschurn, Austria. Its rated power is 525 MW, and it was commissioned in 2009 [45]. Because of their many potential benefits, a new 360 MW T-PSH plant named Obervermuntwerk will be commissioned at the end of 2018 in Austria [46]. There is not any T-PSH project in construction or planning in the U.S. Owing to the lack of realistic parameter information, its research and development is behind that of AS-PSH [36]. Only [44] shows a basic model for T-PSH. Some details of the model like the shared-penstock in HSC mode are not included.

CHAPTER 3 TERNARY PUMPED STORAGE HYDROPOWER

In recent years, T-PSH technology has attracted more attention and more interests from industry. However, as mentioned before, few works from academia show the detailed T-PSH system modeling. There is an urgent need for a detailed model of T-PSH system which can be used in research and in industrial application. In this chapter, a detailed T-PSH system modeling study will be introduced. Especially, the unique operation mode-hydraulic short-circuit (HSC) mode-with special water interaction in the penstocks will be studied.

3.1 Introduction

T-PSH is a structural innovation based on C-PSH. Without changing the original structure of C-PSH, an additional pump system is added to connect with the turbine system on the same shaft. This configuration was first proposed in [47] and was used in Puente-Bibey underground pumped-storage station in Spain [48]. However, due to technical limitations at that time, the turbine and pump can only be operated separately. Obviously, the pump and the turbine can be operated together to implement a new operation mode [44]. This new mode named HSC mode is the most important feature of T-PSH technology by allowing abilities of frequency regulation while pumping water. Meanwhile, this configuration does not require the shaft to reverse direction in different operation mode, which significantly reduces the wait a long time caused by the large inertia during the operation mode switching. Thus, quick operation mode switching becomes possible in T-PSH unit whereas the C-PSH unit always needs 3-4 minutes to switch from pumping to generating and vice versa. Therefore, modelling for this new configuration and the new

operation mode is the most important thing in the whole system modeling.

In order to model T-PSH system, the system is divided into many parts as shown in the block diagram in Figure 3.1. Owing to evolution from C-PSH, the synchronous machine and excitation system in C-PSH modelling can still be used in T-PSH system. However, due to the new configuration and the additional HSC mode in T-PSH technology, the separated governor model used in C-PSH cannot be used. A new combination governor model needs to be created to model the most important feature of T-PSH in which both the turbine and pump work simultaneously.

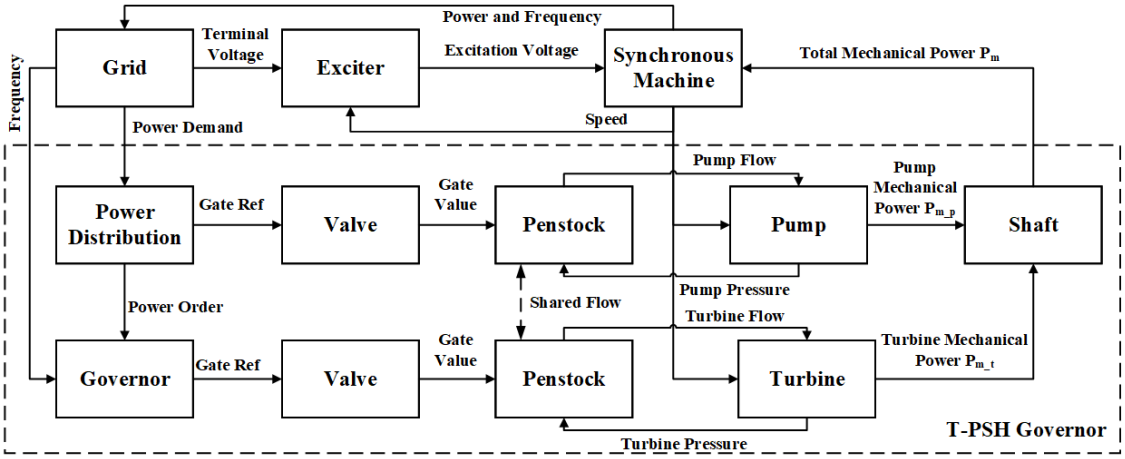

Figure 3.1 Block diagram of the T-PSH system

3.2 Synchronous Machine and Excitation System Modeling

Since T-PSH technology retains the synchronous machine used in C-PSH technology, the model of the synchronous machine and its DC excitation system in the C-PSH system model can be used in the T-PSH system model. When implementing the machine system used in T-PSH system in the PSLF platform, the built-in salient pole synchronous machine and its DC exciter models are adopted. The introduction of these models is presented in this section.

3.2.1 Synchronous Machine Modeling

The synchronous machine is the core of the entire T-PSH system and is used to convert electrical energy into kinetic energy in the pumping mode or to convert kinetic energy into electrical energy in the generating mode. An existing three-phase salient pole machine model in the PSLF platform is used in this study. This model is called GENSAL, which means salient pole synchronous machine is represented by equal mutual inductance rotor modeling [49]. Before introducing the model, two references should be defined. First, the q-axis leads the d-axis by 90 degrees. Second, the rotor angle is the angle of the q-axis with respect to the network a phase axis [50]. A schematic of the synchronous machine and these definitions is shown in Figure 3.2.

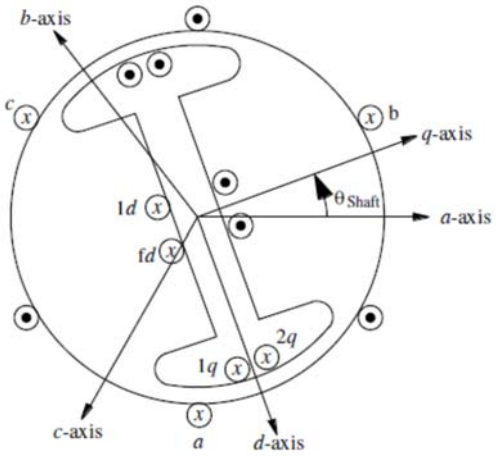

Figure 3.2 Synchronous machine schematic [51]

According to the fundamental Kirchhoff's, Faraday's and Newton's laws, the relationship between current and flux linkage and swing equation in the synchronous machine are given below:

$$v_a = i_a r_s + \frac{d\psi_a}{dt} \tag{1}$$

$$v_b = i_b r_s + \frac{d\psi_b}{dt} \tag{2}$$

$$v_c = i_c r_s + \frac{d\psi_c}{dt} \tag{3}$$

$$v_{fd} = i_{fd} r_{fd} + \frac{d\psi_{fd}}{dt} \tag{4}$$

$$v_{1d} = i_{1d} r_{1d} + \frac{d\psi_{1d}}{dt} \tag{5}$$

$$v_{1q} = i_{1q} r_{1q} + \frac{d\psi_{1q}}{dt} \tag{6}$$

$$v_{2q} = i_{2q} r_{2q} + \frac{d\psi_{2q}}{dt} \tag{7}$$

$$2H \frac{d\omega}{dt} = T_m - T_e - T_{f\omega} \tag{8}$$

where ψ is flux linkage, *r* is winding resistance, *H* is the inertia constant, T_m is the mechanical torque on the shaft, T_e is the electrical torque and $T_{f\omega}$ is a friction torque on the shaft.

After doing a Park's transformation and linearization, the linear magnetic circuit model used in GENSAL is derived [51]. Ignoring saturation in the generator, the relationship between flux linkage and current on the d-axis can be expressed as:

$$T'_{do} \frac{dE'_q}{dt} = E_{fd} - E'_q - (X_d - X'_d)[I_d + \frac{X'_d - X''_d}{(X'_d - X_l)^2}(E'_q - \psi'_d - (X'_d - X_l)I_d)] \tag{9}$$

$$T''_{do} \frac{d\psi'_d}{dt} = E'_q - \psi'_d - (X'_d - X_l)I_d \tag{10}$$

$$\psi''_d = \frac{X''_d - X_l}{X'_d - X_l} E'_q + \frac{X'_d - X''_d}{X'_d - X_l} \psi'_d \tag{11}$$

Assuming T'_{qo} is 0 to get a simple q-axis relationship, the relationship between flux linkage and current on the q-axis can be written as [51]:

$$T''_{qo} \frac{d\psi''_q}{dt} = -\psi''_q - (X_q - X''_q)I_q \tag{12}$$

The relationship between synchronous machine and network, after doing a Norton transformation is written as:

$$V_d + jV_q = (-\psi''_d + j\psi''_q)(1+\omega) \tag{13}$$

$$I_{d\_norton} + jI_{q\_norton} = \frac{V_d + jV_q}{R_a + jX''_d} \tag{14}$$

The swing equation can be expressed below:

$$\frac{d\delta}{dt} = \omega \times \omega_0 \tag{15}$$

$$\frac{d\omega}{dt} = \frac{1}{2H}\left(\frac{P_{mech} - D\omega}{1+\omega} - T_{elec}\right) \tag{16}$$

$$T_{elec} = \psi''_d I_q + \psi''_q I_d \tag{17}$$

where P_m is the mechanical power on the shaft and all the parameters in the equations are shown in Table 3.1.

Table 3.1 Parameters in the GENSAL model [49]

Parameter	Description	Units
T'_{do}	d-axis transient rotor time constant	sec
T''_{do}	d-axis sub-transient rotor time constant	sec
T''_{qo}	q-axis sub-transient rotor time constant	sec
X_d	d-axis synchronous reactance	p.u.
X_q	q-axis synchronous reactance	p.u.
X'_d	d-axis transient reactance	p.u.
X''_d	d-axis sub-transient reactance	p.u.
X''_q	q-axis sub-transient reactance	p.u.
X_l	Stator leakage reactance	p.u.
R_a	Stator resistance	p.u.
H	Inertia constant	sec
D	Damping factor	p.u.

After finishing this simplified one-axis model for the synchronous machine, a diagram according for the GENSAL model is shown in Figure 3.3.

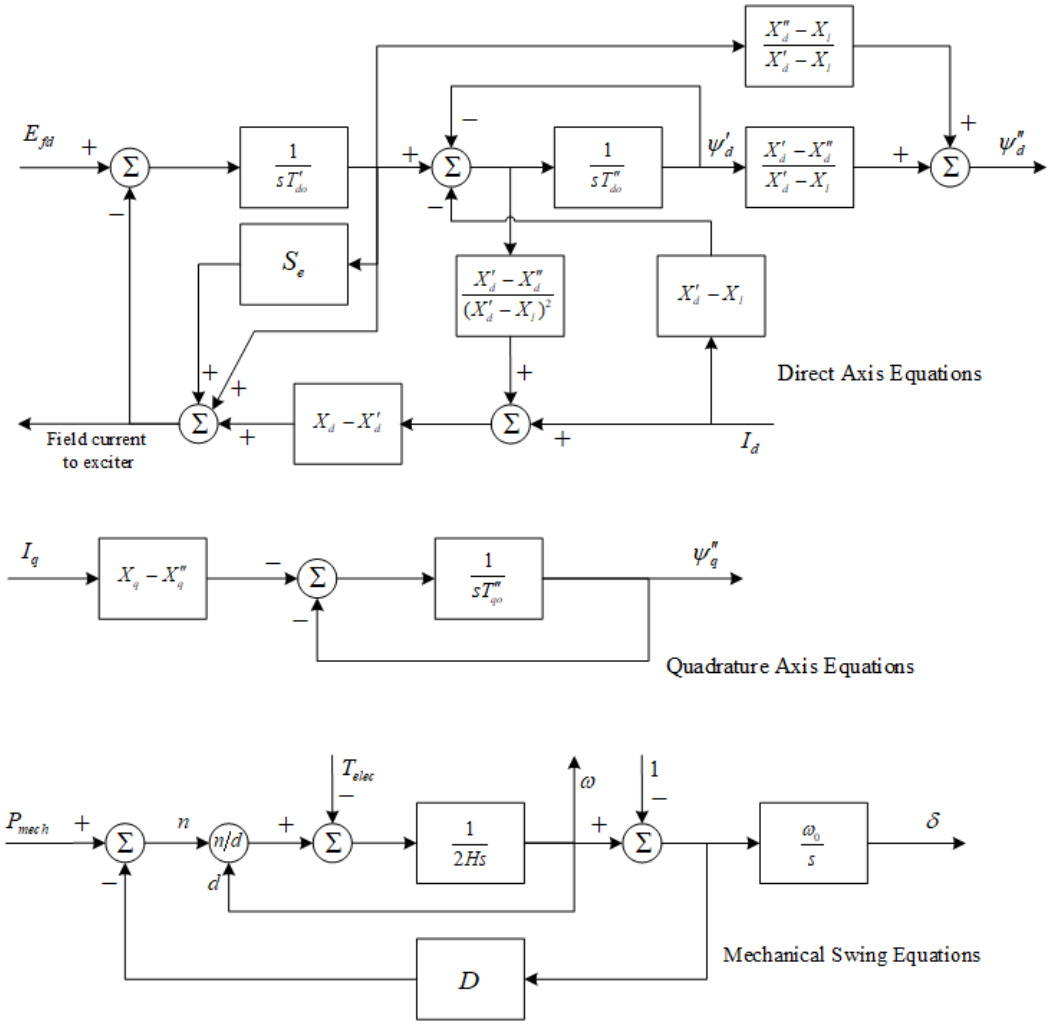

Figure 3.3 Diagram of the GENSAL synchronous machine model [49]

3.2.2 Excitation System Modeling

The excitation system in the synchronous generator provides DC current to the field winding, which induces three phases voltages on the armature winding. Meanwhile, the additional functions of exciter include voltage control, reactive power flow control, system stability enhancement and

generation system protection [52]. In this T-PSH study, the IEEE (1968) Type 1 DC excitation system model is used to model the DC exciter [53]. This excitation system is representative of a modern system in service. In the later IEEE standard [54, 55], this IEEE (1968) Type 1 DC exciter has been modified as Type DC1A DC excitation system. When implementing this excitation system in PSLF, the existing exciter model 'IEEET1' shown in Figure 3.4 is used [49].

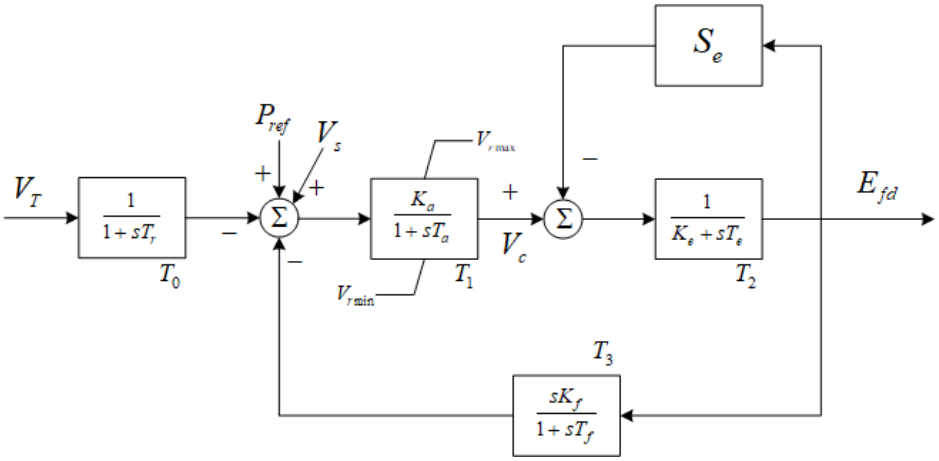

Figure 3.4 Transfer function diagram of the IEEET1 excitation system

In this model, the input is the generator terminal voltage V_T, reference voltage V_{ref} and scheduled voltage V_s. Before getting the error of voltage at the first summing point, there is a first order filter T_0 to filter out clutter in the input of the generator terminal voltage. At the first summing point, the voltage error is generated by combining all the inputs and the feedback voltage which is filtered by damping function T_3. The feedback loop used here can stabilize the system quickly. After the first summing point, the error is sent to the main regulator transfer function T_1. A windup function is embedded in this main regulator to limit its output V_c to meet the function shown below:

$$V_{r\min} < V_c < V_{r\max} \tag{18}$$

The variables $V_{r\min}$ and $V_{r\max}$ are lower and upper limits of windup function, respectively. At the second summing point, the output of the main regulator subtracts the signal from the saturation function. This saturation signal is calculated by multiplying exciter output voltage or generator field voltage by a saturation factor S_e. This factor can be calculated by using:

$$S_e = \frac{B(E_{fd} - A)^2}{E_{fd}} \tag{19}$$

where A and B are defined as the exciter excitation to produce the output voltage on the constant-resistance-load saturation curve and the air gap line shown in Figure 3.5, respectively [53].

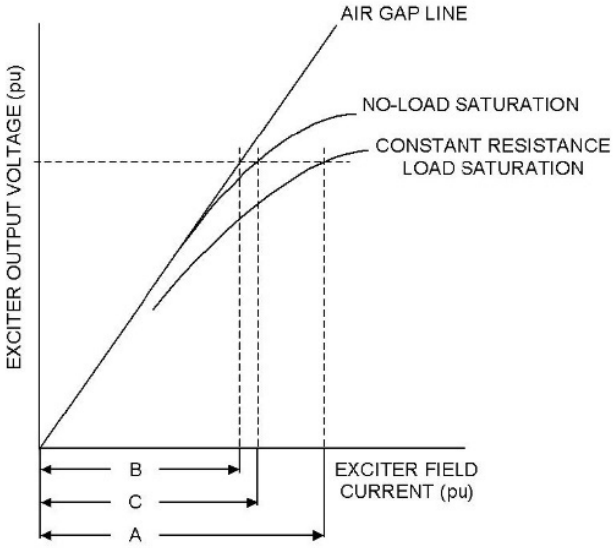

Figure 3.5 Exciter saturation characteristics [55]

The voltage error at the second summing point is applied to the exciter transfer function T_2. After this transfer function, the exciter output voltage E_{fd} is obtained as follows:

$$E_{fd} = \frac{T_1 T_2}{T_1 T_2 T_3 + S_e T_2 + 1} \times (V_{ref} + V_s - T_0 V_T)$$
$$where\ T_0 = \frac{1}{1+sT_r},\ T_1 = \frac{K_a}{1+sT_a},\ T_2 = \frac{1}{K_e + sT_e}\ and\ T_3 = \frac{sK_f}{1+sT_f} \quad (20)$$

Additional parameters in this transfer function are shown in Table 3.2

Table 3.2 Parameters in the transfer function of IEEET1 model [49]

Parameter	Description	Units
T_r	Transducer time constant	sec
K_a	Voltage regulator gain	p.u.
T_a	Voltage regulator time constant	sec
K_e	Exciter field resistance line slope margin	p.u.
T_e	Exciter field time constant	sec
K_f	Rate feedback	p.u.
T_f	Rate feedback time constant	sec

3.3 Governor modeling

Unlike the synchronous machine and exciter model, the governor model cannot directly use the C-PSH one due to the innovative structure of the governor in T-PSH system. A new dynamic governor model, whose diagram is shown in Figure 3.6, is developed based on the 'HYGOV' model. This dynamic model is a general hydropower turbine and governor model, which is universally used in hydropower generation modeling [49]. Here, it will be used to model the turbine part in the governor. The model describes a straightforward hydroelectric plant governor with a simple hydraulic representation of the penstock with unrestricted head race and tail race, and no surge tank [56]. In order to describe the pumping mode and HSC mode, additional pump part with complete detailed water flow regulator and penstock system is added into the 'HYGOV' model [57]. A new function to describe the single shaft system with the turbine runner, pump runner,

and synchronous machine connected is implemented in the model. Meanwhile, a distribution block is designed in this governor model to calculate and send the power reference to turbine part and pump part, which can control or switch the operation mode of the T-PSH. In addition, a part is added to the shared-penstock hydro model to describe the water flow interaction between the turbine penstock and pump penstock during the HSC mode.

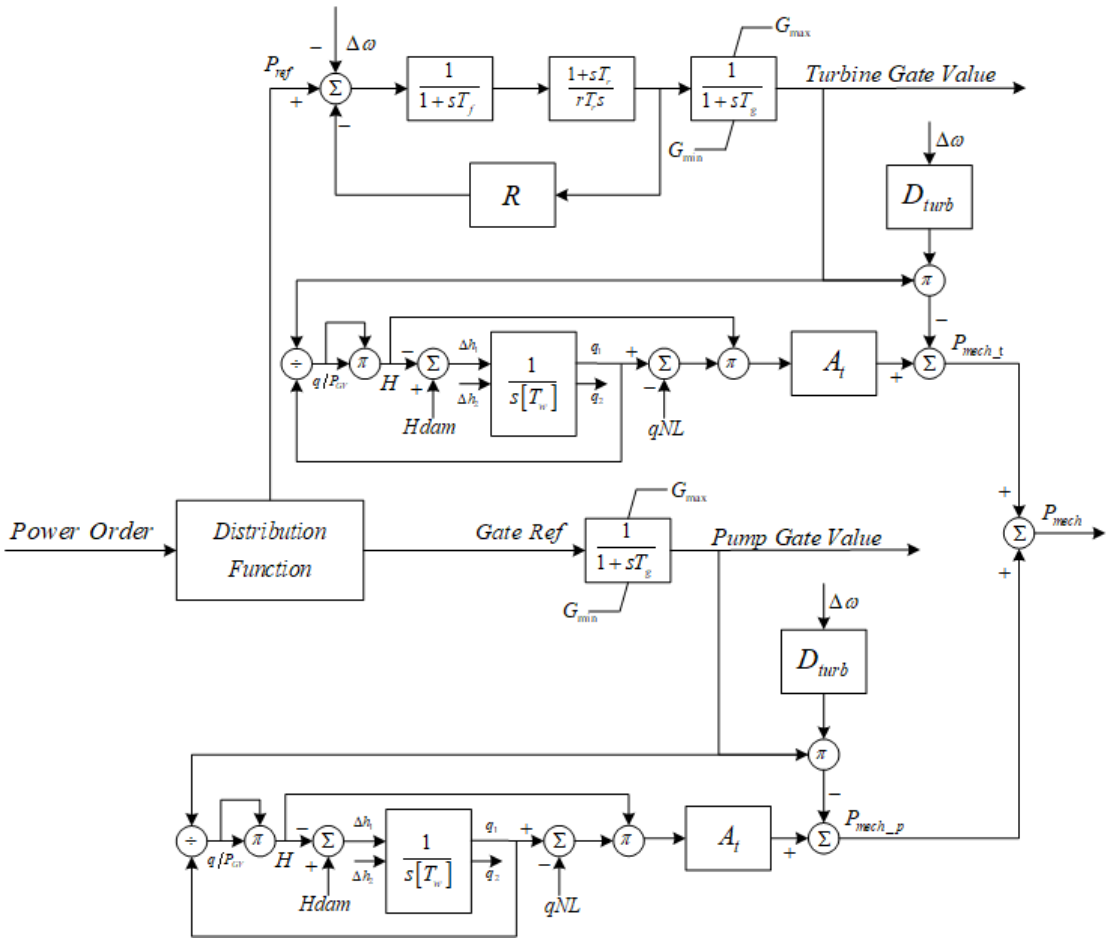

Figure 3.6 Transfer function diagram of the T-PSH governor

3.3.1 Distribution Block Design

As a combination governor model is used in T-PSH modeling, an operation mode controller

is added to control the three T-PSH operation modes. In this controller, a pair of distribution coefficients are defined by

$$\begin{aligned} &\text{Generating Mode：} K_{d\_p}=0, K_{d\_t}=1 \\ &\text{Pumping Mode：} K_{d\_p}=1, K_{d\_t}=0 \\ &\text{HSC Mode：} \frac{P_{rate}}{P_{gen}}>K_{d\_p}>1, K_{d\_t}=1-K_{d\_p} \end{aligned} \tag{21}$$

where K_{d_t} is the distribution coefficient for the turbine part, K_{d_p} is the distribution coefficient for the pump part, P_{rate} is the rated capacity of the T-PSH unit, and P_{gen} is current power requirement of the T-PSH in HSC mode. These coefficients are set in the distribution block and share with the turbine part and the pump part to make them know the current working status of the T-PSH. And, the clutches and the gates will be controlled according to these coefficients to meet different operational needs in different operation mode. In order to control mechanical coupling between the turbine and the pump and the shaft, this controller achieves a combination of operation of turbine and pump (separately or together) to generate positive or negative mechanical power signal to the synchronous machine in the specific simulation case. This kind of design also allows a practical way for the customer to add any special operating situation in the future model updates or extend more function in the model.

According to these distribution coefficients, a power reference calculation function is defined in (22) to generate the power order for each part during the initialization and the simulation.

$$\begin{cases} P_{gen\_pump}=-K_{d\_p}\times\left|P_{gen}\right| \\ P_{gen\_\text{turbine}}=K_{d\_t}\times\left|P_{gen}\right| \end{cases} \tag{22}$$

where P_{gen} is the active power of the synchronous machine in per unit, P_{gen_pump} is the power order

of the pump part, $P_{gen\_turbine}$ is the power order of the turbine part, K_{d_t} is the distribution coefficient for turbine part, and K_{d_p} is the distribution coefficient for pump part. During the initialization, the power order for each part will be calculated according to the power demand from the grid and initial the T-PSH system. During the simulation, this power order will be updated in each simulation iteration.

3.3.2 Modelling of the Gate Controller in Turbine Part

By using a combination of turbine and pump, the gate controller for each part should be modelled separately. In T-PSH system, the pump works in a fixed setting value whether in the pumping mode or in the HSC mode. The output power cannot be adjusted automatically because there is no controller in the pump part. As a result, the power reference calculated in (22) from distribution block is sent directly to the gate as the gate reference signal. The gate value will keep constant regardless of grid status.

However, unlike the pump part, the turbine part is operated as conventional hydropower generation. There is a droop controller shown in Figure 3.7 in the turbine part to adjust the gate value automatically according to both power reference received from the distribution block and the frequency variance from the grid. When a system frequency error or power reference change occurs, the gate value is increased to increase mechanical power output and vice versa. After that, the difference between the requirement and actual output will be decreased. In this way, droop speed control helps to keep a stable grid frequency. The amount of power produced is strictly proportional to the error between the actual turbine speed and speed reference [52].

The transfer function of the governor is shown as:

$$g_{ref} = \frac{T_r s + 1}{rT_f T_r s^2 + RT_r s + rT_r s + R} \cdot (P_{ref} - \Delta f) \tag{23}$$

where g_{ref} is the gate reference, P_{ref} is the power reference from the distribution block, Δf is the frequency difference input, T_r is the washout time constant, T_f is the filter time constant, r is the temporary droop constant, and R is the permanent droop constant.

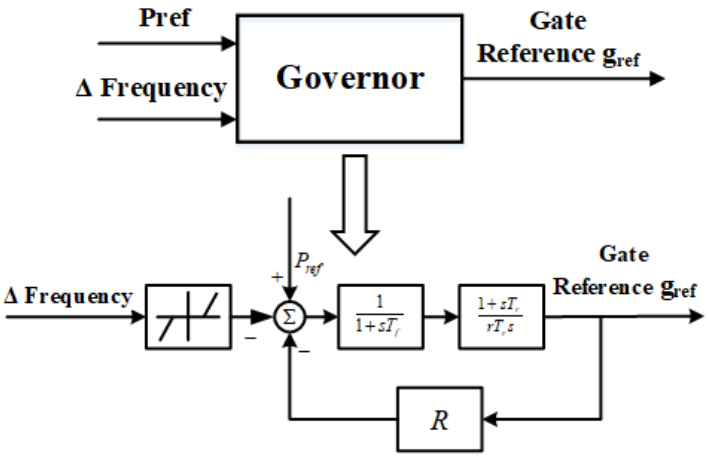

Figure 3.7 Block diagram of the turbine gate controller

3.3.3 Gate valve modeling

The amount of mechanical power directly depends on the inflow of water in the turbine runner or outflow of water in the pump runner. The rate of water flow is controlled directly by the gate valve. As a result, by using gate valve to adjust the water flow can make T-PSH meet the power requirement according to the system demand. To work with the clutch system, the gate valve can even switch T-PSH operation mode in daily operation. In the real gate valve for the Pelton turbine, there are two mechanical devices to control the water flow, one is injector and another is deflector

as shown in Figure 3.8. These two components will be modelled separately and combined to form a gate valve model.

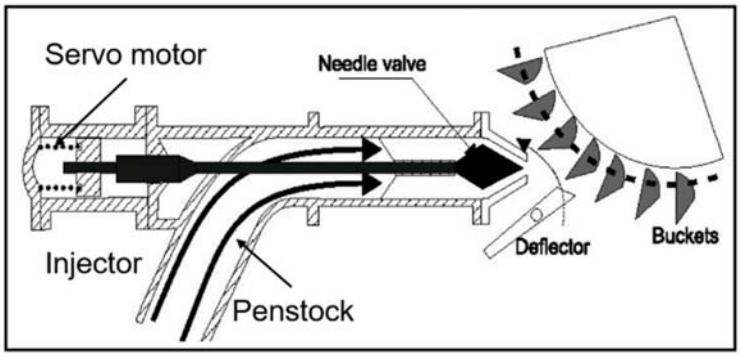

Figure 3.8 Slicing diagram of the valve in T-PSH [58]

The injector is used to control the amount of the water flow in daily operation and has two parts: the needle valve and the servo motor. The needle valve in the nozzle is driven by a servo motor to adjusts the amount of water flow into the turbine runner and the pump runner. The physical response delay of the servo motor is modeled by a first order delay as shown in Figure 3.9, and the transfer function is shown in (24).

$$g = \frac{1}{1+T_g s} \cdot g_{ref} \tag{24}$$

where g is the gate value, g_{ref} is the gate reference, and T_g is the time constant of the gate servo. The time of execution for the servo motor and the needle valve is described as a linear speed limit function. The constant 'Velm' in this ramp function indicates the time spent for the injector to open from 0% to 100% per unit (same in 100% to 0%). Meanwhile, an extremum limit is added into the gate valve block to set the injector's value between 0 and 1 per unit, which imitates the actual range of gate. This extremum limit can avoid unreasonable simulation caused by excessive gate

reference input.

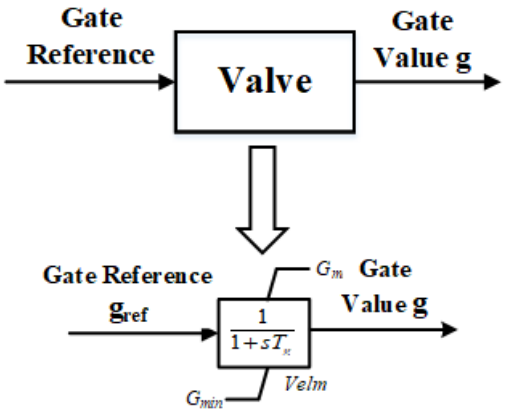

Figure 3.9 Block diagram of the injector

The deflector shown in Figure 3.8 is at the end of the penstock and can be treated as a water flow switch. It is a kind of on/off mechanical switch which can adjust the direction of water inflow. As shown in Figure 3.8, the deflector is between the Pelton turbine and the end of the penstock. The deflector can block the water jet from hitting the rotating bucket, thus removing the mechanical input torque on the shaft. Compared with the injector, the deflector cannot stop the water flow from the penstock, but it can deflect the water within several seconds. A logic function with a short time delay is used to model the function of the deflector in the valve model. Because of its quick response, it can be used for emergency protection like transmission line disconnection. After the quick deflection, the injector closes the valve according to the protective command to stop the water flow input completely.

These two components make up the valve system in the T-PSH system. The quick response of the deflector can help T-PSH switch the operation mode or do the protective generator tripping in seconds. The injector, with a minute level response, plays an important part in adjusting

mechanical power output.

3.3.4 Modelling of Turbine Runner and Penstock System

After finishing the controller and the gate valve modelling, another important part is the turbine runner and penstock system. This system is the bridge between the control system and mechanical power output. It models the conversion process from potential energy in the water to kinetic energy on the shaft, which will give practical meaning to the whole governor model.

The penstock is modelled by assuming an incompressible fluid and the penstock head loss is ignored. According to Newton's law of motion, the force of water in the penstock system can be defined by [59, 60]:

$$F_{net}=\rho L\frac{dq}{dt}=A\rho g(H_0-H) \tag{25}$$

where F_{net} is the force of water in the system, ρ is the water density, L is the length of the penstock, q is the flow rate of the water in the penstock, A is the cross-sectional area of the penstock, g is the gravitational constant, H is the dynamic head at the bottom of the penstock and H_0 is the nominal steady-state head at the bottom of the penstock. The rate of change of water flow in the penstock can be rewritten according to (25):

$$\frac{dq}{dt}=\frac{gA}{L}\cdot(H_0-H) \tag{26}$$

After converting to per unit, this function is shown as:

$$\frac{dq}{dt}=\frac{(1-\mathrm{H})}{T_w} \tag{27}$$

where T_w is water time constant with units in seconds which can be defined as:

$$T_w = \frac{L}{gA} \cdot \frac{q_{base}}{H_{base}} \tag{28}$$

where q_{base} is the base water flow, which is chosen as the value of water flow when the gate is fully opened, and H_{base} is the static head of the water column.

After finishing the model of the penstock, the relationship between water flow and turbine output should be found. An ideal model given in (29) describes the relationship among water flow, gate position and water head [61].

$$q = G\sqrt{H} \tag{29}$$

where *G* is the gate position. This function shows the value of water that flows through the turbine. The last step in the turbine modelling is to determine an expression for mechanical power output. In the ideal turbine model, output mechanical power is proportional to the water flow and water head. However, in reality, the turbine cannot work in an ideal situation with 100% efficiency. There is a minimum water requirement called no-load water flow to operate the turbine. Under this no-load flow, the turbine runner cannot be driven by this amount of water flow. Also, there is a similar definition in the pump part. Always, in the turbine runner and pump runner, frictional resistance appears on the rotating shaft. After adding these factors to the ideal model of turbine, a more realistic model can be expressed:

$$P_m = A_t H(q - q_{NL}) - D_{turb} G\Delta f \tag{30}$$

where P_m is the mechanical power output, A_t is a constant of turbine gain, *H* is the dynamic head at the bottom of the penstock, q_{NL} is the no-load water flow, *q* is the flow rate of the water,

D_{turb} is the damping factor of friction, G is the gate position and Δf is the difference of input frequency.

Combining the turbine model and the penstock water flow model together, a whole hydro model for turbine and pump in the T-PSH is shown in Figure 3.10. This model is used in the generating mode and pumping mode. The interaction of water flow in the HSC mode will be introduced in the next section.

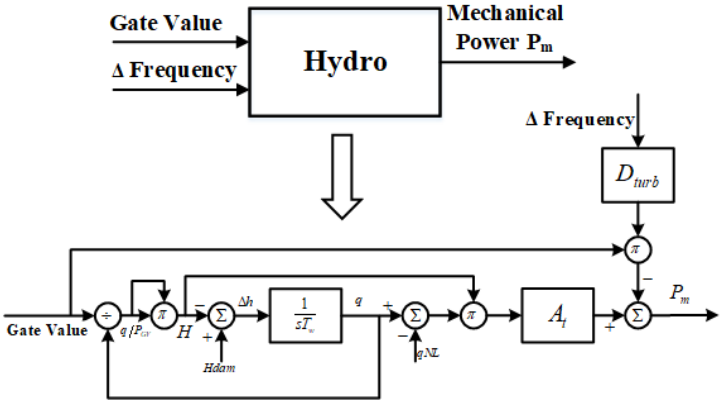

Figure 3.10 Block diagram of hydro penstock and turbine/pump

3.3.5 Hydraulic Short-circuit Modeling

Hydraulic short-circuit, as a new feature in the T-PSH system, occurs because both the turbine runner and the pump runner work together. When T-PSH consists of a set of separated parallel penstocks, water flow in the pump part and turbine part flow between the higher reservoir and the lower reservoir by themselves. Obviously, the direction of water flow in two units, pump and turbine, are different. But the water flow in these parallel penstocks cannot affect each other owing to the reservoir used in T-PSH system, which can be treated as an infinite water resource. As a

result, simply combine the turbine part and the pump part to achieve the HSC mode. Under the control of the distribution block, the pump part is operated with a fixed output whereas the turbine part provides variable output. The negative constant pump torque, countering the variable positive turbine torque, results in a variable net torque which is described in (31)

$$P_m = P_{m\_t} + P_{m\_p} \tag{31}$$

where P_m is the total mechanical power output of the governor, P_{m_t} is the mechanical power output of the turbine part, and P_{m_p} is the mechanical power output of the pump part. This function is added into the governor model to describe the combination of torque on the shaft. At the same time, there are some changes in the hydro model. Based on water flow model shown in (27), a second order matrix system is derived to describe this HSC mode:

$$\begin{bmatrix} T_{w\_t} & 0 \\ 0 & T_{w\_p} \end{bmatrix} \cdot \begin{bmatrix} \frac{dq_t}{dt} \\ \frac{dq_p}{dt} \end{bmatrix} = \begin{bmatrix} \Delta H_t \\ \Delta H_p \end{bmatrix} \quad \mathrm{T}_{w\_t,p} = \frac{L_{t,p}}{gA_{t,p}} \cdot \frac{q_{base}}{H_{base}} \tag{32}$$

where T_{w_t}, T_{w_p} are the water time constants for the entire penstock length of the turbine part and the pump part; q_{w_t}, q_{w_p} are the turbine flows in per unit for the turbine part and pump part; and $\Delta H_{w\_t}, \Delta H_{w\_p}$ are the turbine head differences in per unit for the turbine part and pump part.

If a two-stage penstock structure is employed to save excavation costs, the HSC mode constitutes a circulating flow as shown in Figure 3.11. In this structure, the primary penstock is used to connect the reservoirs and chambers of T-PSH unit. A secondary penstock is split from primary penstock to connect each chamber in the T-PSH unit. The water flow in the secondary

penstock forms a circuit of water flows in the HSC mode. The pump runner drives the water flow from lower reservoir to higher reservoir as shown in Figure 3.11 by the arrows from bottom left to upper right. Meanwhile, the turbine runner is driven by part of pumped water flow to generate torque, which is superimposed with the power on the shaft. The water flow through the turbine recombines with the water flow from the lower reservoir reflow into the pump. The water flow in the turbine part can be treated as a short-circuit water flow and will affect the whole water flow in the T-PSH hydro system. As a result, the previous method used for parallel penstock system cannot accurately describe the interaction of water flow in the turbine part and the pump part under HSC situation. A new water flow model should be designed to model this interaction.

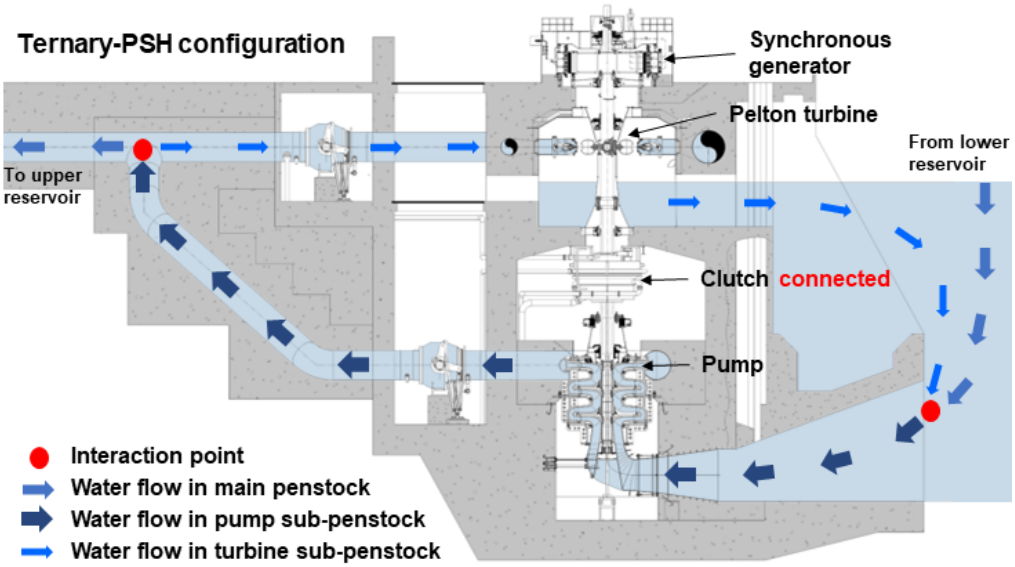

Figure 3.11 Water flow in the HSC mode with two-stage penstock [source: GE]

Based on (26) introduced in the previous section, a function is derived for water flow in primary penstock located between higher reservoir and split point (two red points in Figure 3.11):

$$H_0 - H = -\frac{L_c}{gA_c} \cdot \frac{dq}{dt} \tag{33}$$

where L_c is the length of the primary penstock, A_c is the cross-sectional area of the primary penstock. And, according to the water flow continuity equation,

$$q = q_p - q_t \tag{34}$$

Water flow can be split into two parts to flow into the secondary penstocks. Equation (33) can be rewritten as:

$$H_0 - H = -\frac{L_c}{gA_c} \cdot (\frac{dq_p}{dt} - \frac{dq_t}{dt}) \tag{35}$$

In the same manner, a function to describe the water flow in the pump part secondary penstock (from the split point to pump runner) can be written as:

$$H - H_p = -\frac{L_p}{gA_p} \cdot \frac{dq_p}{dt} \tag{36}$$

Combining (35) and (36) together, a new water flow function is derived:

$$H_0 - H_p = -(\frac{L_c}{gA_c} + \frac{L_p}{gA_p}) \cdot \frac{dq_p}{dt} + \frac{L_c}{gA_c} \cdot \frac{dq_t}{dt} \tag{37}$$

This function describes the relationship between water head and water flow in the penstock (from higher reservoir to the pump runner) By using the same per-unit as in (28), a new set of water time constants for the pump part can be defined as:

$$T_{w\_pp} = -(\frac{L_c}{gA_c} + \frac{L_p}{gA_p}) \cdot \frac{q_{base}}{H_{base}} \quad T_{w\_pt} = \frac{L_c}{gA_c} \cdot \frac{q_{base}}{H_{base}} \tag{38}$$

where T_{w_pp} is the water time constant for the entire penstock length of the pump part, and T_{w_pt}

is the water time constant for the shared-penstock length from the pump part to the turbine part. When using the same analysis method for the turbine part, the analysis of water flow between high reservoir and turbine runner is shown below:

$$H_0 - H_t = (\frac{L_c}{gA_c} + \frac{L_t}{gA_t}) \cdot \frac{dq_t}{dt} + \frac{L_c}{gA_c} \cdot \frac{dq_p}{dt} \tag{39}$$

Therefore, the water time constants for the turbine part water flow can be derived:

$$T_{w\_tt} = (\frac{L_c}{gA_c} + \frac{L_t}{gA_t}) \cdot \frac{q_{base}}{H_{base}} \quad T_{w\_tp} = -\frac{L_c}{gA_c} \cdot \frac{q_{base}}{H_{base}} \tag{40}$$

where T_{w_tt} is the water time constant for the entire penstock length of the turbine part, and T_{w_tp} is the water time constant for the shared-penstock length from the turbine part to the pump part. After collecting the water time constants, a new water flow model can be written as:

$$\begin{bmatrix} Tw_{tt} & Tw_{tp} \\ Tw_{pt} & Tw_{pp} \end{bmatrix} \cdot \begin{bmatrix} \frac{dq_t}{dt} \\ \frac{dq_p}{dt} \end{bmatrix} = \begin{bmatrix} \Delta H_t \\ \Delta H_p \end{bmatrix} \tag{41}$$

Especially, in the HSC mode, T_{w_pt} and T_{w_tp} in the water constant matrix describe the interaction between two separate secondary penstocks whose water flow are in a different direction at the same time. If T-PSH only works in the generating or pumping mode, this water time constant is still suitable by only setting value for T_{w_pp} or T_{w_tt} and set other three elements as zero.

After analyzing the hydraulic short-circuit, the complete hydro model with detailed hydraulic short-circuit function, shown in Figure 3.12, is developed to use both in the turbine part and the pump part. The total mechanical power output still follows the original formula (31).

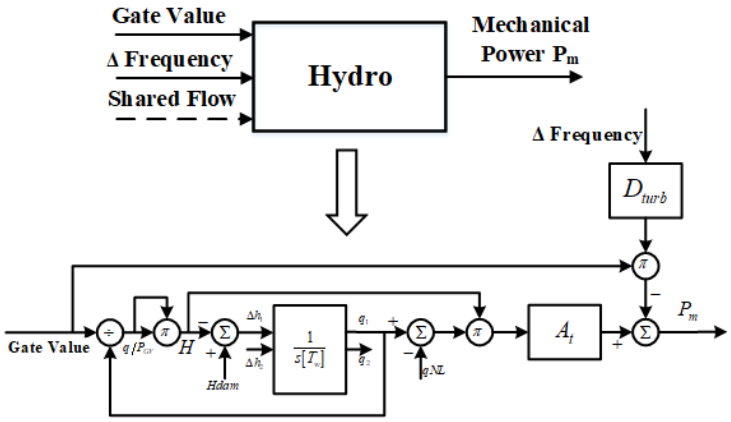

Figure 3.12 Block diagram of hydro system

3.3.6 Hydro Model Linearization

After finishing this nonlinear hydro model for dynamic simulation, it is easy to find that this nonlinear hydro model is hard to write as a transfer function. This makes it difficult to do the system analysis, design the droop controller and test the frequency response of system. Because of this, it is necessary to linearize this hydro model.

According to the linearized mechanical power function (42), a linear model can be derived as:

$$\begin{aligned} \Delta q &= \frac{\partial q}{\partial G}\Delta G + \frac{\partial q}{\partial H}\Delta H \\ \Delta P_m &= \frac{\partial P_m}{\partial H}\Delta H + \frac{\partial P_m}{\partial q}\Delta q - D_{turb} G \Delta f \end{aligned} \tag{42}$$

Combine (42) with water flow function shown below:

$$\Delta q = \frac{\Delta H}{sT_w} \tag{43}$$

Then we can get a relationship between mechanical power and gate position:

$$\Delta P_m = \frac{\left[\frac{\partial q}{\partial G}\frac{\partial P_m}{\partial q} - sT_w\frac{\partial q}{\partial G}\frac{\partial P_m}{\partial H}\right]}{1+sT_w\frac{\partial q}{\partial H}}\cdot\Delta G - D_{turb}G\Delta f \tag{44}$$

Put (29) and (30) into this linear model, the whole hydro system can be modelled as a first order lead-lag function with damping:

$$\Delta P_m = A_t\frac{\alpha_1 - sT_w\alpha_2}{1+\frac{1}{2}sT_w\alpha_3}\cdot\Delta G - D_{turb}G\Delta f \quad \text{where } \alpha_1 = \sqrt{H^3}, \alpha_2 = \left(\Delta q - q_{NL}\right)\sqrt{H}, \alpha_3 = \frac{G}{\sqrt{H}} \tag{45}$$

It is worth mentioning that Δq is the water flow difference for penstock. After ignoring the friction force on the shaft and no-load water flow in the penstocks, the system can be simplified as a lead-lag function:

$$\Delta P_m = A_t\frac{\alpha_1 - sT_w\alpha_2}{1+\frac{1}{2}sT_w\alpha_3}\cdot\Delta G \quad \text{where } \alpha_1 = \sqrt{H^3}, \alpha_2 = \Delta q\sqrt{H}, \alpha_3 = \frac{G}{\sqrt{H}} \tag{46}$$

Further simplifying (46) by setting water head *H* and gate value *G* to 1 p.u., when system is at steady-state, a simplifies hydro model can be derived:

$$\frac{\Delta P_m}{\Delta G} = A_t\frac{1-sT_w}{1+\frac{1}{2}sT_w} \tag{47}$$

These linear hydro models can be used in the simplified T-PSH system analysis. When choosing the simplest hydro model (47), the mechanical power output for the turbine part can be written as:

$$P_{m\_t} = \frac{T_r s+1}{rT_fT_rs^2 + RT_rs + rT_rs + R}\cdot\frac{1}{1+sT_g}\cdot A_t\frac{1-sT_w}{1+0.5sT_w}\cdot\left(K_{d\_t}\left|P_{gen}\right| - \Delta f\right) \tag{48}$$

In the same way, the mechanical power output for pump part can be written as:

$$P_{m\_p} = \frac{1}{1+sT_g}\cdot A_t\frac{1-sT_w}{1+0.5sT_w}\cdot\left(-K_{d\_p}\left|P_{gen}\right| - \Delta f\right) \tag{49}$$

By using (31), the total mechanical power can be got by adding (48) and (49) together.

3.4 Operation Mode Introduction

In the generating mode, T-PSH is operated as a conventional hydropower plant with only the turbine part participating in the operation. The power reference for the governor is calculated by the setting power order in (22), where K_{d_t} is equal to 1 and K_{d_p} is equal to 0. The droop controller in the governor can respond to the system variance dynamically by changing the gate value. The water flow in the penstock flows from the higher reservoir to the lower reservoir which is shown in Figure 3.13. The potential energy stored in the water is transferred into the kinetic energy of the shaft. Finally, the synchronous machine converts kinetic energy into electrical energy. Because of the droop controller, T-PSH in the generating model can achieve governor speed control, which means that it can provide frequency regulation service to a system to help stabilize the system under a contingency.

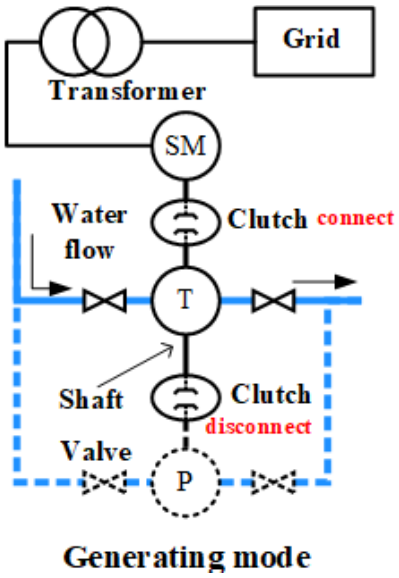

Figure 3.13 Water flow of T-PSH in generating mode

In the pumping mode, T-PSH is operated as a fixed-speed pump which is same as C-PSH—i.e., only the pump is in operation. The desired gate value of the pump is calculated by the power order in (22), where K_{d_t} is equal to 0 and K_{d_p} is equal to 1. The water flows from the lower reservoir to the higher reservoir as shown in Figure 3.14. The electrical energy is absorbed by the T-PSH and transferred to the potential energy which is stored in the higher reservoir. However, different from the turbine part, no any droop controller exists in the pump part. T-PSH in this pumping mode cannot participate in governor speed control because its fixed power absorption during this operation. This means that in pumping mode T-PSH cannot respond to a system disturbance to provide any frequency regulation service.

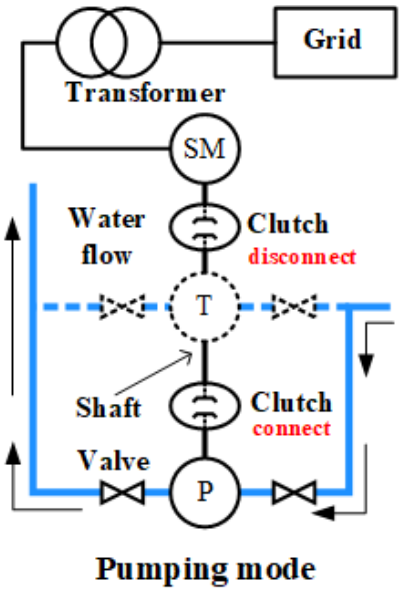

Figure 3.14 Water flow of T-PSH in pumping mode

In HSC mode, both the turbine part and the pump part are in operation. The power order for each part will be calculated by K_{d_t} and K_{d_p}, shown in (22), where K_{d_t} and K_{d_p} is

satisfied according to the relationship shown in (21). The net torque is a combination of variable turbine torque and fixed pump torque resulting in a negative variable torque (absolute value of pump torque is larger than turbine torque). As a result, T-PSH behaves as a load to absorb power from the power grid. The water flow in this mode is from the lower reservoir to the higher reservoir as shown in Figure 3.15. This variable negative mechanical power output makes T-PSH in HSC mode can respond to a system disturbance by adjustment provided from turbine part. In this mode, T-PSH has the ability to provide ancillary service in the pumping water whereas the C-PSH cannot in pumping mode.

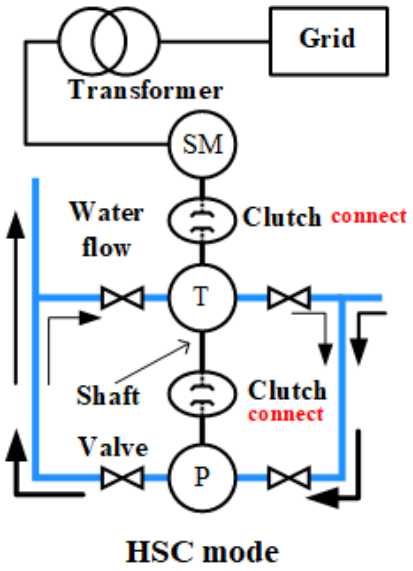

Figure 3.15 Water flow of T-PSH in HSC mode

3.5 Introduction of Transition Time

Because of the unique ternary design, the T-PSH system is an irreversible PSH technology. The pump and the turbine have the same rotation direction. As a result, T-PSH system does not require to reversal of the rotation direction of the shaft when changing the operation mode. The

impacts from hydraulic transients are thus significantly reduced, and the T-PSH can switch its operation mode quickly. It is worth mentioning that the reversible PSH technologies like C-PSH and AS-PSH must change rotation direction when changing from generating to pumping and vice versa. However, today's PSH system always has a huge and heavy mechanical system results in a very large inertia for the PSH system. If the PSH unit changes its operation mode, much time is required for the shaft to be slowed to a stop before the rotation direction can be reversed. As a result, too much time is wasted waiting for the mechanical system to stop. A comparison of transition times for T-PSH, C-PSH and AS-PSH are shown in Figure 3.16 and Table 3.3. T-PSH technology can switch its three operation modes in less than one minute, whereas the other two reversible PSH technologies always need about six minutes to change from generating mode to pumping mode and about three and half minutes to switch from pumping mode to generating mode. It is obvious that T-PSH has advantages in shorter transition time.

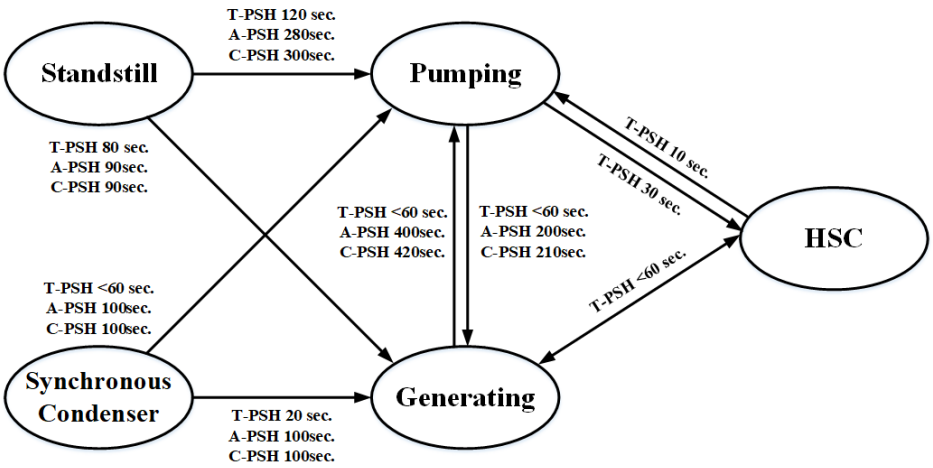

Figure 3.16 Transition time of three types of PSH technology

Table 3.3 Comparison of transition times

Type	A	B	C	D	E	F
C-PSH	210s	420s	90s	300s	100s	100s
AS-PSH	200s	400s	90s	280s	100s	100s
T-PSH	<60s	<60s	80s	120s	20s	<60s

where A is pumping to generating, B is generating to pumping, C is standstill to generating, D is standstill to pumping, E is synchronous condenser to generating, and F is synchronous condenser to pumping

When deploying T-PSH in the grid, itcan be switched quickly form generating mode to pumping mode in less than 60 seconds to absorb and store the excess power generated from renewable energy. In contrast, the AS-PSH or C-PSH requires about seven minutes to finish switching its operation mode. However, this often misses the best period of storage because of the variation and discontinuity of renewable energy generation. Moreover, T-PSH can not only play an important role in storage, but also shows its outstanding performance when providing ancillary service. If a contingency arises, the T-PSH working in pumping mode can respond in one minute by switching to the generating mode or HSC mode according to the severity of the contingency. This quick switching ability makes T-PSH much more flexible and reliable as an ES unit. In addition, T-PSH can provides a variety of solution according to the types of contingency because of its large capacity and system inertia. In contrast, BESS can respond quicker because of its power electronic interface. However, it has many limitations when facing a serious contingency owing to its limited capacity and instantaneous current withstand capability of power electronic device. In a word, T-PSH can significantly reduce the transition time in operation switching which increases flexibility in providing frequency regulation service and balancing energy use.

CHAPTER 4 T-PSH SYSTEM IMPLEMENTATION

After finishing the T-PSH modeling, system implementation on commercial software is important work, because there is no T-PSH model exists in a simulation platform. In this chapter, the T-PSH model implementation in the GE Positive Sequence Load Flow (PSLF) will be introduced. T-PSH system will be built both in power flow analysis and dynamic simulation. Platform and model operation mechanism will also be introduced. A detailed model implementation procedure by using the user-defined model in PSLF is presented. Some pseudocode fragments will be used to show the structure of the model.

4.1 PSLF introduction

PSLF is a package of programs developed by GE for studying power system transmission networks and equipment performance in both steady-state and dynamic environments [49]. PSLF is a platform which can handle large scale simulation with a large number of data to show the system performance effectively and accurately. The power flow analysis can be performed on systems with up to 80,000 buses. This capability makes analysis and simulation of a realistic wide-area system possible. The whole platform can be divided into several parts shown below [49]:

- Menu and Command Selector
- Main Load Flow Program and Working Case Maintenance Commands (PSLF)
- Graphics Subsystem (OLGR)
- Short-Circuit Subsystem (SCSC)
- Dynamics Subsystem (PSDS)

- Dynamic Results Viewer (PLOT)
- Control Language Processor (EPCL)
- Linearized Network Analysis Subsystem (LINA)
- Economic Dispatch Subsystem (ECON)

In the PSLF simulation, the first step is the construction of a model of the tested electric power system which is called the working case [49]. Most of the test and simulation process programs work based on this system model as shown in Figure 4.1. In PSLF, the model of system is described by many data tables. For example, buses are represented by their serial numbers, names and base voltages. Transmission lines are defined by starting bus number and ending bus number, as well as the line impedance. Other working devices like loads, generators, transformers, etc. are assigned on the located bus with various specific parameters.

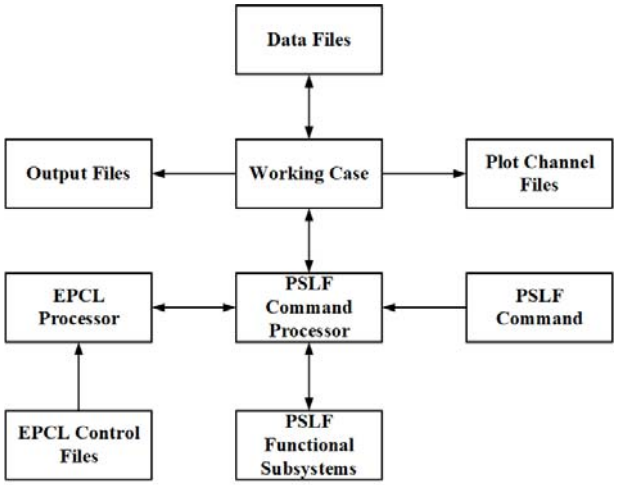

Figure 4.1 Basic Structure of PSLF

The working case can be seen, edited and controlled through these data tables. Once, the data tables have been established, PSLF has all information about the tested system. The power flow

analysis can be finished based on the data tables. In each step of the power flow solution, the contents of the data tables will be overwritten. The power flow analysis is the key and basic analysis embedded in the PSLF platform. Other analyses like the dynamic simulation and economic dispatch are executed based on the results of the power flow analysis.

4.1.1 Dynamic Simulation Introduction

For the study of T-PSH system, the dynamics subsystem (PSDS) in the PSLF platform is used as the main tool to test. Dynamic simulation is a combination of dynamic model simulation and electrical network simulation. In this dynamic simulation, the tested power system is described by a set of algebraic equations, and the components in the power system are modelled by differential equation [49]. up to 50,000 dynamic models can be set up in one dynamic simulation case. These models are invoked in the dynamic model library of dynamics subsystem.

When doing the dynamic simulation, first, the dynamics subsystem reads the declared models used in this simulation by using an 'RDYD' command to read the dynamic simulation data file. This command tells the dynamics subsystem which model is enabled in the system, where it is connected and what are the specific parameters of the model. Second, the dynamics subsystem traverses the entire dynamic model library to find out the invoked models in the current simulation case. If the model in the dynamic model library is found, a set of code modules will be enabled to be included in the simulation case. All the activated models are attached on the appropriate buses virtually and set up all the parameters. After that, the dynamics subsystem finishes all the preparation to establish the dynamic model system. Third, the initialization for each dynamic

model will be executed in the dynamics subsystem by using the 'INIT' command. Each dynamic model is described by differential equation, and the initial values are needed for each model. At the same time, the dynamics subsystem reads the power flow data stored in the data tables to know the current system status and help finish the initialization. The last step in the initialization is that all the output results are assigned to different output channels. These channels are written into the output channel file to show the simulation results. After initialization, the dynamic simulation will be executed step by step with a specific sampling interval. During each step in the simulation, the network parameters like the voltage will be calculated according to the network equation and several boundary conditions. Especially, the first-time solution is solved based on the initialization. Differential equations in each dynamic model will be solved in order by using numerical methods with network parameters in the previous step. Some variables in the results, which are declared in the output table, are sent to the output channel in each simulation step. As a result, the simulation results are discrete and will be connected into lines in the output image. The detailed dynamic simulation process is shown in Figure 4.2.

Algorithm 1: Dynamic simulation structure

```
   Data: Dynamic model table and simulation parameters
   Result: Dynamic simulation results
 1 Read dynamic model assignments;
 2 Initialization;
 3 while do dynamic simulation do
 4 |   Calculate generator network boundary currents;
 5 |   Solve system network boundary voltages and
   |    currents;
 6 |   Calculate secondary variables in dynamic model;
 7 |   Send output variables to store;
 8 |   Run integration step for next simuation step;
 9 |   if Terminate simualtion then
10 |   |   break;
11 |   end
12 end
```

Figure 4.2 Pseudocode for the Basic Dynamic Simulation Process Steps

4.1.2 User-defined Dynamic Model

The user-defined dynamic model is a special type of dynamic model that can be defined by the user. This allows users to customize some models that are not in the dynamic model library. The user-defined model is developed by using the engineering process control language (EPCL), which is a built-in programming language in PSLF and closely couples with the PSLF core.

EPCL is usually used for two purposes: customized function and EPCL application. Customized function is typically used to control PSLF like running multiple simulation cases. The EPCL application is used to implement a user-defined model. Different from the customized function, EPCL user-defined dynamic model must work with the PSLF C code model called 'epcmod'. This C mode model is the bridge between the EPCL dynamic model and the PSLF core. Because of this, the EPCL model must be written in a fixed structure. The user deploys the EPCL language to implement custom functions under the structure of the epcmod model. An inherent simulation order is shown in Figure 4.3. Five blocks of code, except 'NTWK' which is executed in the PSLF core, are needed to be involved in the EPCL user-defined model. Each stage is explained in the follows [49]:

- INIT: dynamic model initialization.
- SORC: dynamic model network boundary source conditions calculation.
- NTWK: network boundary calculation. (execution in PSLF core)
- ALGE: secondary variables calculation.
- RATE: state variable derivative calculation.

- OUTP: output variables setting.

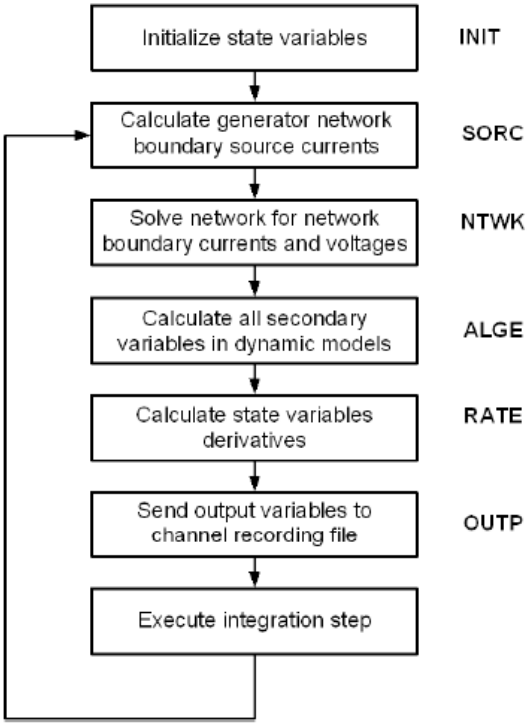

Figure 4.3 Flow chart of a dynamic simulation [49]

For one dynamic simulation case, the initialization part is executed once at the beginning of the simulation. After that, all other 5 sub-steps are executed in a fixed order and repeat until the end of the simulation. If there are more than one EPCL model in a simulation case, all EPCL models will be first initialed together followed by sequential execution. Different from the single EPCL model, the execution of a multi-model case obeys a pre-set order, which is defined as a number from 0 to 49 in a parameter table and is treated as a sequence table for the compiled EPCL model. This number must be unique for each EPCL user-defined model. If an EPCL model is used several times in one simulation case, the same assigned number should be used. During simulation, the PSLF core will call the blocks of code in the EPCL model according to their fixed order shown

in Figure 4.3. These blocks of structure in an EPCL model are implemented by using the function of multiple choices 'switch function' shown in Figure 4.4.

Algorithm 2: EPCL model structure

```
   Input: Network Parameters
   Output: Output Channel
 1 switch @mode do
 2 |   case RATE do
 3 |   |   calculate state variable derivative;
 4 |   |   break;
 5 |   case ALGE do
 6 |   |   calculate secondary variables;
 7 |   |   break;
 8 |   case SORC do
 9 |   |   calculate dynamic model network boundary
   |   |    source conditions;
10 |   |   break;
11 |   case OUTP do
12 |   |   Send output variables to record channels;
13 |   |   break;
14 |   case INIT do
15 |   |   Initial state variables;
16 |   |   break;
17 |   end
18 end
```

Figure 4.4 Pseudocode for structure of EPCL model

4.2 T-PSH System Implementation in PSLF

In order to use the T-PSH system dynamic simulation in the PSLF platform. Several steps are required. First, as previously introduced, a system parameter table for power flow calculation is set up by using PSLF loadflow file (*.epc) or retrieving a previous load flow file (*.sav). Note that, *.sav file is in binary format, which can only be viewed or edited in PSLF platform, whereas *.epc file is in ASCII format and can be opened by other software. Second, the power flow is solved based on the parameter table to get the power flow results in steady state. This result will provide the basis for further analysis. Third, a dynamic model table is set up by using the PSLF dynamics model data file (*.dyd). After that, initialization is a dispensable step to prepare initial values for

each dynamic model. Last, dynamic simulation is executed after some necessary parameters are set like simulation duration and step size. The flow chart shown in Figure 4.5 introduces the whole process to finish a dynamic simulation. To simplify the entire process, remove the manual step. An example of running a dynamic simulation controlled by EPCL code is shown in Figure 4.6.

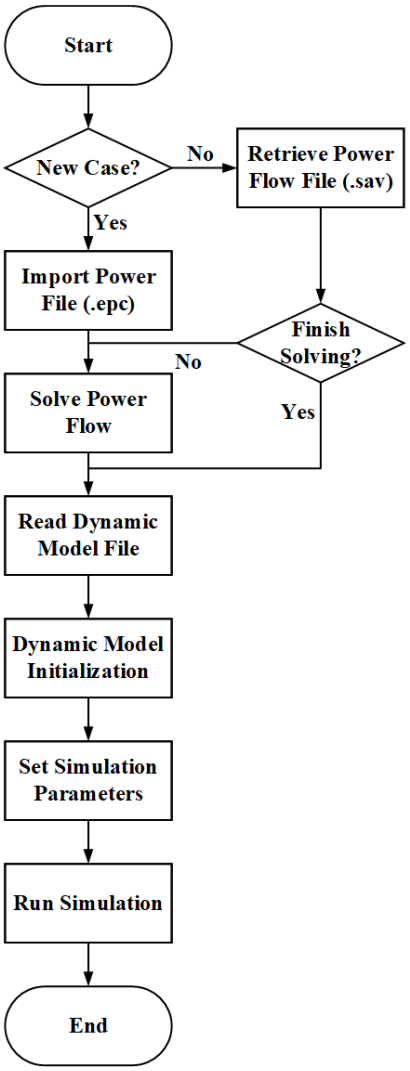

Figure 4.5 Flow chart for dynamic simulation in PSLF

Algorithm 3: EPCL dynamic simulation control

Data: History data table files
Result: Run dynamic simulation

```
1  @ret = getf() ;      // Read loadflow file for power
     flow analysis.
2  @ret = solv() ;          // Solve system power flow.
3  @ret = savf() ;               // Save loadflow file.
4  @ret = psds() ;  // Clear memory space for dynamic
     simulation.
5  @ret = getf() ;
6  @ret = rdyd() ;  // Read loadflow file and dynamic
     model table file.
7  @ret = init() ;   // Initial simulation parameters.
8  Set simulation parameters;
9  @ret = run() ;           // Run dynamic simulation.
10 @ret = dsst() ; // Terminates a dynamic simulation
     run.
```

Figure 4.6 Pseudocode for simulation control by EPCL

4.2.1 Power Flow Data Table Implementation

After figuring out the simulation process, power flow data table establishment is the cornerstone of all work. When creating a T-PSH system in the power flow analysis, a system network is needed that include buses, transmission lines, loads and generators. For the definition of each element in the system, there are different parameters in the PSLF platform. A simple example contains commonly used components as shown in Figure 4.7. The T-PSH unit is described as a synchronous machine in the power flow analysis. As introduced in the example, if implementing a T-PSH system into an existing system network, an electric machine is the only thing to be declared in a specific bus node.

```
bus data  [1] ty  vsched volt angle ar zone vmax vmin date_in date_out pid L own /
st latitude  longitude island sdmon vmax1 vmin1 dvmax
    1 "Bus1" 138.00 : 0 1.06000 1.060000 0.00000 1 1 1.1000 0.9000 400101 391231 /
0 0 1 0 0.00000 0.00000 0 0.00000 0.00000 0.00000

branch data  [1] ck  se  ----------long_id_---------- st resist react charge /
rate1 rate2  rate3  rate4 aloss  lngth
    1 "Bus1" 138.00 2 "Bus2" 138.00  "1"  1 "␣" : 1 0.019380 0.059170 0.052800 /
0.0 0.0 0.0 0.0 0.000 1.0 1 1 0.0000  0.0000  1.0000 400101 391231 0 1 0 0.0 0.0/
 0.0 0.0 1 1.000 0 0.000 0 0.000 0 0.000 0 0.000 0 0.000 0 0.000 0 0.000 0 0

generator data  [1] id  ----------long_id_---------- st --no--  reg_name /
prf  qrf  ar zone  pgen  pmax  pmin  qgen  qmax  qmin  mbase  cmp_r cmp_x /
gen_r gen_x hbus tbus date_in date_out pid N
    1 "Bus1" 138.00 "1" "␣" : 1 1 "Bus1" 138.00  0.0000  1.0000  1 1 232.3917 /
10000.0000 -10000.0000 -16.5494  0.0000  0.0000 615.0000 0.000 0.000 0.000 1.000 /
-1 "␣" 0.00 -1 "␣"  0.00 400101 391231 0 0  0.0000 0.0000 1.0000 1 1.000 0 0.000 /
0 0.000 0 0.000 0 0.000 0 0.000 0 0.000 0 0.000 0 0 0 0 0 0 0 0.0 0 0 1.0000

load data  [1] id  ----------long_id_---------- st mw mvar mw_i mvar_i mw_z /
mvar_z ar zone date_in date_out pid N own M nonc thr_bus flg
    1 "Bus1" 138.00 "1" "␣" : 1 21.6999 12.7000 0.0000 0.0000 0.0000 0.0000 1 1 /
400101 391231 0 0  1 0 0 0 "" 0.00 0
```

Figure 4.7 Example of power flow table

4.2.2 Dynamic Model Table Implementation

Same as the power flow data table, the dynamic model table is the basis of the dynamic simulation. Different from power flow analysis, T-PSH is no longer just described as an electric machine, but all dynamic characteristic of the T-PSH system should be present. As a result, three elements-synchronous machine, exciter and user-defined governor model should be included in the dynamic model table. A fragment of program shown in Figure 4.8 shows a commonly used declaration. Especially, the name ‘epctrb’ shown in the example is the model name for the user-defined EPCL model whose model type is a turbine whereas the common one mentioned earlier is ‘epcmod’. This specially differentiated model has the same dynamic model type as the ‘HYGOV’ hydro turbine and governor model which helps the PSLF platform to better distinguish dynamic model categories.

```
# Synchronous machine:                                    Tpdo    Tppdo   Tppqo   H
gensal 1 "Bus1"  24.00  "1" : #9 mva=1176.0000 12.0000 0.0730 0.3400 5.5800 /
#   D       Ld      Lq      Lpd     Lppd    Ll      S1      S12     Ra      Rcomp   Xcomp
    0.0000 1.0500 0.7000 0.2770 0.2000 0.1300 0.1700 0.3600 0.0000 0.0000 0.0000
# DC exciter:                                   Tr      Ka      Ta      Vrmax   Vrmin
ieeet1 1 "Bus1"  24.00  "1" : #1 0.0500 50.0000 0.0600 1.0000 -0.4000 /
#   Ke      Te      Kf      Tf      spare   E1      SE1     E2      SE2
    0.2060 1.6300 0.0200 1.2000 0.0000 2.5000 0.0200 3.6000 0.0400
# User-defined governor model:
epctrb 1 "Bus1"  24.00  "1" : #7 "hygovt.p" 3.0000 "Tg" 0.500 "Tw11" -1.1700 /
    "Tw12" 0.0000 "Tw22" 1.1700 "Tw21" 0.000 "At" 1.480 "Dturb" 0.3000 /
    "qnl" 0.1 "hdam" 1.0000 "Tr" 6.880 "Tf" 0.0500 "R" 0.040 "r" 0.310 /
    "Gmax" 1.0 "Gmin" 0.0 "Kd" 0 "Velm" 0.05
```

Figure 4.8 Example of dynamic model table

4.3 User-defined EPCL Governor Model Implementation

When the establishment of the parameter tables is completed, programming of the EPCL governor model is the last thing in T-PSH system implementation. Different from dynamic models come from the dynamic model library, this user-defined governor model must be written using the EPCL language with a fixed structure. Especially, the governor dynamic model should be initialized by a preset way in the initialization part. Combining with the declaration in the dynamic model table, this governor model can achieve its function correctly and completely.

4.3.1 EPCL Model Programming

EPCL is a built-in language in PSLF platform and was introduced previously. Commonly used statements such as mathematical operations and logic statements are almost the same as C language or MATLAB programming. In this governor model, the core of EPCL programming is the description of the differential process. Unlike the C language, EPCL has several specific state variables to describe a state. These three state variables are state variable, state variable derivative and integrator storage variable which can be used to describe different transfer functions. Here are

examples, shown in Figure 4.9 and Figure 4.10, to introduce programming of a first-order lag function and the integration function, which are the most commonly used transfer functions in dynamic modelling.

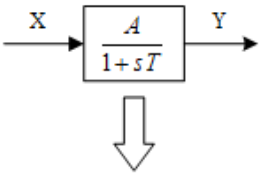


```
@mode = dypar[0].mode
@mx = dypar[0].cmi
switch(@mode)
    case RATE
        epcmod[@mx].ds0 = (epcmod[@mx].A * X - epcmod[@mx].s0)
                          / epcmod[@mx].T
        break
    case ALGE
        epcmod[@mx].v0 = epcmod[@mx].s0
        break
    case INIT
        epcmod[@mx].s0 = Y
        X = Y / epcmod[@mx].A
        break
    endcase
end
```

Figure 4.9 EPCL example of first order lag function

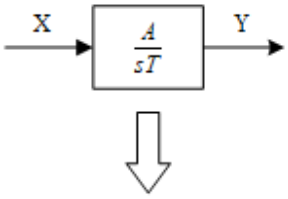


```
@mode = dypar[0].mode
@mx = dypar[0].cmi
switch(@mode)
    case RATE
        epcmod[@mx].ds0 = epcmod[@mx].A * X
        break
    case ALGE
        epcmod[@mx].v0 = epcmod[@mx].s0
        break
    case INIT
        epcmod[@mx].s0 = Y
        X = 0
        break
    endcase
end
```

Figure 4.10 EPCL example of integration function

4.3.2 EPCL Model Initialization

Initialization of the model allows the entire system to have data for the first step of the calculation. A correct initialization can help PSLF get more accurate dynamic simulation results and spend less time to get stable in the dynamic simulation. The initialization for the user-defined model is based on steady-state power flow results. The mechanical power output for the turbine part and the pump part in the steady state is assumed as $p_{m_{0\_t}}$ and $p_{m_{0\_p}}$. These mechanical power outputs, in the steady state, are equal to power demand from the distribution block. Therefore, a relationship can be derived according to (22)

$$\begin{cases} p_{m_{0\_p}} = -k_{d\_p} \times \left| p_{gen} \right| \\ p_{m_{0\_t}} = k_{d\_t} \times \left| p_{gen} \right| \end{cases} \tag{50}$$

where p_{gen} is the power generation results from the power flow calculation and k_{d_p} and k_{d_t} are current distribution coefficients for turbine part and pump part, respectively. According to the modelling work in the last chapter, the hydro model in the turbine part can be rewritten as:

$$p_{m\_t} = A_t H_t (q_t - q_{NL}) - D_{turb} G_t \Delta f \tag{51}$$

In the steady state, the frequency difference is zero. The function can be simplified as:

$$p_{m\_t} = A_t H_t (q_t - q_{NL}) \tag{52}$$

According to (27), in the steady state, the changing rate of water flow is equal to zero. Therefore, the initial value of water head is obtained:

$$h_0 = 1 \tag{53}$$

Inserting (53) into (52), the initial value of water flow in the turbine part is:

$$q_{0\_t} = \frac{p_{m\_t}}{A_t h_0} + q_{NL} \tag{54}$$

After initialing the hydro model in the turbine part, the initial value of the gate can be easily obtained by inserting (53) and (54) into (29)

$$g_{0\_t} = \frac{q_{0\_t}}{\sqrt{h_0}} \tag{55}$$

It is easy to get that the changing rate of gate position is equal to zero. According to this, the initial value of the gate reference is derived as:

$$g_{ref_{0\_t}} = g_{0\_t} = \frac{q_{0\_t}}{\sqrt{h_0}} \tag{56}$$

Because the changing rate of output of the droop controller is equal to zero and the frequency difference input is equal to zero in steady state, the initial value of the power reference is shown as:

$$p_{ref_{0\_t}} = Rg_{0\_t} \tag{57}$$

By using the same method, the initialization of the pump part in the governor model is shown below:

$$q_{0\_p} = \frac{p_{m\_p}}{A_p h_0} + q_{NL} \tag{58}$$

$$g_{0\_p} = \frac{q_{0\_p}}{\sqrt{h_0}} \tag{59}$$

Note that the water flow here has the different direction compared to the turbine part.

CHAPTER 5 T-PSH SYSTEM VALIDATION

The focus of this chapter is to validate the modelling work of the T-PSH system, especially the user-defined governor model, developed in the previous chapter in both MATLAB and PSLF. The validation work in MATLAB is to test the correctness and integrity of the design of the governor model. The transient simulation of the governor is built in the Simulink package based on the MATLAB environment. A single bus system is built in this simulation. The governor is set to work with an existing synchronous machine model in Simulink. Another validation test based on a small power system is built in the PSLF platform. By using the dynamic simulation package in PSLF, the dynamic performance of the T-PSH under different operation modes and different system scenarios is tested. The correctness and reliability of the EPCL user-defined governor model are also validated in this small system. In addition, the validation study for the T-PSH system on a large system is also presented.

5.1 Governor Model Validation

MATLAB is a widely and commonly used scientific numerical computing environment. Simulink, as a built-in package in MATLAB, is a graphical programming environment for dynamic simulation. Before implementing the T-PSH system in PSLF, the function of the governor should be verified on this platform to simplify validation work in PSLF. In the Simulink package, its embedded continuous function blocks and discontinuous function blocks can be used to easily develop such functions as PI controller and saturation function, which are used in T-PSH governor model [62]. Moreover, the existing model of the synchronous machine and its DC excitation

system makes T-PSH implementation easier. In this section, we will use the Simulink package to validate the function of the T-PSH governor in three operation modes.

5.1.1 Validation in All Operation Modes

In order to do the validation simulation of the governor design, a single bus system is established in the Simulink. The test T-PSH system is connected on a bus whose capacity is 28.9 MW. In order to balance the system, a 20 MW load is connected on this bus. In pumping mode case and HSC mode case, a synchronous generator is connected as shown in Figure 5.1. The existing model of a synchronous machine and its exciter are used to simplify the simulation.

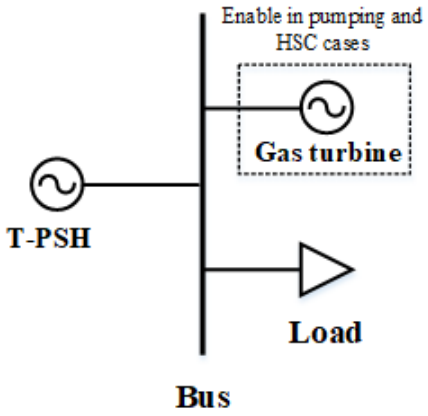

Figure 5.1 Circuit diagram of the single bus system

To validate the T-PSH in the generating mode, the T-PSH unit is operated to supply 20MW (0.692 p.u.) power to the load. By using the initialization method introduced previously, the governor gives the correct mechanical power data as shown in Figure 5.2. After the calculation, the gate value provided by the governor and the calculation value of the gate value are consistent. The governor model provides an accurate function in the generation mode validation simulation.

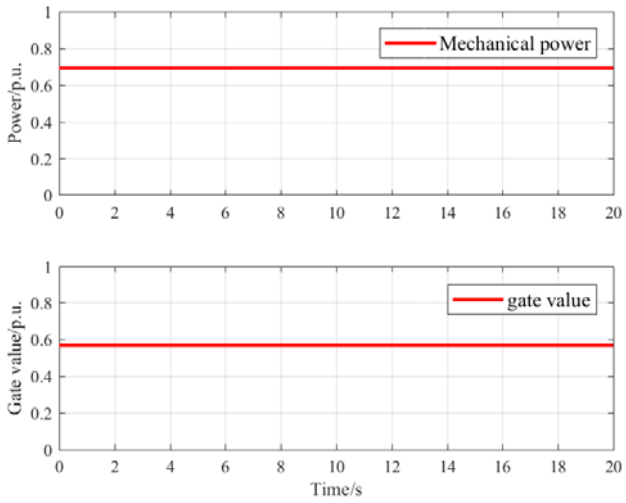

Figure 5.2 Output of governor in generating mode

To validate the pumping mode, the T-PSH unit is set to absorb 20 MW (-0.962 p.u.) power from the gird. In order to balance the system, the synchronous generator is enabled to supply 40 MW power. The results in Figure 5.3 show that the output of governor is correct and stable. Because the absolute value of the power for the T-PSH unit in generating case and pumping case are same, the gate values in these two cases are same. As a result, the design of the gate valve and penstock system in the governor model is proved to be correct.

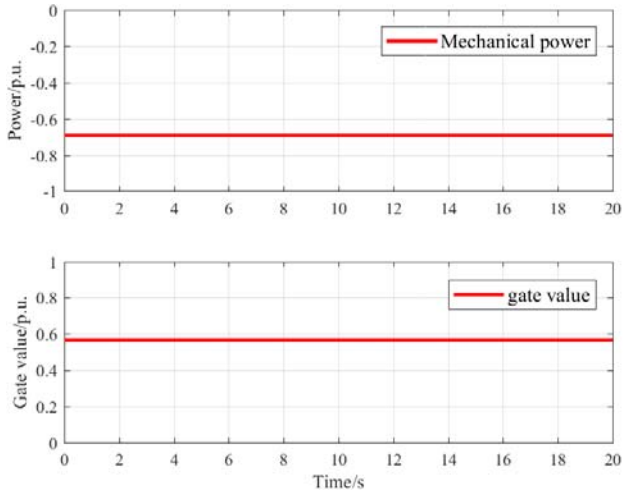

Figure 5.3 Output of governor in pumping mode

The HSC mode validation of the governor model is the most important part as it has a unique feature in the T-PSH technology. The turbine part and pump part are operated together with or without the shared-penstock situation in this simulation. The T-PSH unit total output is set at -15 MW (-0.519 p.u.) which means the total mechanical power output by the governor is 0.519 p.u. The turbine part and pump part in the governor are operated at 5 MW (0.173 p.u.) and -20MW (-0.692 p.u.) separately. The synchronous generators in the system supply the 35 MW power to the T-PSH system and load.

In the non-shared-penstock case, each part in the governor outputs mechanical power accurately and steadily as shown in Figure 5.4. The gate valve and water flow results shown in Figure 5.5 and Figure 5.6 prove the design of governor model can simulate the T-PSH system in the HSC mode.

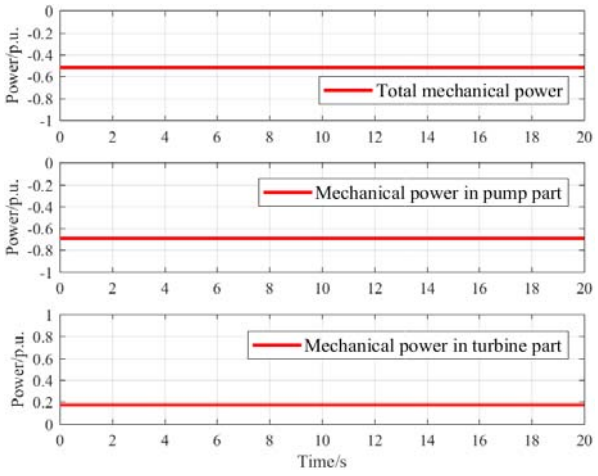

Figure 5.4 Mechanical power in HSC mode without shared-penstock

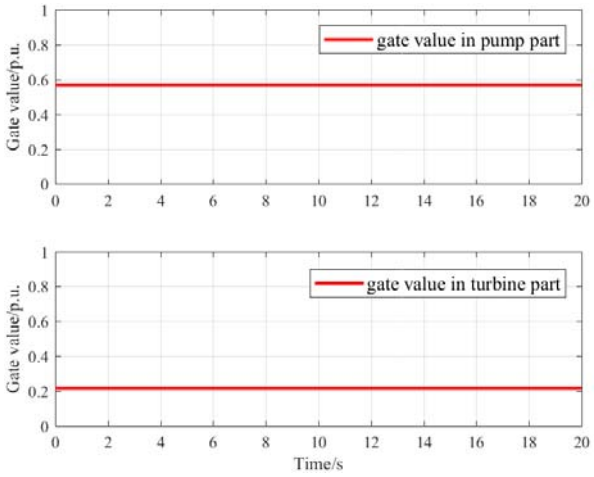

Figure 5.5 Gate value in HSC mode without shared-penstock

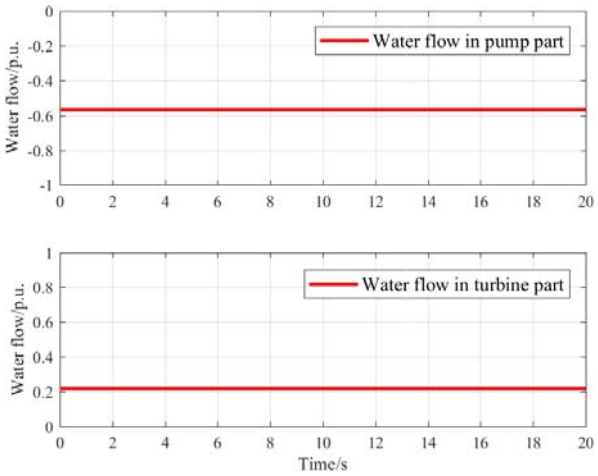

Figure 5.6 Water flow in HSC mode without shared-penstock

After enabling the shared-penstock situation, the governor model becomes more complicated. The governor keeps the same mechanical power output in each part as the previous HSC mode case as shown in Figure 5.7. Compared with the non-shared-penstock case, the gate value shown in Figure 5.8 and the water flow shown in Figure 5.9 have no obvious difference. This proves that the shared-penstock situation has no obvious influence on the system in the case of stable operation of the T-PSH system in the HSC mode. The detailed study of the influence caused by the water

interaction under the shared-penstock situation will be presented later.

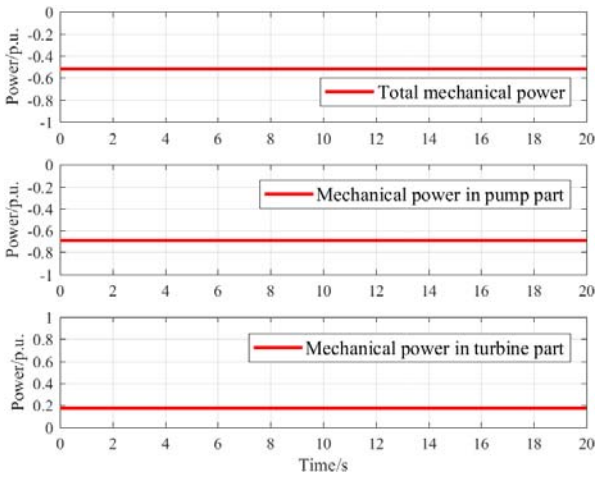

Figure 5.7 Mechanical power in HSC mode with shared-penstock

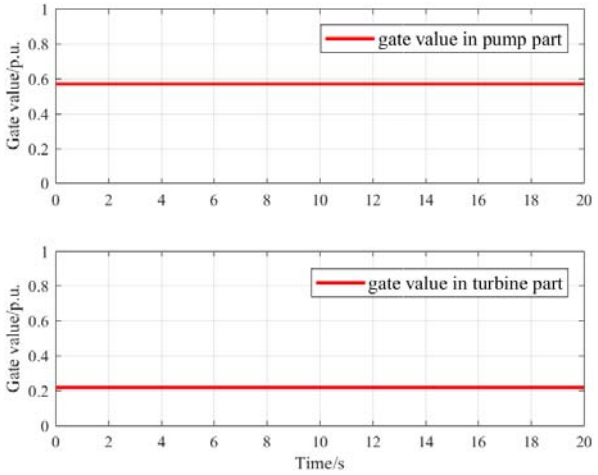

Figure 5.8 Gate value in HSC mode with shared-penstock

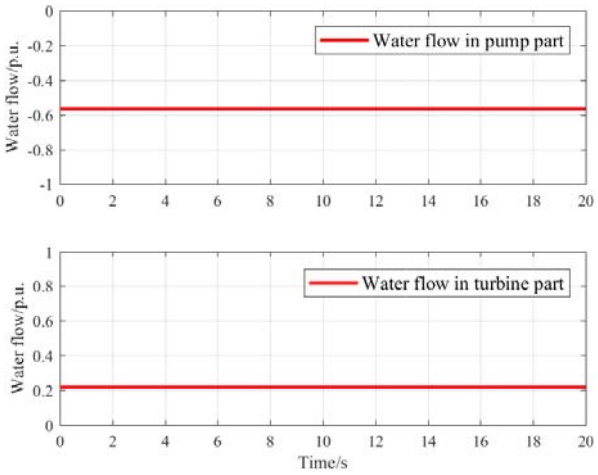

Figure 5.9 Water flow in HSC mode with shared-penstock

Considering all the results, the design of the new T-PSH governor is correct, its basic function is correct, it works well in all operation modes, and it can be implemented in the PSLF platform. Especially, the influence of the shared-penstock in HSC mode should be studied in detail.

5.2 System Performance Validation in a Small System

After completing the validation of the governor model, further functional tests of the T-PSH system, including performance of T-PSH under system disturbance and T-PSH system operation mode switching test, were performed in a small system. The small system has three generators system and is built on the PSLF platform. This validation experiment aims to illustrate the performance of the T-PSH in the power system. The characteristics of the T-PSH will be verified in the small system to provide a basis for large system study.

5.2.1 3-gen Small System Introduction

The small system used for T-PSH dynamic performance validation is the 3-generator and 10-bus system shown in Figure 5.10. In this system, there are three voltage levels, 24 kV, 34.5 kV and

230 kV. Three generating units are arranged in three different buses whose parameters are shown in Figure 5.1. The test T-PSH unit is placed on Bus 19; a gas turbine and a C-PSH unit are placed on Bus 20 and Bus 15, respectively. In the different simulation cases, different capacities of the generator will be chosen to yield a balanced system. In particular, the capacity of the T-PSH that exceeds the actual size of PSH can effectively demonstrate its influence and response in the system. Moreover, in order to better reflect characteristics of T-PSH, the governor and exciter for the gas turbine will be disabled in some simulation cases to make the gas turbine do not respond to the frequency event. At the same time, the swing bus will also be assigned to different buses in the different simulations. There are two loads with different rated capacity connected on Bus 11. The smaller load (No.2) is used to generate a system disturbance in the system. By tripping or connecting this 100 MW load, the over-frequency or under-frequency event will be applied in the system. More details of system dynamic model table are provided in Appendix A to Appendix C.

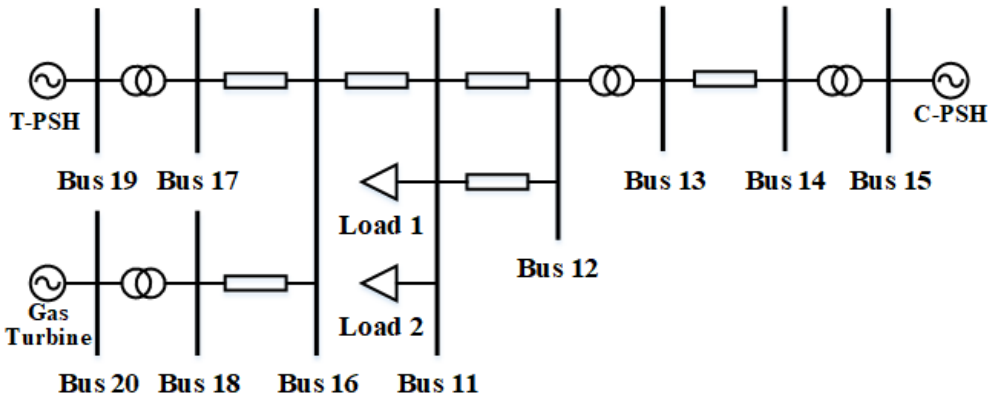

Figure 5.10 Circuit diagram of the 3-gens system

Table 5.1 Details of system components

	Generating Mode Case	Pumping Mode Case	HSC Mode Case
Bus 15 C-PSH	GENSAL IEEET1 HYGOV 28.9MW		
Bus 19 T-PSH	GENSAL IEEET1 EPCTRB		
	1176.0 MW	1276.0 MW	1276.0 MW
Bus 20 Gas Turbine	GENROU	GENROU EXAC1 GAST	GENROU
	200.0 MW	2400.0 MW	2400.0 MW
Bus 11 Load	No.1 1000.0 MW, No.2 100.0 MW		
Measurements	IMETR VMETR FMETR		
Swing Bus	Bus 19	Bus 20	

5.2.2 Performance of T-PSH under Different Frequency Events

In these simulation cases, several frequency events were applied to the system where the test T-PSH unit is operated in three different operation modes: generating mode, pumping mode and HSC mode. The swing bus was set as Bus 19 in the generating mode case, whereas the Bus 20 was the swing bus in other two simulation cases. Meanwhile, in the generating mode case and HSC mode case, the gas turbine was operated without a governor or exciter to make it not respond to the frequency event, which helps to highlight the response of T-PSH. In contrast to this, in the pumping mode case, the gas turbine unit will work with governor and exciter to respond to the frequency event to keep system balance as there is no frequency support from T-PSH in the pumping mode.

In the generating mode case, the test T-PSH, as the main generator in the system, supplies 83.70% of the generating capacity. The test T-PSH unit was the main response unit for the frequency event whereas the gas turbine is operated so as to not respond to the frequency event. Before the simulation, the valve velocity was 1/20 p.u./s, which means the injector needed 20

seconds to open from minimum to the maximum (same in opposite action) when the larger loads (1000MW) on Bus 11 were connected into the system. At the beginning of the simulation, the T-PSH, in the generating mode, supplied 900 MW (0.765 p.u.) power to the system as shown in Figure 5.11. At 10 seconds, load 2 with rated power is 100 MW was connected to apply an under-frequency event, and at 50 seconds, the same load was tripped from the system to apply an over-frequency event. Throughout the simulation, although the pump part in the T-PSH is disabled, the gate in the pump part still opened to its minimum value because there is no-load water flow in the pump part penstock. However, only on-load water flow in the penstock made the mechanical power output from pump part zero. When frequency events occur, the frequency difference is not zero. The governor in the turbine part adjusted the valve reference according to the frequency reference to make the mechanical power meet the system requirement to help the system frequency return to balance. Because of governor adjustment, T-PSH in generating mode provided frequency regulation when a system contingency occurred.

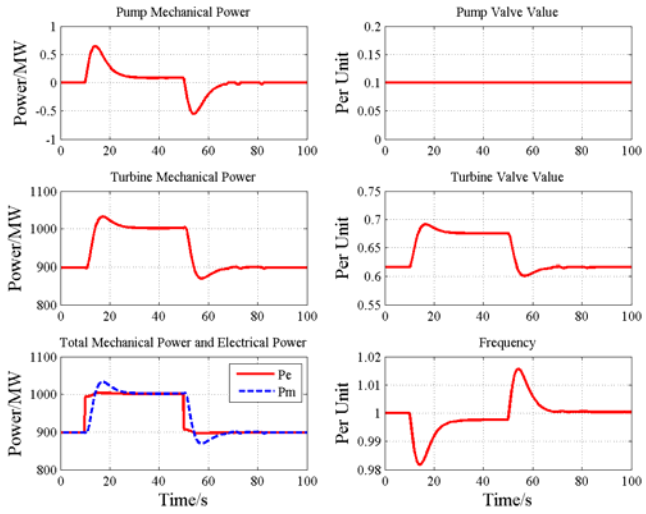

Figure 5.11 Dynamic responses of T-PSH in generating mode

In the pumping mode case, the T-PSH is operated as an inductive load which absorbed 500 MW (-0.392 p.u.) power from the system at the beginning. As in the generating mode case, the valve velocity limit was set as 1/20 p.u./s, and only larger load (1000 MW) was connected to the system. The 100 MW frequency events were applied at 10 seconds and 50 seconds, respectively, by connecting and tripping load 2. After the frequency events, the T-PSH did not respond to the frequency events owing to its fixed pump output as shown in Figure 5.12. There is no governor in the pump part and the turbine part was disabled in this simulation so that the T-PSH operating in pumping mode did not respond to any frequency events in the system. Especially, the small variances in the mechanical power output after the frequency events were caused by the frequency fluctuations. These fluctuations, although they cannot affect the gate value, it slightly impacted the frictional resistance on the shaft, which caused the variances in the mechanical power output in both the turbine part and the pump part. This case illustrates that the T-PSH in the pumping mode cannot respond to frequency events, which means no power regulation ability in the pumping mode.

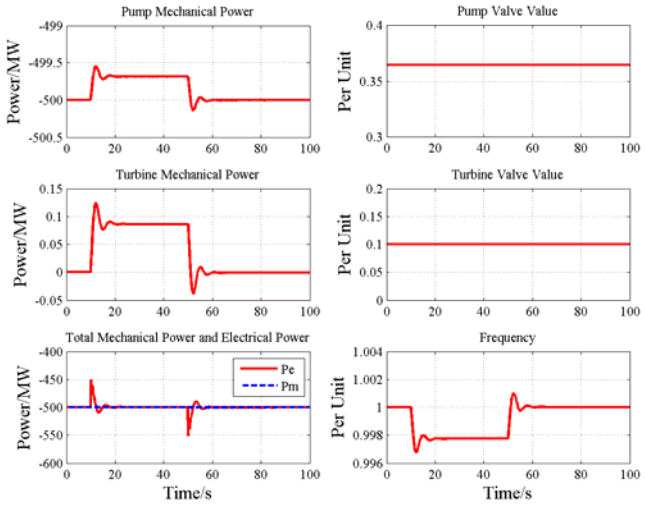

Figure 5.12 Dynamic responses of T-PSH in pumping mode

In the last validation case, HSC mode case, the T-PSH was set in the HSC mode absorbing 500 MW (-0.392 p.u.) power from system as the initial condition. The valve velocity limit was kept same as the previous cases (1/20 p.u./s). And only 1000MW load was connected in the system. At 10 seconds, the 100 MW load 2 was added to the system to apply an under-frequency event, and it was tripped at 70 seconds to apply an over-frequency event. Because the T-PSH in HSC mode is a combination of turbine and pump, after each frequency event, the turbine part adjusted the valve reference by using the governor to let mechanical power output meet the power demands. At the same time, the pump part kept the power output constant, although there was a small variance in the mechanical power output caused by the frequency fluctuation after the system frequency event. This case shown in Figure 5.13 illustrates that the turbine part gives the T-PSH system frequency regulation ability in HSC mode. Compared with the pure pumping mode, T-PSH in the HSC mode can provide power adjustment to help stabilize the system after the frequency event.

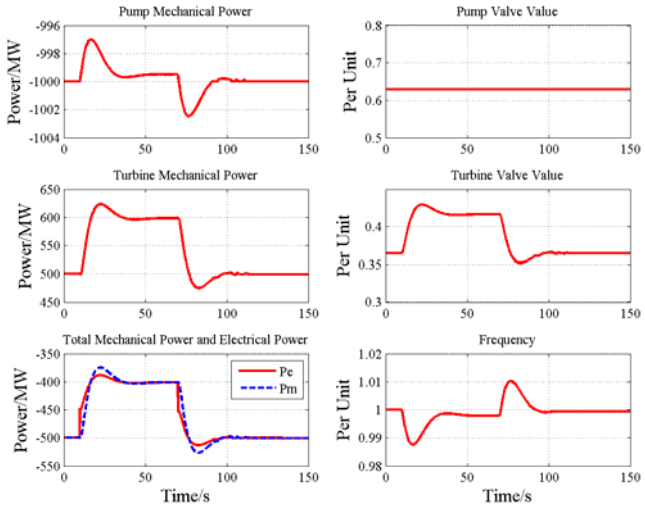

Figure 5.13 Dynamic responses of T-PSH in HSC mode

After these validation cases, the performance of T-PSH in different operation modes is shown. Benefitting from the adjustment provided by turbine part, the T-PSH can provide frequency regulation both in generating and pumping water (HSC mode). Moreover, the reliability of T-PSH model working in a small system has been verified, and the correctness of user-defined EPCL governor model has been determined.

5.2.3 Operation Mode Switching Validation

Another important feature in T-PSH technology is operation mode switching which is validated in this case. Three operation modes are switched clockwise according to the sequence shown in Figure 5.14 (from generating mode, to pumping mode, then to HSC mode, and finally back to generating mode). The different transition times from actual operation, according to actual operation data shown in Figure 5.14, for each switching event was set as 25seconds, 30 seconds and 60 seconds separately which means the valve velocity was 0.25 p.u./s, 1/30 p.u./s, and 1/60 p.u./s, respectively. In this case, Bus 20 was assigned as the swing bus where the gas turbine was located. In order to help the system remain steady during the T-PSH operation mode switching, the governor model and exciter model were enabled in the gas turbine system to regulate the grid frequency. At the beginning, the T-PSH was operated in the generating mode with 500 MW (-0.392 p.u.) power output. The switching event was applied at 10 seconds, 30 seconds and 150 seconds sequentially as shown in Figure 5.15. The results verify the operation mode switching ability of T-PSH. Especially, the design of the user-defined governor model allowed the T-PSH system to do the switching during the simulation case. The different transition times used in this case

demonstrate that the user-defined governor model has the ability to modify the valve velocity limit during the simulation.

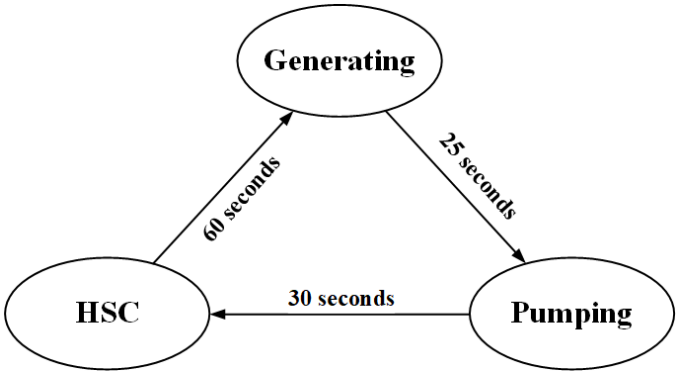

Figure 5.14 Operation mode switching sequence and transition time

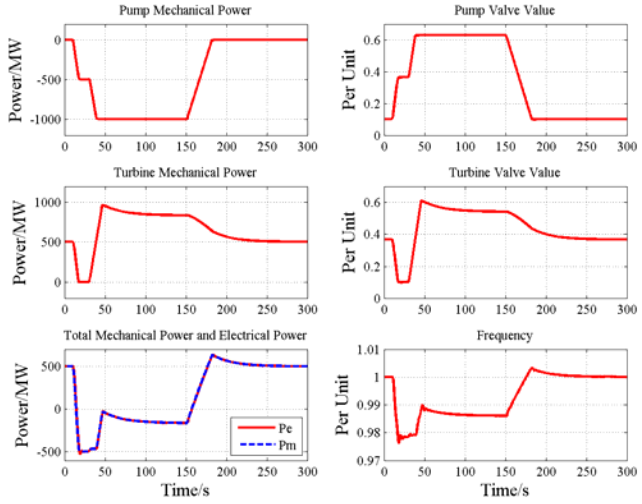

Figure 5.15 Dynamic responses of T-PSH in operation mode switching

5.2.4 Comparison Between T-PSH and C-PSH

After verifying the basic frequency response and operation mode switching, a comparison case between T-PSH and C-PSH was designed to better understand the characteristics of the HSC mode. Because the only difference between T-PSH and C-PSH is the additional HSC mode, this section focuses on the difference between T-PSH in HSC mode and C-PSH in pumping mode. In

two simulations, the test unit was set to T-PSH unit and C-PSH unit with the same parameters, respectively. At the beginning, both test units were operated as absorbing 500 MW (-0.392 p.u.) power from the system. The 2400 MW gas turbine on the swing bus (Bus 20) with the governor model and exciter model helped keep the system stable during the frequency event. At the beginning only Load 1 (1000 MW) was connected. An under-frequency event was applied at 1 second by connecting Load 2 (100 MW) into the system.

As mentioned before, the T-PSH in the HSC mode can respond to the frequency event as shown in Figure 5.16 and Figure 5.17. After the frequency event, the governor in the turbine part adjusted the gate valve reference to increase the mechanical power output as shown in Figure 5.18. In addition, the output of the pump part remains the same. This power regulation increased system frequency by 68.49 mHz at steady state and by 11.16 mHz at the frequency nadir compared with the pumping case. In the T-PSH case, frequency regulation is provided by the gas turbine and T-PSH unit, although the contribution of the T-PSH is limited owing to its limited capacity. On the contrary, the C-PSH in the pumping mode cannot provide any support during the frequency event.

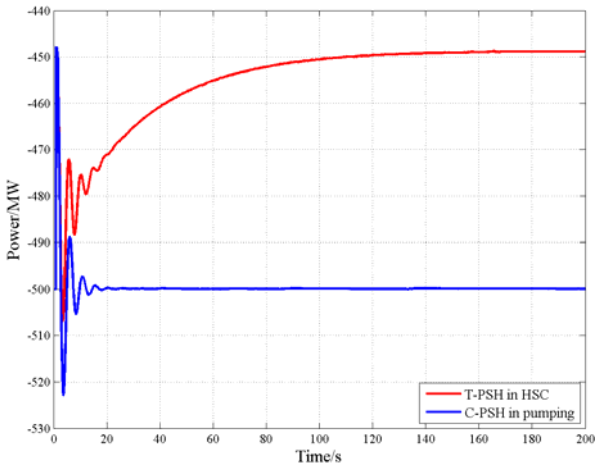

Figure 5.16 Comparison of electrical power between T-PSH and C-PSH

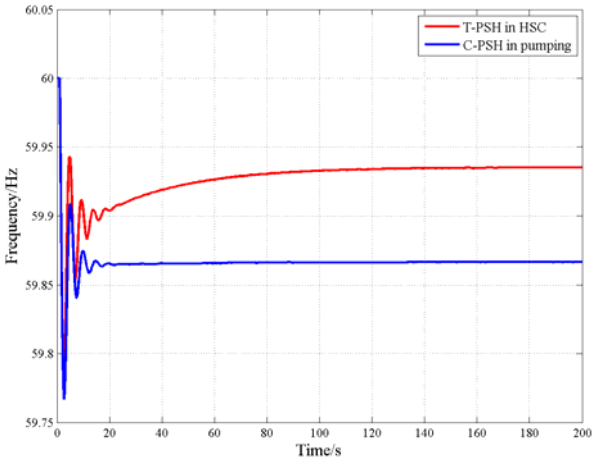

Figure 5.17 Comparison of frequency response between T-PSH and C-PSH

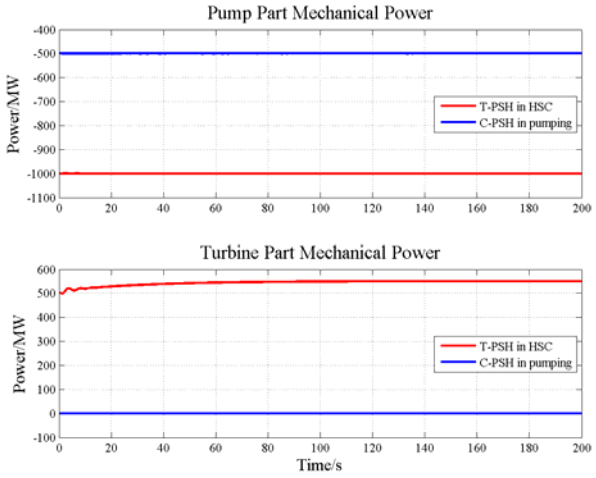

Figure 5.18 Comparison of mechanical power between T-PSH and C-PSH

5.3 System Validation in the Western Interconnection

After finishing the T-PSH validation in the small system, this section is dedicated to studying the performance of T-PSH in the Western Interconnection (WI) system. This system is one of three major interconnected systems in the continental power transmission grid of the United State. It covers 12 states in the United States, 2 provinces in Canada and a small area in Mexico as shown

in Figure 5.19. Therefore, the validation results of T-PSH obtained by testing in this wide area system are representative.

Figure 5.19 Geography scope of Western Interconnection [63]

5.3.1 2022 Light Spring Case Introduction

The 2022 Light Spring (LSP) scenario base case was constructed as a planning case to create a high renewable energy penetration environment in a large and real system [64]. It is implemented in the PSLF platform with about 116.66 GW total online generation and about 367.29 GW total capacity. It includes more than 19,000 buses and has the system inertia of 2.89 [65]. More than 4,000 generators are modelled by their own dynamic model and parameters based on real data. The penetration of total online renewable is 23.51% with details shown in Figure 5.20. This detailed modelled system is the representative of the actual system chosen for this study. Especially, this high penetration level is very suitable for studying the performance of T-PSH in a such a

system.

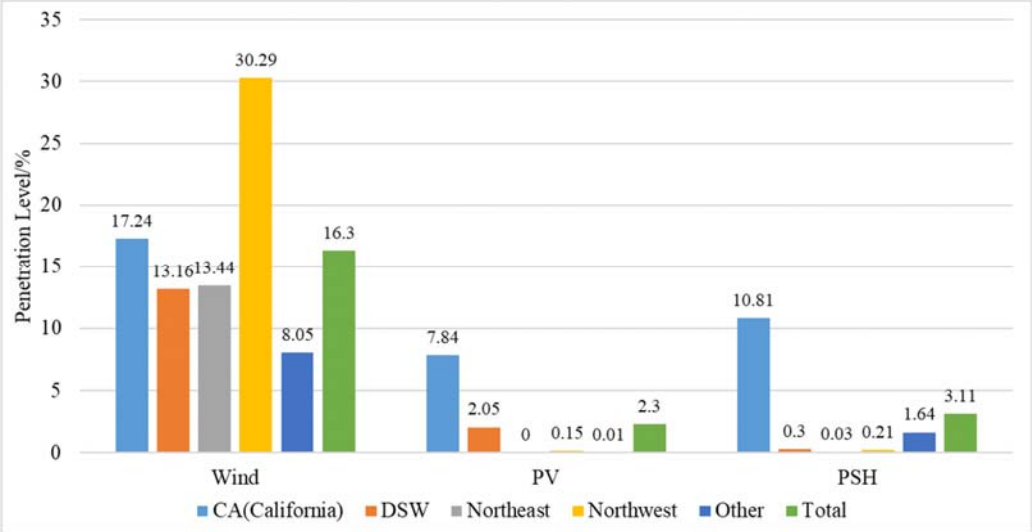

Figure 5.20 Percentage of renewable energy penetration level in each area

5.3.2 Comparison Between T-PSH and C-PSH

As the results showed previous experiments, a significant advantage of the T-PSH is that it can provide the frequency regulation in HSC mode even if it is pumping water. To verify this advantage in a real system, a comparison case between T-PSH and C-PSH was undertaken in the 2022 LSP case. In order to combine this comparison case with later test cases under high penetration level, the T-PSH system was placed in an area with high penetration. The California area, including five small transmission areas was chosen for several cases to test the performance of T-PSH in a large real system, because it has a higher renewable penetration than other areas. Five C-PSH units in California were replaced by T-PSH units [20, 24, 66-68]. These C-PSH units exit and continue to operate every day. The geographic locations and details of the units are given in Figure 5.21 and Table 5.2.

Figure 5.21 Geographic location map of five C-PSH units

Table 5.2 Details of five replaced C-PSH units

Name	Num of Unit	Total Capacity	Online Power
Castaic	6	1500 MW	-894 MW
Helms	3	1287 MW	-930 MW
Hyatt	6	714 MW	-469 MW
San Luis	8	424 MW	-53 MW
Big Creek	1	222 MW	-207 MW
Total	24	4147 MW	-2553 MW

After replacing these C-PSH units by T-PSH units in 2022 LSP case, a comparison case between these two types of PSH was constructed. In order to find out the frequency response difference between T-PSH and C-PSH after the frequency event and prove that the previous results are also correct in this large system, the largest N-2 contingency was chosen [69]. To simulate this contingency, two nuclear generators at Palo Verde, AZ, with a total generation of 2.7 GW (2.96% of total power generation), were tripped at 10 seconds. A significant under-frequency event was created in the system. Meanwhile, the protection devices were disabled to show the influence and

performance of T-PSH in the WI system. In the test case, five T-PSH units is operated in HSC mode with absorbing 2.55 GW power. In the comparison case, five C-PSH units is operated in pumping mode with same absorbing 2.55 GW power. The results shown in Figure 5.22 and Figure 5.23 illustrate the same inertial response in both T-PSH and C-PSH cases after the frequency event. However, after the inertial response, compared with C-PSH results, governor response in the T-PSH case provided a larger frequency improvement. The governor in the T-PSH turbine part helped the five T-PSH units feed more 267 MW back to the system by the end of the simulation. This additional power increased frequency by 13.8 mHz at the frequency nadir and by 21.2 mHz at the end of the simulation in the T-PSH case. Since the total capacity of the five T-PSH units is small in the WI system (about 1.13%), there is a very small frequency improvement from these T-PSH units. Although it was a negligible improvement for the whole system, this indicates the effectiveness of the T-PSH frequency regulation ability in HSC mode (pumping water). If more C-PSH units in the WI system were replaced, the improvement would be better and more obvious. In the C-PSH case, all the governor responses came from other generators in the system. The five test C-PSH units did not contribute to this frequency event. Above all, T-PSH units in the HSC mode can provide significant frequency regulation during the system frequency event for a large contingency, whereas C-PSH in pumping mode cannot.

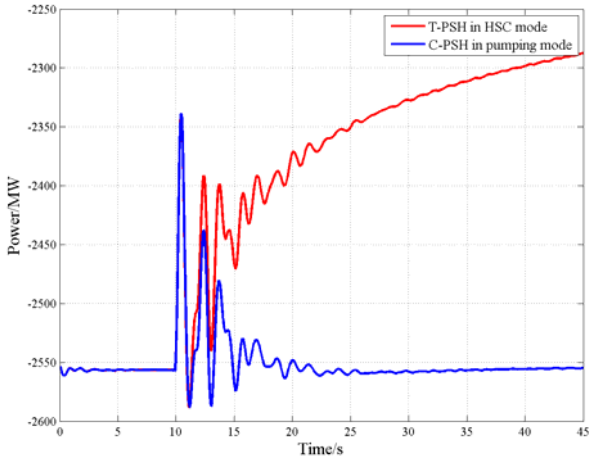

Figure 5.22 Total electrical power of 5 testing PSH units

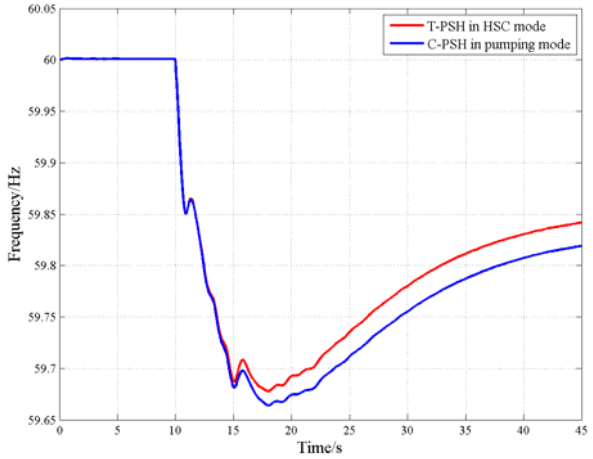

Figure 5.23 Frequency response of 5 testing PSH units

CHAPTER 6 SENSITIVITY STUDY OF GATE VALVE AND SHARED-PENSTOCK

In the previous operation mode switching validation cases, the transition time affected the frequency response performance of T-PSH. In addition, the shared-penstock was not included include in the previous validation simulation. However, the shared-penstock, as one of the most important features in T-PSH technology, should be studied in detail. This chapter is focused on the impact of different transition time and shared-penstock situation on system performance. Several comparison cases for transition time and shared-penstock in different operation of T-PSH are studied.

6.1 Influence of Valve Velocities to T-PSH Response

In the T-PSH modelling, the transition time is quantified as gate valve velocity. In the daily operation, the gate valve in the T-PSH unit requires 30 to 60 seconds to open the valve from minimum to maximum (same time in closing). In addition, the largest transition time of T-PSH unit is about 60 seconds during operation mode switching. The time spent in the valve adjustment delays the water flow, which in turn, leads to a delay of mechanical power output. Because of this, the transition time definitely affects the performance of T-PSH response in daily operation. Several sensitivity study cases for T-PSH in different operation scenarios are studied in the small test system used in the previous chapter to illustrate the impact of the transition time.

6.1.1 Sensitivity Study of Valve Velocities in General Operation

In daily operation, T-PSH unit will adjust its output power according to the operation plan and power system status. Therefore, the adjustment of the valve is essential. According to the

governor model, the speed of the valve adjustment directly affects the rate of output mechanical power. In this sensitivity study, the test T-PSH with 400 MW capacity was operated in generating mode and pumping mode separately. Bus 20 was assigned as the swing bus where the gas turbine unit was operated with governor and exciter models in two cases. There are four types of gate valve velocity in each case. The first one used a deflector to cut the mechanical torque off the shaft immediately, which is always used in system protection. In this operation, the gate valve, actually the injector, is not operated. The other three groups use the injector to adjust water flow at different velocities. One of them has no velocity limit, which means the gate valve can adjust the value as quickly as possible. The other two have velocities of 1/30 p.u./s, and 1/60 p.u./s (30 and 60 seconds from minimum to maximum), respectively.

In the generating case, T-PSH was operated at a maximum of 400 MW initially and then set to zero output at 1 second to simulate the system terminates power generation. At 100 seconds, it was returned to maximum to re-power the system. The response results of different gate valve velocities shown in Figure 6.1 indicate that there is still a delay in the no velocity limit case, which is an inherent characteristic of the injector. In the frequency response and electrical power results shown in Figure 6.2 and Figure 6.3 respectively, significant overshoot and longtime oscillation occurred in the deflector case and the no velocity limit case. In contrast, in the 1/30 p.u./s, and 1/60 p.u./s cases, there was not any obvious overshoot and oscillation after the power output adjustment.

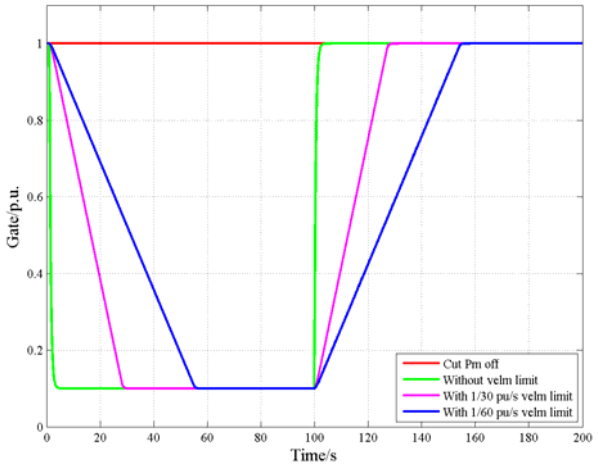

Figure 6.1 Gate valve of T-PSH in general generating adjustment with different valve velocities

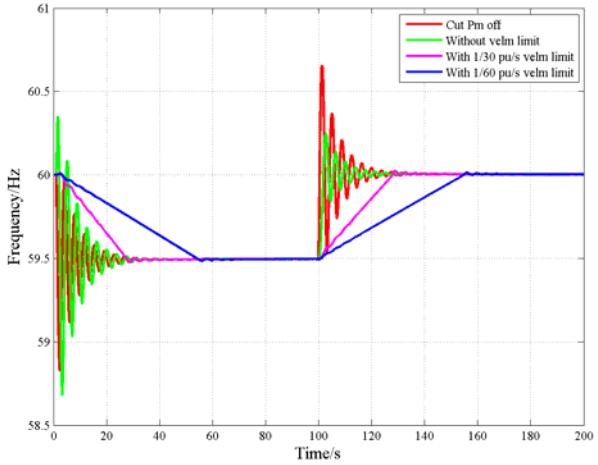

Figure 6.2 Frequency response of T-PSH in general generating adjustment with different valve velocities

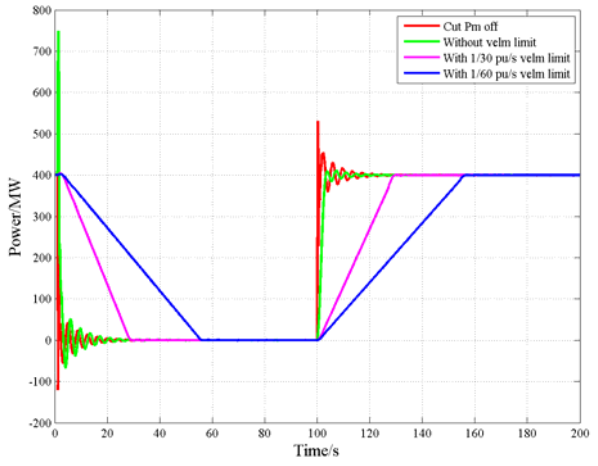

Figure 6.3 Electrical power of T-PSH in general generating adjustment with different valve velocities

In the pumping case, the T-PSH was operated at -400 MW (-0.313 p.u.) at the beginning, which is the maximum pumping output. At 1 second, the unit is adjusted to zero output to simulate no excess energy generation in the system. After that, the T-PSH was returned to maximum pumping output at 100 seconds. The velocity groups and other system parameter were the same as the generating case. Similar to the previous results were obtained and as shown in Figure 6.4, Figure 6.5 and Figure 6.6. Again a near zero transition time caused significant influence in the system after output adjustment. Conversely, a larger transition time can effectively minimize the effect of the adjustment.

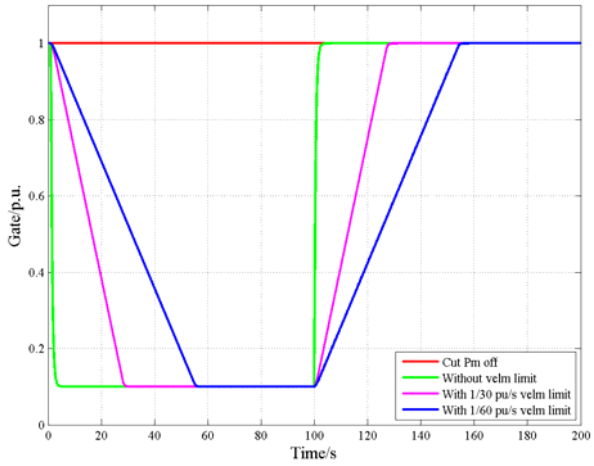

Figure 6.4 Gate valve of T-PSH in general pumping adjustment with different valve velocities

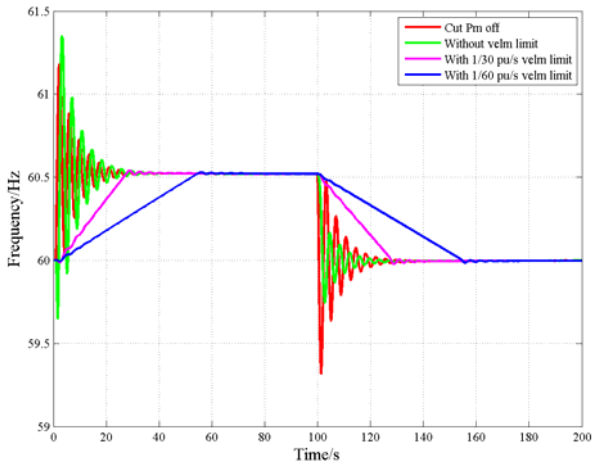

Figure 6.5 Frequency response of T-PSH in general pumping adjustment with different valve velocities

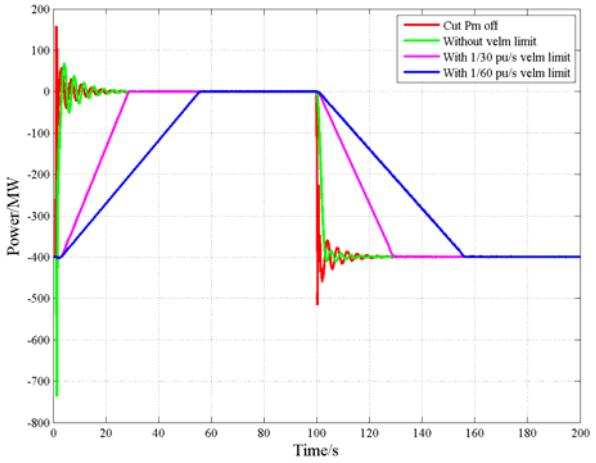

Figure 6.6 Electrical power of T-PSH in general pumping adjustment with different valve velocities

Based on these results, in the daily output adjustment, a suitable transition time should be utilized for T-PSH unit to minimize the impact on the system. It is obviously found that smaller transition time of T-PSH unit is not good for power system. The system inertia always prevents a quick adjustment, which will cause a significant bad effect in the system. It is worth mentioning that the protective cut-off action does cause a significant influence on the system, even though it

always is used to protect the T-PSH unit.

6.1.2 Sensitivity Study of Valve Velocities in Frequency Response

After clarifying the influence of valve velocity in the daily adjustment, the next issue studied concerned is the effect on the frequency response of T-PSH after the frequency event. Recalling that the pump part cannot respond to the frequency event, this sensitivity study is based on T-PSH in the generating mode. In addition, the frequency response of T-PSH after the frequency event is mainly provided by the gate valve adjustment, which is controlled by the governor. Because of this, the deflector case is not included in this study, whereas injector was included in the other three cases. The gas turbine was set without the governor model and the exciter model so that it did not respond to the system frequency event. The swing bus, in this case, was the Bus 19 where the T-PSH is located. Both of these two settings were used to better reflect response of the T-PSH unit.

In the beginning, both loads on the Bus 11 with total of 1100 MW were connected into the system and the T-PSH unit provides the majority of power (about 1 GW) to the system. At 1 second, a 100 MW over-frequency event is applied in the system by tripping Load 2. The response results of the T-PSH, shown in Figure 6.7 and Figure 6.8, with 1/30 p.u./s coincided with the results without a velocity limit. This means the valve speed at 1/30 p.u./s was short enough to respond to this frequency event. Namely, 30 seconds was shorter than the inherent response time of the test T-PSH unit. When compared with results of 1/30 p.u./s and 1/60 p.u./s, there was a significant delay in the 1/60 p.u./s case. This indicates that a valve velocity longer than the T-PSH unit inherent

response time will cause an obvious delay in the response after the frequency event. Similarly, this valve velocity effect is also applicable in the HSC mode, owing to only the turbine part responding to the frequency event in this mode.

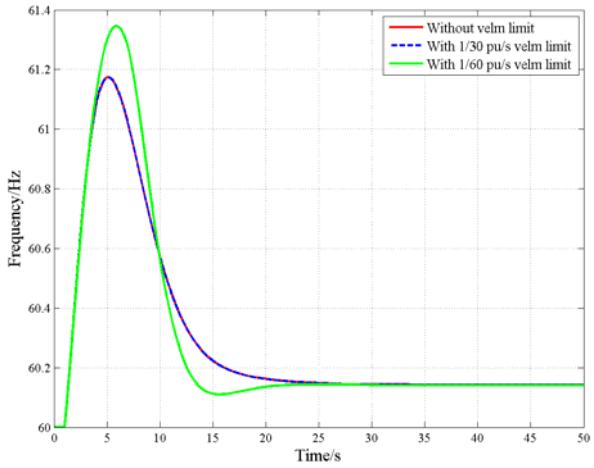

Figure 6.7 Frequency response of T-PSH after frequency event under different valve velocities

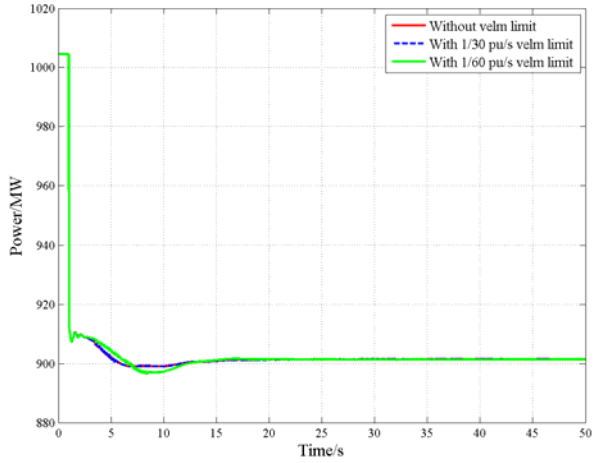

Figure 6.8 Electrical power of T-PSH after frequency event under different valve velocities

6.1.3 Sensitivity Study of Valve Velocities in Mode Switching

As a PSH unit, another common scenario is operation mode switching. As previously introduced, switching between different modes yields different transition time. In this sensitivity study, a comparison case was set up to show the influence of valve velocity on operation mode

switching. In order to make the system stable in this case, the swing bus was changed to gas turbine's bus (Bus 20), and the gas generator's governor model and exciter model were enabled. The test groups were same as groups in the general operation study. Among them, the deflector case (cut Pm off) was simulated as an extreme protective operation mode switching. Usually, this operation mode should use the injector and clutch to switch. The simulation began with the T-PSH operating in generating mode with an output of 500 MW. At 1 second, the operation mode switching was switched from generating to pumping. After the operation mode switching, T-PSH absorbed 500 MW (-0.425 p.u.) from the system. In the results shown in Figure 6.9 and Figure 6.10, there are some significant delays in 1/30 p.u./s and 1/60 p.u./s cases. Although a great delay existed in these two cases, especially in the 1/60 p.u./s case, the oscillation was much smaller compared with the no velocity limit and the deflector cases. When looking at the deflector case and the no velocity limit case, they both responded quickly but caused great oscillation in the system. There was a small delay in the no velocity limit case compared with the deflector case due to the inherent delay in the gate valve. Therefore, the selection of valve velocity should consider both the response speed and the impact on the system.

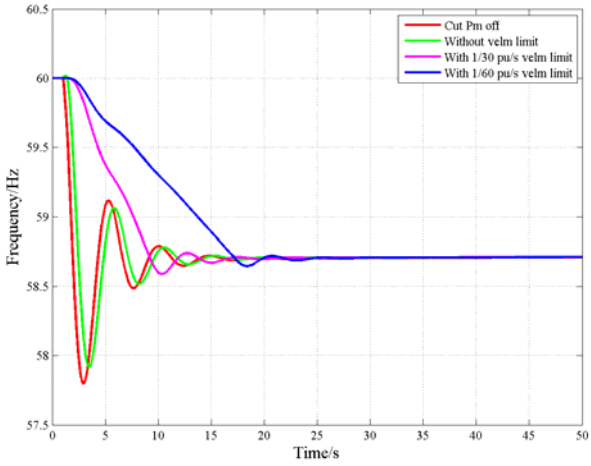

Figure 6.9 Frequency response of T-PSH in operation mode switching with different valve velocities

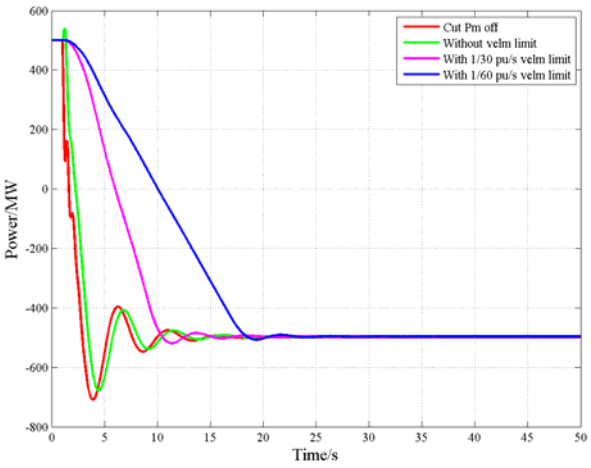

Figure 6.10 Electrical power of T-PSH in operation mode switching with different valve velocities

Above all, an appropriate gate valve velocity can make the T-PSH respond quicker in general operation and frequency response and reduce the impact on the system in the operation mode switching. In the actual project, the valve velocity should be selected smaller than the reciprocal of the T-PSH response time in mode switching and larger than the reciprocal of inherent response time in the general operation and in the system frequency event.

6.2 Influence of Shared-penstock to T-PSH Response

In actual construction, ideal parallel penstocks between the higher reservoir and lower reservoir do not exist because of its high excavation cost. There is always only one main penstock to connect T-PSH unit chambers and reservoirs. When this main penstock is excavated near T-PSH chambers, it is split into two sub-penstocks to connect the turbine part and the pump part. The water flow of these two parts in the sub-penstocks have different directions in the HSC mode. Because of this, the ideal parallel penstock cannot be simply used in the T-PSH simulation, especially in HSC mode. This requires water interaction at the junction of these penstocks to be studied. Two sensitivity study cases in different operation scenario are shown in this section to illustrate the influence of the shared-penstock in T-PSH operation.

6.2.1 Sensitivity Study of Shared-penstock in HSC Mode

As introduced before, there is only a hydraulic short-circuit situation when the T-PSH is operated in HSC mode. In this section, the T-PSH unit in HSC mode with the shared-penstock model will be operated with 500 MW (0.392 p.u.) at the beginning and tested under system frequency event in the 3-gen system. A 100 MW over-frequency event was applied at 1 second by tripping Load 2 on Bus 11. The gas generator was operated with exciter and governor to help keep the system stable after the frequency event. The baseline for this study is a none-shared case whose T_{w_pt} and T_{w_tp} were set equal to zero which is the same as the cases tested in the small system. Three shared-penstock cases with different water time constant were used to simulate different length to cross-sectional area ratios for the penstocks. Here, the water time constants were not at

zero to describe the interaction between sub-penstocks. The results shown in Figure 6.11 and Figure 6.12 indicate that the shared-penstock modeling does not have a significant effect on the frequency response during the system frequency event. Different length to cross-sectional area ratios in the penstocks cannot affect the frequency response performance of T-PSH. The difference in frequency at maximum point among four cases was less than 0.005 Hz. Because of this, the shared-penstock can be ignored in the dynamic simulation. The hydraulic short-circuit situation in HSC mode cannot affect the final response of T-PSH during system frequency event.

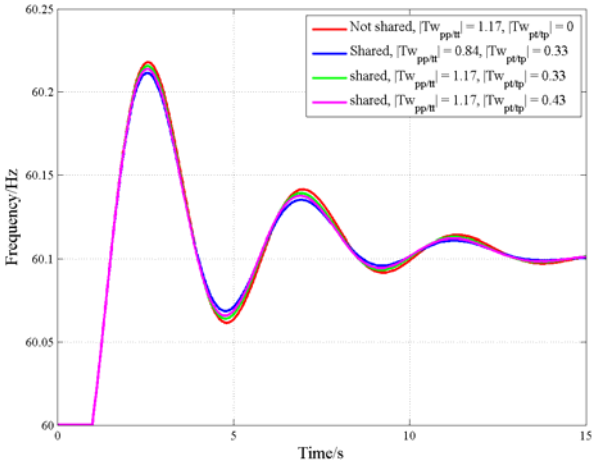

Figure 6.11 Frequency response of T-PSH in HSC mode under different penstock conditions

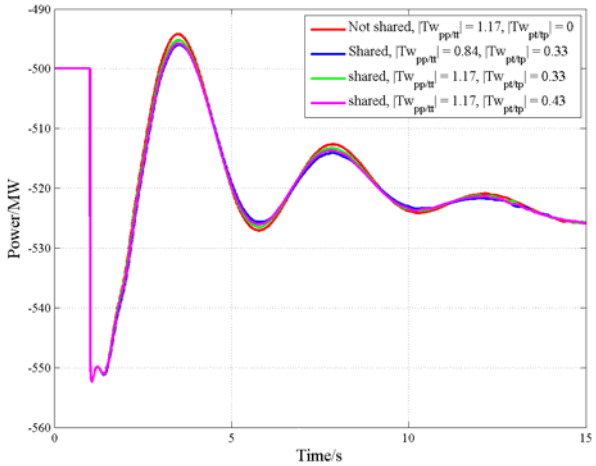

Figure 6.12 Electrical power of T-PSH in HSC mode under different penstock conditions

6.2.2 Sensitivity Study of Shared-penstock in Operation Mode Switching

The shared-penstock influence on operation mode switching is studied in this section by using the same simulation parameters as the last section. The mode switching event was applied at 1 second to switch the T-PSH from HSC mode to pumping mode. The T-PSH unit has the same output -500MW (-0.392 p.u.) before and after switching. The results shown in Figure 6.13 and Figure 6.14 illustrate that all of them have a significant oscillation in the response. The shared-penstock cases all have a significant overshoot in the response compared with non-shared case. The interaction constants, T_{w_pt} and T_{w_tp} ,produced a larger overshoot into the system compared with the non-shared case (baseline). The larger main water constants, T_{w_tt} and T_{w_pp}, in the two shared-penstock cases yielded more significant oscillation in the response. Here, the larger main water constants mean the larger length to cross-sectional area ratio in penstock parameters which indicates the penstock has the longer length or the smaller cross-section area. Meanwhile, another set of coefficients, T_{w_pt} and T_{w_tp} , result in smaller overshoot when they are smaller. The overshoot after the operation mode switching was positively related to the interaction constants, T_{w_pt} and T_{w_tp} , and main water constants T_{w_tt} and T_{w_pp} . Above all, an appropriate set of penstock parameter should be considered when designing the T-PSH unit, because the water interactions in shared-penstock do affect the output performance during the operation mode switching.

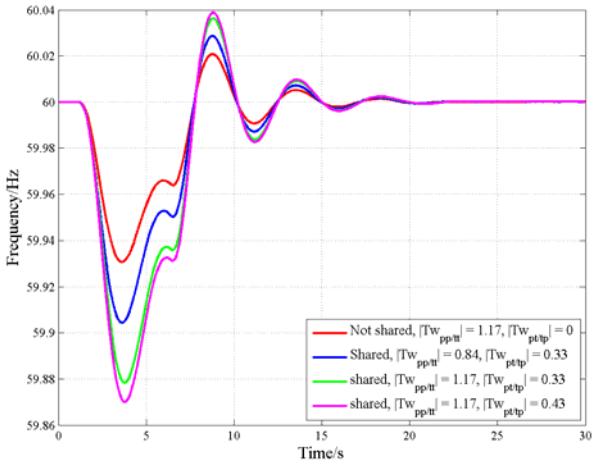

Figure 6.13 Frequency response of T-PSH in the mode switching under different penstock conditions

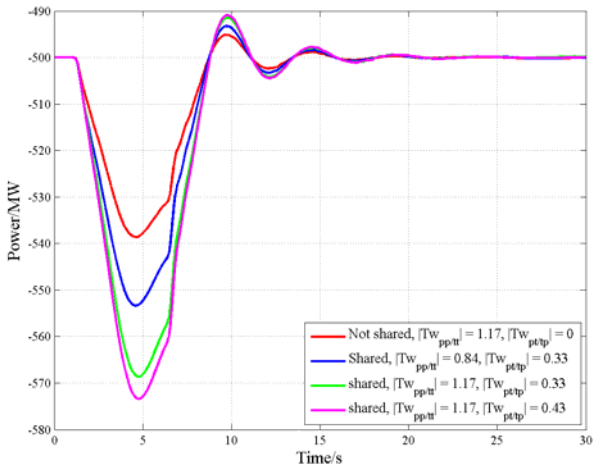

Figure 6.14 Electrical power of T-PSH in the mode switching under different penstock conditions

CHAPTER 7 PERFORMANCE OF T-PSH ON HIGH RENEWABLE PENETRATED WESTERN INTERCONENCTION

Because of the additional HSC mode, T-PSH can provide frequency regulation during pumping water. Also, T-PSH has the ability to quickly change the operation mode switching due to its unique design of dual hydro runners. In order to reveal the advantages when T-PSH units are deployed in the future large-scale use of renewable energy generation, the dynamic benefit from T-PSH under extremely high renewable penetration has been compared with the non-T-PSH case in this chapter. The impact of T-PSH on the different renewable penetrated WI system after a contingency is studied. In addition, operation mode switching application as a fast and effective way to adjust frequency when an extremely high penetrated system meets a serious contingency is discussed.

7.1 High Renewable Penetration Scenario Development

Based on the 2022 LSP WI system used in previous wide area system test, four different renewable penetration cases varying from 20% to 80% were set up. To increase the WI system renewable penetration level, the traditional thermal power plants were replaced by photovoltaic (PV) plants [70]. The first change was to replace the fossil fuel power plants, the second was the hydropower plants, and the last was the nuclear plants. This replacement was based on existing PV resource data and PV technical potential estimation in the National Solar Radiation Database [69, 71]. The detailed penetration parameters are shown in Figure 7.1 and Table 7.1, in which the penetration level of the wind power remained basically the same, and the penetration level of solar

energy increased linearly. The remaining penetration comes from the PSH units when implemented in these cases. In PSLF, only the dynamic models of these thermal power plants were replaced by a GE Type 4 wind power plant model, as suggested in [72, 73]. As synchronous machines were gradually replaced by PV generation units, the system equivalent inertia decreased linearly with increase in renewable penetration level as shown in Figure 7.1. Especially, the system equivalent inertia is calculated below:

$$H_{sys} = \frac{\sum_{i=1}^{n} H_i \times S_i}{S_{sys}} \tag{60}$$

where H_i is inertia of the ith synchronous generator, S_i is the rating capacity of the ith synchronous generator, and S_{sys} is the rating capacity of grid.

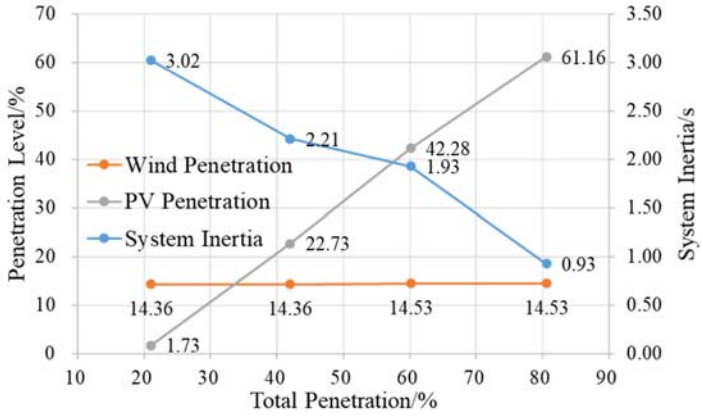

Figure 7.1 System penetration and inertia in each case

Table 7.1 System penetration and inertia of different penetration cases

Case	System Inertia	Wind Penetration	PV Penetration	PSH Penetration	Total Penetration
20% case	3.02	14.36%	1.73%	4.94%	21.03%
40% case	2.21	14.36%	22.73%	4.94%	42.02%
60% case	1.93	14.53%	42.28%	3.35%	60.16%
80% case	0.93	14.53%	61.16%	4.92%	80.61%

7.2 Baseline Contingency Analysis: C-PSH System Under Contingency

Before studying the performance of T-PSH under extremely high renewable penetration level, the system with C-PSH in pumping mode should be analyzed as the baseline. The N-2 contingency used previously was applied at 10 seconds in each penetration case. The C-PSH units were chosen according to Table 5.2. In order to find out the frequency response of C-PSH units under different penetration levels, all protective devices in the WI system were disabled. In order to more accurately show the frequency response of the whole system, the system frequency was calculated by using the center of inertia (COI) frequency which is expressed below:

$$f_{coi} = \frac{\sum_{i=1}^{n} H_i \times f_i}{\sum_{i=1}^{n} H_i} \tag{61}$$

where H_i is inertia of the ith area and f_i is frequency measured in the ith area. Further, the frequency was measured at a randomly selected bus with the highest voltage level in each area.

The frequency results shown in Figure 7.2 illustrate that a system with a higher penetration level of renewable energy has a worse frequency response. Meanwhile, electrical power traces shown in Figure 7.3 show that there is a larger overshoot after the frequency event when the system had a higher penetration level. This overshoot in the electrical power results was caused by the frequency dip. After that overshoot, the results illustrate that the C-PSH units themselves cannot adjust their output by using a governor in the pumping mode. The frequency regulation was provided by the limited number of synchronous generators. The reasons for these worse frequency

responses are reduced system inertia, the slow response of traditional synchronous plants, and limited number of frequency regulation providers. To make matters worse, C-PSH units, as part of synchronous plant in the system, cannot respond to the frequency event when in the pumping mode. Unfortunately, in the 80% case, the frequency nadir was lower than the setting point of the first stage of under-frequency load shedding (UFLS). Thus, protective devices will execute load shedding when frequency falls below 59.5 Hz in the 80% penetration level case. Therefore, a certain degree of power outage will occur in the 80% renewable penetrated WI system case. Although 60% penetration case was spared from protective load shedding, the frequency nadir shown in Figure 7.4 indicates that the nadir is already very close to the setting point of the UFLS. Because of this, the WI system with C-PSH units whose renewable penetration level was higher than 60% will not survive in this N-2 contingency.

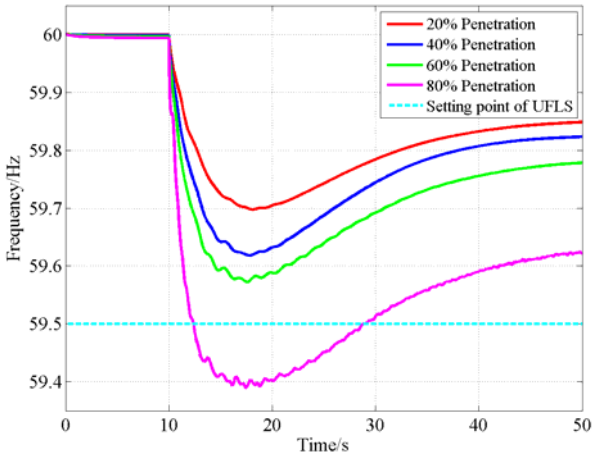

Figure 7.2 COI Frequency responses of C-PSH units under different renewable penetration levels

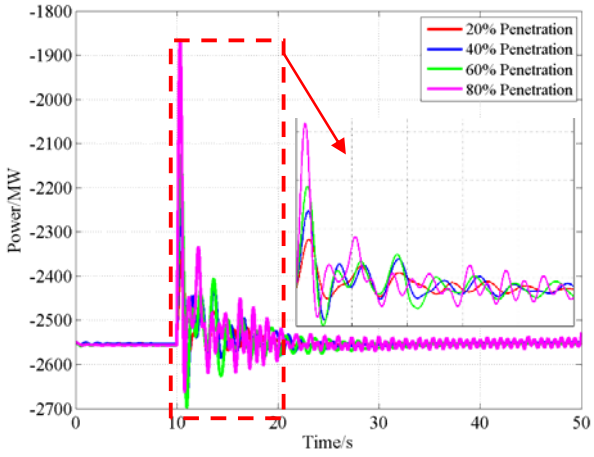

Figure 7.3 Electrical power output of C-PSH units under different renewable penetration levels

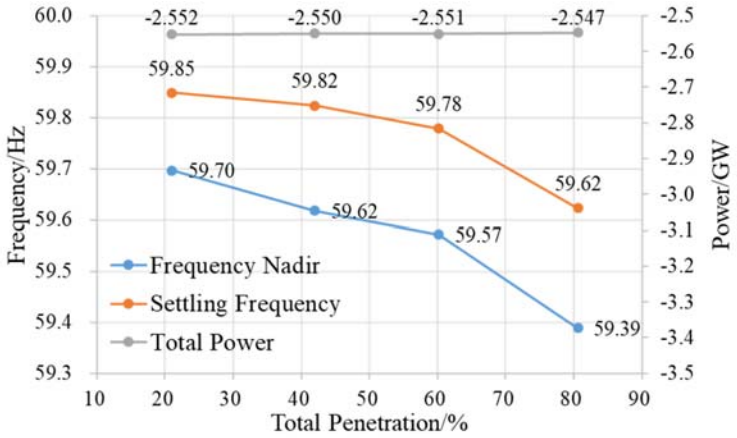

Figure 7.4 Frequency nadir, settling frequency, and total power outputs of the C-PSH in each case

7.3 HSC Mode of T-PSH Under Generation Loss

In order to understand the role and performance of T-PSH in the extremely high renewable penetrated system, several comparison cases between T-PSH in HSC mode and C-PSH in pumping mode were set up in the different penetrated WI system used in the previous section. These T-PSH units have the same parameters as for validation of T-PSH system in 2022 LSP WI system. The same largest N-2 contingency used previously was applied at 10 seconds in each case to create an

under-frequency event.

7.3.1 Study of 20% Renewable Penetration Level

In the 20% renewable penetration case, T-PSH units increased about 14.1 mHz at the frequency nadir as shown in Figure 7.5. Since the total capacity of T-PSH units was limited in the total capacity of synchronous machine in the power grid, the frequency increase was relatively small in this 20% renewable penetration level. In addition, the power regulation from other synchronous generators was still adequate which led to the T-PSH units only feeding an additional 283 MW (0.068 p.u.) back to the grid. In the electrical power results shown in Figure 7.6, output power was smooth after the inertial response, which benefits from the larger system inertia and sufficient capacity of synchronous generators. Although the regulation from T-PSH in HSC mode was limited in this 20% penetration case, it still helped the system to maintain at high frequency resulting in a reduction in the workload of secondary frequency adjustment.

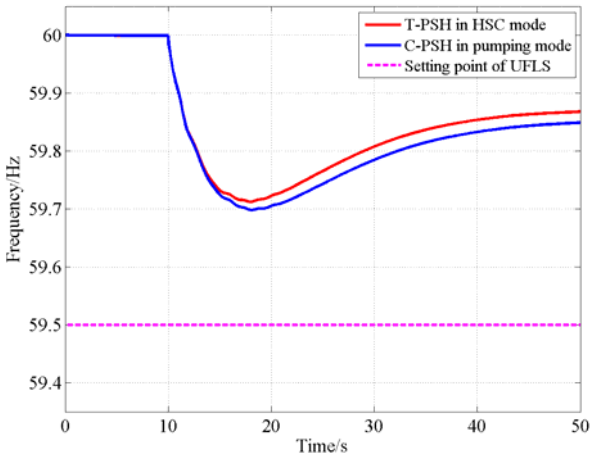

Figure 7.5 COI frequency response of T-PSH units under 20% penetration level

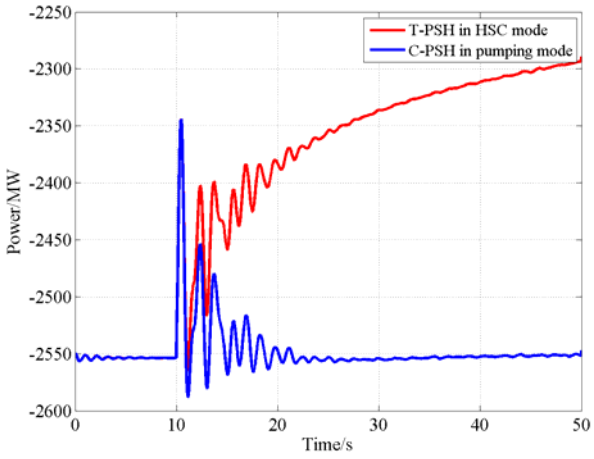

Figure 7.6 Electrical power output of T-PSH units under 20% penetration level

7.3.2 Study of 40% Renewable Penetration Level

As the penetration level increased to 40%, T-PSH units have an increased role in the regulation of the system. The frequency improvement provided by T-PSH in HSC mode, shown in Figure 7.7, was about 22.5 mHz in comparison to the with C-PSH in the pumping mode case. Owing to the total capacity of the online synchronous generators has decreased, the additional power feed by the T-PSH units was increased to 294 MW (0.071 p.u.) which is shown in Figure 7.8. Because of reduced system inertia, the electrical power required more time to stabilize after the inertial response compared to the results of the 20% penetration case.

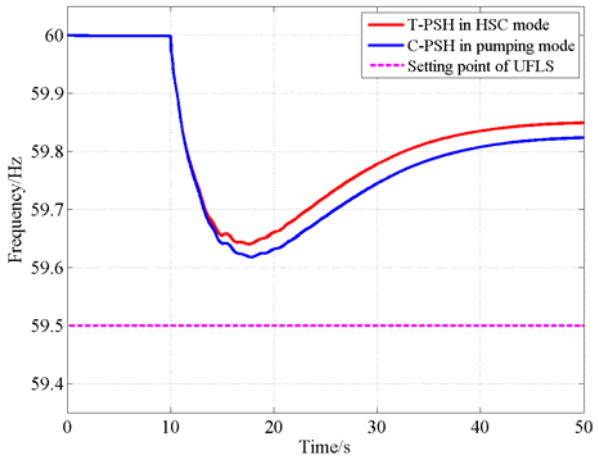

Figure 7.7 COI frequency response of T-PSH units under 40% penetration level

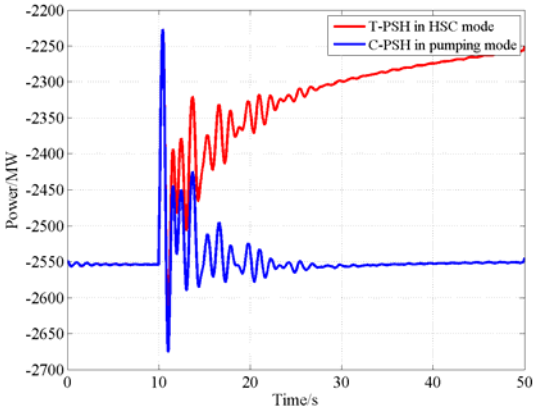

Figure 7.8 Electrical power output of T-PSH units under 40% penetration level

7.3.3 Study of 60% Renewable Penetration Level

With the further increase of renewable penetration level, the impact of T-PSH units in the frequency regulation became more obvious. In the C-PSH case, insufficient frequency regulation provided by the synchronous generators made the COI frequency nadir of the system lower than 59.6 Hz. Actually, the system frequency in some area was lower than 59.5 Hz, which is low enough to trigger the USLF. In contrast, in the T-PSH case, the frequency nadir, shown in Figure 7.9, was 29.6 mHz higher than C-PSH case, which is higher than 59.6 Hz. This effectively alleviates the

possibility of triggering UFLS. In addition, the T-PSH in HSC mode feeds more 344 MW (0.083 p.u.) back to the grid as shown in Figure 7.10. Especially, more obvious oscillation occurs in the output electrical power after the inertial response and more time is spent to reach the steady state all related to the small system inertia.

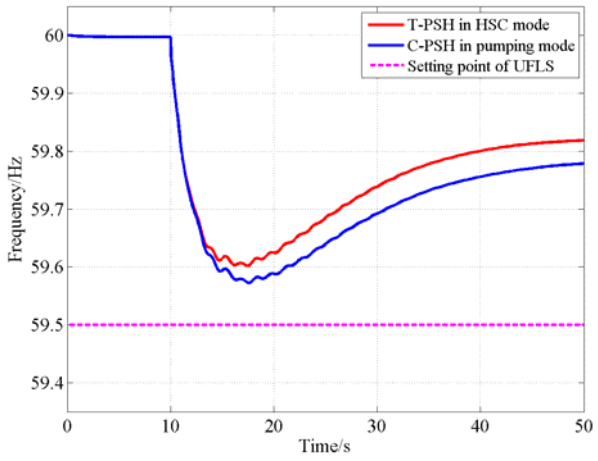

Figure 7.9 COI frequency response of T-PSH units under 60% penetration level

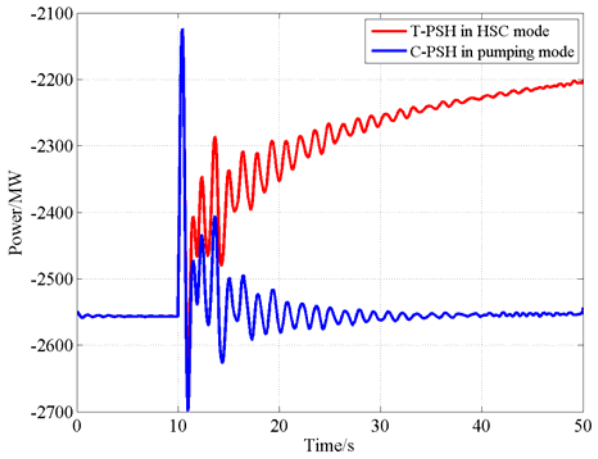

Figure 7.10 Electrical power output of T-PSH units under 60% penetration level

7.3.4 Study of 80% Renewable Penetration Level

In the 80% penetration case, the frequency regulation provided by the T-PSH units in HSC mode is obvious as shown in Figure 7.11. The 526 MW (0.127 p.u.) additional power provided by

the T-PSH units, shown in Figure 7.12, was twice that in the 20% penetration case. However, the system was not particularly stable after the frequency event both in C-PSH case and T-PSH case. The T-PSH units have not been able to effectively improve the stability of the system in this extremely high penetration level, although the T-PSH units increased 63.4 mHz at the frequency nadir and 94.0 mHz at the settling frequency.

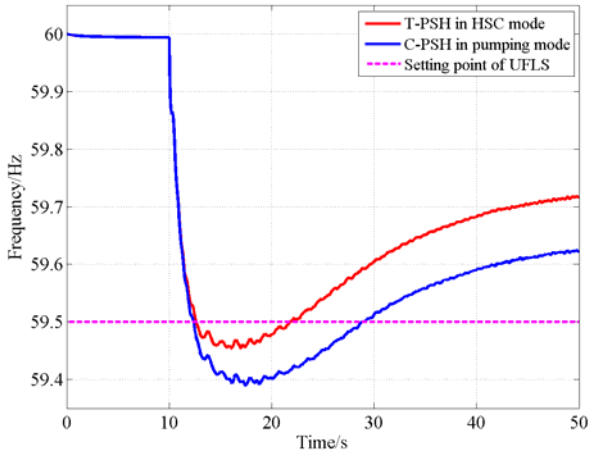

Figure 7.11 COI frequency response of T-PSH units under 80% penetration level

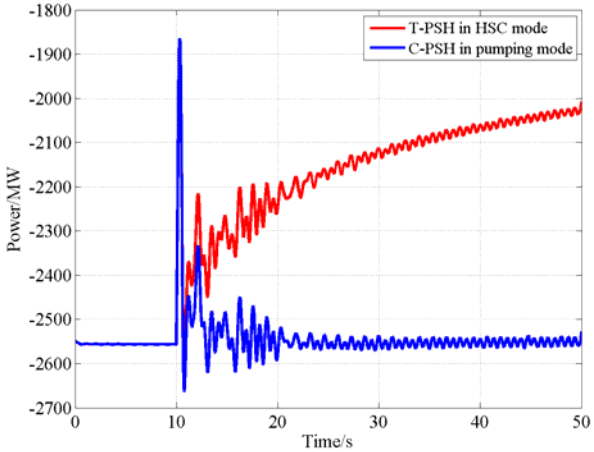

Figure 7.12 Electrical power output of T-PSH units under 80% penetration level

7.3.5 Results Analysis

After finishing the study of T-PSH units under different renewable penetration levels, the

detailed comparison of results in all penetration cases is shown in Figure 7.13 and Table 7.2. As the penetration level increased, the improvements of frequency both at frequency nadir, settling frequency and regulation of electrical power became more and more significant. In contrast to the baseline cases, C-PSH units in the pumping mode not only cannot respond to the frequency event, but also cannot improve the response performance of system. Because of this, T-PSH in HSC mode can effectively improve the frequency response when system has a high renewable penetration level, especially higher than 60%.

However, the frequency nadir is still less than 59.5 Hz, which is the set point of the first stage of USLF, when the T-PSH units were deployed in the 80% renewable penetrated system. Although T-PSH units in HSC mode provide a significant frequency improvement, they still cannot prevent the load shedding by the UFLS devices. More than 20% of power supplied by the T-PSH units in the 80% penetration case was effective but still insufficient to deal with this level of contingency. It is very urgent to consider a solution to effectively deal with the problem caused by a serious contingency under extremely high penetration level. The customers' power outage caused by load shedding protection will actually exist in the future owing to the great growth of renewable energy. Therefore, it should be resolved to reduce the customers' economic losses.

Table 7.2 Details of improvement by T-PSH units in HSC mode

Case	Frequency Nadir	Settling Frequency	Ratio of Extra Power
20% case	14.1 mHz	18.9 mHz	10.14%
40% case	22.5 mHz	25.7 mHz	11.52%
60% case	29.6 mHz	40.0 mHz	13.47%
80% case	63.4 mHz	94.0 mHz	20.60%

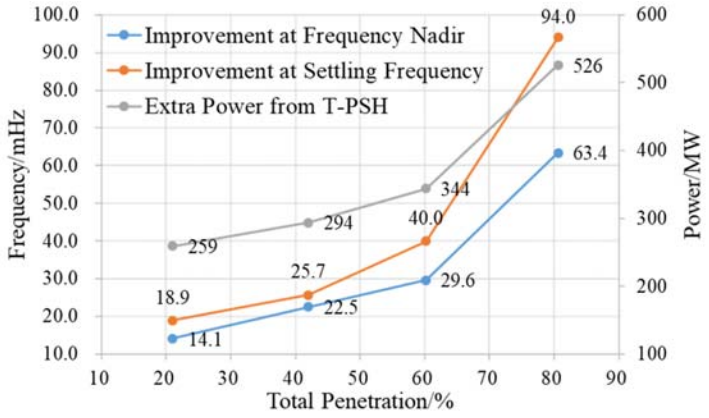

Figure 7.13 Improvements of T-PSH units under different penetration levels

7.4 Operation Mode Switching Application Under Generation Loss

The participation of T-PSH units operated in HSC mode was proven to be beneficial to the high renewable penetrated system. However, under an extremely high renewable penetration level like 80%, limited governor response in the turbine part provided by a small number of T-PSH units operated in the HSC mode cannot prevent the protective load shedding. In the future, the growth of new energy is inevitable. It is not realistic to build a large number of T-PSH units or upgrade C-PSH units to T-PSH units in a short period of time to face the increase of renewable penetration level. Therefore, quick operation mode switching as another advantage of T-PSH was considered to further improve frequency response performance of system after the serious contingency.

A comparison simulation among operation mode switching, HSC mode, and conventional pumping mode of the T-PSH is presented in this section. Based on the 2022 LSP WI system, five T-PSH units were operated to absorb 2.6 GW at the beginning. Especially, the T-PSH units for operation mode switching case were operated in pumping mode at the beginning. The same largest N-2 contingency was applied at 10 seconds to create a generation loss contingency. In order to

detect the frequency event and get the value of the generation loss, rate of change of frequency (ROCOF) measurement expressed below was employed

$$\Delta P = 2\sum_{i=1}^{n} H_i \frac{df_{coi}}{dt} \tag{62}$$

where ΔP is the power change in the system, H_i is the system inertia in i[th] area and f_{coi} is the center of inertia frequency. A new block for this measurement was designed and added into T-PSH system and is shown in Figure 7.14. Figure 7.15 introduces the entire process of detection and implementation for the operation mode switching. In order to simplify the design, the T-PSH units were pre-selected according to the N-2 contingency. Here, the pre-selected T-PSH units were the Castaic PSH plant and Hyatt PSH plant.

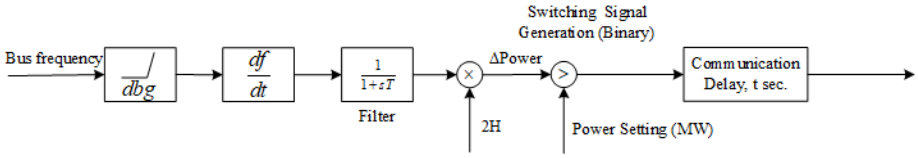

Figure 7.14 Block diagram of ROCOF measurement

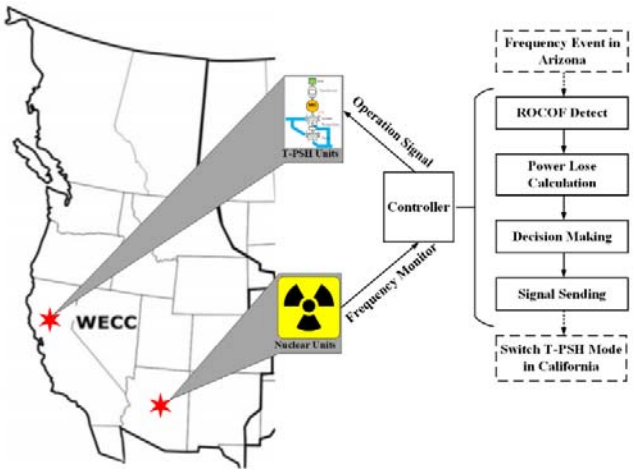

Figure 7.15 Schematic diagram of T-PSH operation mode switching application

After the frequency event, the measurements of ROCOF and generation loss estimation are shown in Figure 7.16 and Figure 7.17. Sampling interval for the ROCOF calculation was 0.1 second. The error of generation loss estimation was 2.51% which is acceptable to do the mode switching. Furthermore, a delay of 0.5 seconds was added in the switching trigger signal to simulate the actual inherent delay in the frequency event detection and signal communication as shown in Figure 7.17. When the measurement block generated the trigger signal (changes to 1), the pre-selected T-PSH units will be switched immediately.

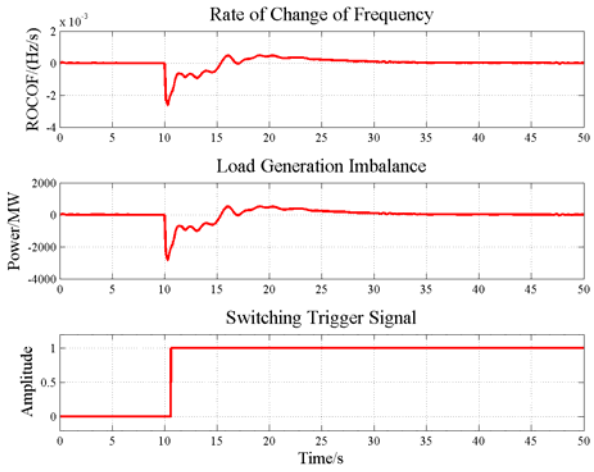

Figure 7.16 Measurements in the ROCOF block

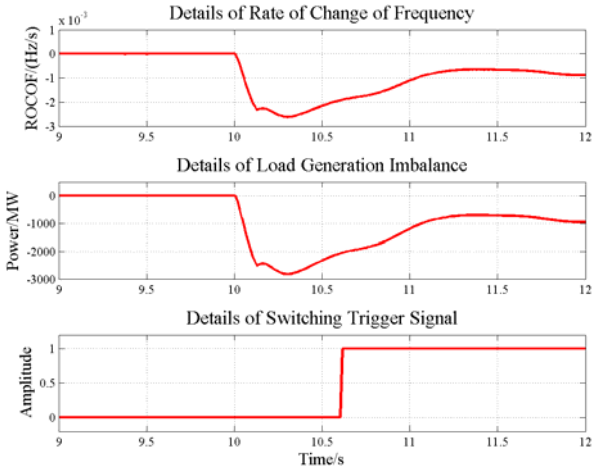

Figure 7.17 Details of measurements in the ROCOF block

When the T-PSH units receive the switching trigger signal, the Castaic and Hyatt units were switched from pumping mode to generation mode with 20 seconds of transition time. Meanwhile, the other three T-PSH units were kept in conventional pumping mode. Figure 7.18 illustrates that the switched T-PSH units can do the quick mode switching and provide a larger proportion of power back to the grid in about 10 seconds. After this, the governor in the turbine part continues to adjust the electrical power output.

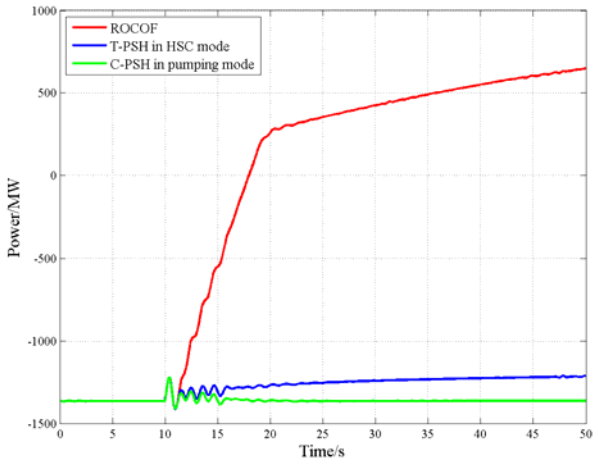

Figure 7.18 Electrical power output of switched T-PSH units

The electrical power and frequency response, shown in Figure 7.19 and Figure 7.20, illustrates that the operation mode switched T-PSH units improve the system frequency response significantly by feeding a large amount of power back to the system. The important thing is that the switching application brings the settling frequency to 59.95 Hz, which directly solved the problem of triggering UFLS and greatly reduce the need for subsequent frequency regulation. The frequency improvement and addition injection power given by two switched T-PSH units are compared with HSC mode case and conventional pumping case and are shown in Table 7.3.

Combining all these results, the operation mode switching application can significantly improve performance of the system after the contingency. Meanwhile, the natural inertia of T-PSH can assist in stabilizing system. Because of this, the ability of operation mode switching is a preferable solution to deal with the serious contingencies under extremely high renewable penetration level. The wide range of power injection provided by switching operation mode makes T-PSH have the potential to participate in wide-area control.

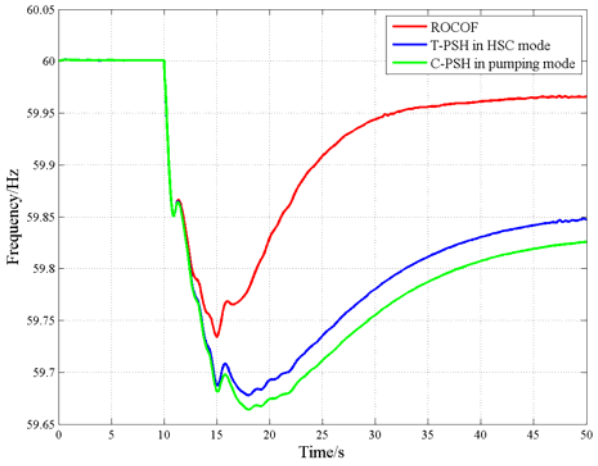

Figure 7.19 Frequency response of T-PSH units in operation mode switching

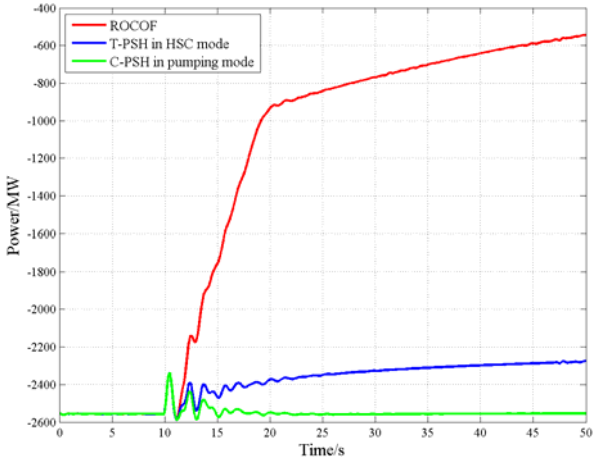

Figure 7.20 Total electrical power output of T-PSH units in operation mode switching

Table 7.3 Details of improvement by T-PSH in operation mode switching

Metrics	Compared with HSC	Compared with Pumping
Frequency nadir	59.40 mHz	70.50 mHz
Settling frequency	119.22 mHz	140.12 mHz
Extra power	1727.5 MW	2010.5 MW

CHAPTER 8 CONCLUSION AND FUTURE WORK

In this work, the first governor dynamic model of T-PSH in the GE PSLF platform has been developed with detailed modeling of gate valve and shared-penstock. A highlight in the development is that this model can simulate the unique hydraulic short-circuit mode of T-PSH and continuously simulate the switch between different operation modes. The validation simulations of T-PSH system were completed in both a small test system and the WI system. Several sensitivity studies of some parameters have been investigated to reveal the influence on the system. The improvements provided by the T-PSH system under the extremely high renewable penetration level was also analyzed. All the research is summarized in this chapter, and a suggestion for future work is provided.

8.1 Summary of Research

The first detailed governor, modeled in T-PSH system, has been successfully implemented in the GE PSLF platform by using the EPCL user-defined model. The functional validations of this model were both completed in the MATLAB/Simulink platform and the GE PSLF platform to prove the correctness of the design and show the smooth operation for T-PSH system in three operation modes. Also, the implementation of this governor model in the WI system indicated that this model works well in large practical systems, which shows the flexibility of this model different size systems.

The operation mode studies of T-PSH system in the 3-gens system revealed the system characteristics in three operation modes. In the generating mode and HSC mode, T-PSH can

respond to the system frequency event by using regulation ability provided by the governor in the turbine part. T-PSH operated in the pumping mode can only provide a fixed power output, always at the maximum value in daily operation. Therefore, T-PSH technology can provide the frequency regulation service both in generating and pumping (HSC mode), where HSC mode is a kind of pumping mode. In addition, the comparison cases between T-PSH in HSC mode and C-PSH in pumping mode were both implemented in the 3-gens small system and the WI system. The results indicated that the T-PSH in HSC mode showed a better performance of frequency response to the system than the pure conventional pumping mode. Because of this, the additional HSC mode in T-PSH technology gives it a more comprehensive and steady frequency regulation capability than C-PSH technology.

The sensitivity studies of valve velocity in the T-PSH system illustrated the influence of transition time (expressed as valve velocity) to the frequency response performance of T-PSH system. Based on the 3-gens testing system, several comparison cases among several sets of valve velocity showed that a too small valve velocity will cause a quite severe system oscillation in normal operation. Especially, the protective cut-off by using a deflector will cause a significant influence on the system. Similarly, too small valve velocity, although the T-PSH can switch operation mode quickly, also yielded large oscillations. However, a large valve velocity, which is longer than the inherent response time of T-PSH system, will bring a delay in the frequency response during the frequency event scenario. In other words, the valve velocity should be selected smaller than the reciprocal of T-PSH response time in mode switching, and larger than the

reciprocal of inherent response time in the general operation and in the system frequency event to have a quicker frequency response while minimizing the oscillations.

The shared-penstock sensitivity study illustrated that it is necessary to model the shared-penstock feature in T-PSH model, because it will affect the power response of T-PSH under HSC mode during the mode switching. The parameters of main penstocks and sub-penstocks split from main penstock to connect chambers both will effectively increase overshoot in the system response after the switching event when it has a larger length to cross-sectional area ratio. Because of this, an appropriate set of penstock parameters should be considered to minimize the water interactions in the HSC mode during operation mode switching without significantly increasing construction costs.

Studies of T-PSH in WI with high penetration levels of renewables illustrate the role of T-PSH system in the future high renewable penetrated system. T-PSH system operated in HSC mode can provide significant frequency support service under various penetration levels when a frequency event occurs. As the penetration level increases, T-PSH system can increase the frequency response in terms of frequency nadir and settling frequency compared with conventional PSH in pumping mode. In addition, after the contingency, the T-PSH system showed superiority in providing more additional power at a higher renewable penetration level.

Furthermore, the quick mode switching capability of T-PSH can provide a large amount of power in a short time. This wide range of power injection gives T-PSH technology the potential to participate in wide-area control to cope with future high renewable penetration level by using HSC

mode and quick operation mode switching.

8.2 Suggestion for Future Work

In the comparison simulation in each test system, the T-PSH technology was only compared with C-PSH technology. There will be follow-up work to compare T-PSH technology and AS-PSH technology, which is also another rapidly developing PSH technology. The AS-PSH system will be added into comparison cases to illustrate the difference among these three types of PSH technologies. At the same time, in order to better develop T-PSH technology, the T-PSH system with the governor model should be implemented in other power system analysis platform like PSS/E.

More parameters in the T-PSH governor should be considered to reveal the influences caused by them. Several sensitivity studies should be planned to analyze the impact of water head and parameters in the droop controller on system characteristics. Also, a non-linear model of the Pelton turbine should be implemented in the governor model to make T-PSH system closer to reality. Another sensitivity study between the linear and non-linear turbine model is worth studying.

Wide-area control is an effective way to deal with the problems caused by the instability and non-sustainability of new energy sources. A simple test in this study only shows the potential of T-PSH technology to be a part of the wide-area control. A smarter and more automatic wide-area control plan with T-PSH units should be designed and tested. Combined with future renewable development, more studies of cooperation of T-PSH technology and renewable generations should be studied.

APPENDIX A

```
Dynamic model table for 3-gen system with T-PSH in generating mode

gensal 19 "HYDRO-LV-NEW"  24.00 "1 ": #9 mva=1176.0000 12.0000 0.0730 0.3400 /
    5.5800 0.0000 1.0500 0.7000 0.2770 0.2000 0.1300 0.1700 0.3600 0.0000 /
    0.0000 0.0000
genrou 20 "GAS-LV-NEW  "  24.00 "1 ": #9 mva=200.0000 6.0000 0.0400 0.6000 /
    0.0500 3.0000 0.0000 1.8000 1.7500 0.4000 0.4000 0.2000  0.1600 0.1500 /
    0.3000 0.0000 0.0000 0.0000 0.0000
gensal 15 "PS-HYDRO     "  24.00 "1 ": #9 mva=28.9000 12.0000 0.0730 0.3700 /
    5.5800 0.0000 1.0500 0.7000 0.2770 0.2000 0.1300 0.1700 0.3600 0.0000 /
    0.0000 0.0000
ieeet1 19 "HYDRO-LV-NEW"  24.00 "1 ": #1 0.0500 50.0000 0.0600 1.0000 -0.4000 /
    0.2060 1.6300 0.0200 1.2000 0.0000 2.5000 0.0200 3.6000 0.0400
ieeet1 15 "PS-HYDRO     "  24.00 "1 ": #1 0.0500 50.0000 0.0600 1.0000 -0.4000 /
    0.2060 1.6300 0.0200 1.2000 0.0000 2.5000 0.0200 3.6000 0.0400
hygov  15 "PS-HYDRO     "  24.00 "1 ": #1 mwcap=28.9000 0.0400 0.3100 6.8800 /
    0.0500 0.5000 0.0500 1.0000 0.0000 1.7200 1.4800 0.3000 0.1000 0.0000 /
    0.0000 0.0000 0.0000 0.0000 0.0000 0.0000 0.0000 0.0000 0.0000 0.0000 /
    0.0000 0.0000 0.0000 0.0000 0.0000 0.0000 0.0000 1.0000 0.0000 0.0000 /
    0.0000 0.0000 0.0000 0.0000 0.0000 0.0000
epctrb 19 "PS-HYDRO     "  24.00 "1 ": #7 "hygovt.p" 3.0000  "Tg" 0.5000 /
    "Tw11" -1.1700 "Tw12" 0.0000 "Tw22" 1.1700 "Tw21" 0.000  "At" 1.4800 /
    "Dturb" 0.3000 "qnl" 0.1000  "hdam" 1.0000 "Tr" 6.8800   "Tf" 0.0500 /
    "R" 0.0400     "r" 0.3100    "Gmax" 1.0000 "Gmin" 0.0000 "Kd" 0.0000 /
    "Velm" 0.0500
vmetr  19 "HYDRO-LV-NEW"  24.00 "1 ": #9 0.0000
imetr  19 "HYDRO-LV-NEW"  24.00 "1 " 17 "HYDRO-HV-NEW" 230.00  "1 "  1: #9 0.0000
fmetr  19 "HYDRO-LV-NEW"  24.00 "1 ": #9 0.0000
fmetr  15 "PS-HYDRO     "  24.00 "1 ": #9 0.0000
vmetr  15 "PS-HYDRO     "  24.00 "1 ": #9 0.0000
imetr  15 "PS-HYDRO     "  24.00 "1 " 14 "WF-LOW2     "  34.50  "1 "  1: #9 0.0000
vmetr  20 "GAS-LV-NEW  "  24.00 "1 ": #9 0.0000
imetr  20 "GAS-LV-NEW  "  24.00 "1 " 18 "GAS-HV-NEW  " 230.00  "1 "  1: #9 0.0000
fmetr  20 "GAS-LV-NEW  "  24.00 "1 ": #9 0.0000
vmetr  11 "LOAD         " 230.00 "1 ": #9 0.0000
fmetr  11 "LOAD         " 230.00 "1 ": #9 0.0000
vmetr  13 "WF-LOW       "  34.50 "1 ": #9 0.0000
fmetr  13 "WF-LOW       "  34.50 "1 ": #9 0.0000
```

APPENDIX B

```
Dynamic model table for 3-gen system with T-PSH in pumping mode

gensal 19 "HYDRO-LV-NEW"  24.00 "1 ": #9 mva=1276.0000 12.0000 0.0730 0.3400 /
    5.5800 0.0000 1.0500 0.7000 0.2770 0.2000 0.1300 0.1700 0.3600 0.0000 /
    0.0000 0.0000
genrou 20 "GAS-LV-NEW  "  24.00 "1 ": #9 mva=2400.0000 6.0000 0.0400 0.6000 /
    0.0500 3.0000 0.0000 1.8000 1.7500 0.4000 0.4000 0.2000  0.1600 0.1500 /
    0.3000 0.0000 0.0000 0.0000 0.0000
gensal 15 "PS-HYDRO    "  24.00 "1 ": #9 mva=28.9000 12.0000 0.0730 0.3700 /
    5.5800 0.0000 1.0500 0.7000 0.2770 0.2000 0.1300 0.1700 0.3600 0.0000 /
    0.0000 0.0000
ieeet1 19 "HYDRO-LV-NEW"  24.00 "1 ": #1 0.0500 50.0000 0.0600 1.0000 -0.4000 /
    0.2060 1.6300 0.0200 1.2000 0.0000 2.5000 0.0200 3.6000 0.0400
ieeet1 15 "PS-HYDRO    "  24.00 "1 ": #1 0.0500 50.0000 0.0600 1.0000 -0.4000 /
    0.2060 1.6300 0.0200 1.2000 0.0000 2.5000 0.0200 3.6000 0.0400
exac1  20 "GAS-LV-NEW  "  24.00 "1 ": #9 0.0500 1.0000 1.0000 40.0000 0.1000 /
    5.0000 -5.0000 0.5000 0.2000 1.0000 0.1000 0.6000 1.0000 1.0000 0.0300 /
    2.0000 0.3000
gast   20 "GAS-LV-NEW  "  24.00 "1 ": #9 mva=2400.0000 0.0500 0.5000 0.5000 /
    3.0000 1.5000 3.0000 1.1000 0.0000 0.0000 0.0 /
    99.0000 99.0000 99.0000  99.0000
hygov  15 "PS-HYDRO    "  24.00 "1 ": #1 mwcap=28.9000 0.0400 0.3100 6.8800 /
    0.0500 0.5000 0.0500 1.0000 0.0000 1.7200 1.4800 0.3000 0.1000 0.0000 /
    0.0000 0.0000 0.0000 0.0000 0.0000 0.0000 0.0000 0.0000 0.0000 0.0000 /
    0.0000 0.0000 0.0000 0.0000 0.0000 0.0000 0.0000 1.0000 0.0000 0.0000 /
    0.0000 0.0000 0.0000 0.0000 0.0000 0.0000
epctrb 19 "PS-HYDRO    "  24.00 "1 ": #7 "hygovt.p" 3.0000  "Tg" 0.5000 /
    "Tw11" -1.1700 "Tw12" 0.0000 "Tw22" 1.1700 "Tw21" 0.000  "At" 1.4800 /
    "Dturb" 0.3000 "qnl" 0.1000  "hdam" 1.0000 "Tr" 6.8800   "Tf" 0.0500 /
    "R" 0.0400     "r" 0.3100    "Gmax" 1.0000 "Gmin" 0.0000 "Kd" 1.0000 /
    "Velm" 0.0500
vmetr  19 "HYDRO-LV-NEW"  24.00 "1 ": #9 0.0000
imetr  19 "HYDRO-LV-NEW"  24.00 "1 " 17 "HYDRO-HV-NEW" 230.00  "1 "  1: #9 0.0000
fmetr  19 "HYDRO-LV-NEW"  24.00 "1 ": #9 0.0000
fmetr  15 "PS-HYDRO    "  24.00 "1 ": #9 0.0000
vmetr  15 "PS-HYDRO    "  24.00 "1 ": #9 0.0000
imetr  15 "PS-HYDRO    "  24.00 "1 " 14 "WF-LOW2     "  34.50  "1 "  1: #9 0.0000
vmetr  20 "GAS-LV-NEW  "  24.00 "1 ": #9 0.0000
imetr  20 "GAS-LV-NEW  "  24.00 "1 " 18 "GAS-HV-NEW  " 230.00  "1 "  1: #9 0.0000
fmetr  20 "GAS-LV-NEW  "  24.00 "1 ": #9 0.0000
vmetr  11 "LOAD        " 230.00 "1 ": #9 0.0000
fmetr  11 "LOAD        " 230.00 "1 ": #9 0.0000
vmetr  13 "WF-LOW      "  34.50 "1 ": #9 0.0000
fmetr  13 "WF-LOW      "  34.50 "1 ": #9 0.0000
```

APPENDIX C

```
Dynamic model table for 3-gen system with T-PSH in HSC mode

gensal 19 "HYDRO-LV-NEW"  24.00 "1 ": #9 mva=1276.0000 12.0000 0.0730 0.3400 /
    5.5800 0.0000 1.0500 0.7000 0.2770 0.2000 0.1300 0.1700 0.3600 0.0000 /
    0.0000 0.0000
genrou 20 "GAS-LV-NEW "  24.00 "1 ": #9 mva=2400.0000 6.0000 0.0400 0.6000 /
    0.0500 3.0000 0.0000 1.8000 1.7500 0.4000 0.4000 0.2000  0.1600 0.1500 /
    0.3000 0.0000 0.0000 0.0000 0.0000
gensal 15 "PS-HYDRO    "  24.00 "1 ": #9 mva=28.9000 12.0000 0.0730 0.3700 /
    5.5800 0.0000 1.0500 0.7000 0.2770 0.2000 0.1300 0.1700 0.3600 0.0000 /
    0.0000 0.0000
ieeet1 19 "HYDRO-LV-NEW"  24.00 "1 ": #1 0.0500 50.0000 0.0600 1.0000 -0.4000 /
    0.2060 1.6300 0.0200 1.2000 0.0000 2.5000 0.0200 3.6000 0.0400
ieeet1 15 "PS-HYDRO    "  24.00 "1 ": #1 0.0500 50.0000 0.0600 1.0000 -0.4000 /
    0.2060 1.6300 0.0200 1.2000 0.0000 2.5000 0.0200 3.6000 0.0400
hygov  15 "PS-HYDRO    "  24.00 "1 ": #1 mwcap=28.9000 0.0400 0.3100 6.8800 /
    0.0500 0.5000 0.0500 1.0000 0.0000 1.7200 1.4800 0.3000 0.1000 0.0000 /
    0.0000 0.0000 0.0000 0.0000 0.0000 0.0000 0.0000 0.0000 0.0000 0.0000 /
    0.0000 0.0000 0.0000 0.0000 0.0000 0.0000 0.0000 1.0000 0.0000 0.0000 /
    0.0000 0.0000 0.0000 0.0000 0.0000 0.0000
epctrb 19 "PS-HYDRO    "  24.00 "1 ": #7 "hygovt.p" 3.0000  "Tg" 0.5000 /
    "Tw11" -1.1700 "Tw12" 0.0000 "Tw22" 1.1700 "Tw21" 0.000  "At" 1.4800 /
    "Dturb" 0.3000 "qnl" 0.1000  "hdam" 1.0000 "Tr" 6.8800  "Tf" 0.0500 /
    "R" 0.0400     "r" 0.3100    "Gmax" 1.0000 "Gmin" 0.0000 "Kd" 2.0000 /
    "Velm" 0.0500
vmetr  19 "HYDRO-LV-NEW"  24.00 "1 ": #9 0.0000
imetr  19 "HYDRO-LV-NEW"  24.00 "1 " 17 "HYDRO-HV-NEW" 230.00  "1 "  1: #9 0.0000
fmetr  19 "HYDRO-LV-NEW"  24.00 "1 ": #9 0.0000
fmetr  15 "PS-HYDRO    "  24.00 "1 ": #9 0.0000
vmetr  15 "PS-HYDRO    "  24.00 "1 ": #9 0.0000
imetr  15 "PS-HYDRO    "  24.00 "1 " 14 "WF-LOW2     "  34.50  "1 "  1: #9 0.0000
vmetr  20 "GAS-LV-NEW "  24.00 "1 ": #9 0.0000
imetr  20 "GAS-LV-NEW "  24.00 "1 " 18 "GAS-HV-NEW  " 230.00  "1 "  1: #9 0.0000
fmetr  20 "GAS-LV-NEW "  24.00 "1 ": #9 0.0000
vmetr  11 "LOAD        " 230.00 "1 ": #9 0.0000
fmetr  11 "LOAD        " 230.00 "1 ": #9 0.0000
vmetr  13 "WF-LOW      "  34.50 "1 ": #9 0.0000
fmetr  13 "WF-LOW      "  34.50 "1 ": #9 0.0000
```

REFERENCE

[1] B. Kroposki, B. Johnson, Y. Zhang, V. Gevorgian, P. Denholm, B.-M. Hodge, *et al.*, "Achieving a 100% renewable grid: Operating electric power systems with extremely high levels of variable renewable energy," *IEEE Power and Energy Magazine,* vol. 15, pp. 61-73, 2017.

[2] A. Tuohy and M. O'Malley, "Pumped storage in systems with very high wind penetration," *Energy policy,* vol. 39, pp. 1965-1974, 2011.

[3] P. Fairley, "Customers seek 100-percent-renewable grids [News]," *IEEE Spectrum,* vol. 54, pp. 12-13, 2017.

[4] C. S. Senate. (2018, Jan 05, 2019). *100% Clean Energy (SB100).* Available: https://focus.senate.ca.gov/sb100

[5] P. Denholm, E. Ela, B. Kirby, and M. Milligan, "The role of energy storage with renewable electricity generation," 2010.

[6] C. Lins, L. E. Williamson, S. Leitner, and S. Teske, "The first decade: 2004—2014: 10 years of renewable energy progress," *Renewable Energy Policy Network for the 21st Century.,* 2014.

[7] M. Beaudin, H. Zareipour, A. Schellenberglabe, and W. Rosehart, "Energy storage for mitigating the variability of renewable electricity sources: An updated review," *Energy for sustainable development,* vol. 14, pp. 302-314, 2010.

[8] B. Dunn, H. Kamath, and J.-M. Tarascon, "Electrical energy storage for the grid: a battery of choices," *Science,* vol. 334, pp. 928-935, 2011.

[9] T. Mahlia, T. Saktisahdan, A. Jannifar, M. Hasan, and H. Matseelar, "A review of available methods and development on energy storage; technology update," *Renewable and Sustainable Energy Reviews,* vol. 33, pp. 532-545, 2014.

[10] I. Hadjipaschalis, A. Poullikkas, and V. Efthimiou, "Overview of current and future energy storage technologies for electric power applications," *Renewable and sustainable energy reviews,* vol. 13, pp. 1513-1522, 2009.

[11] D. Sprake, Y. Vagapov, S. Lupin, and A. Anuchin, "Housing estate energy storage feasibility for a 2050 scenario," 2017.

[12] H. Ibrahim, A. Ilinca, and J. Perron, "Energy storage systems—Characteristics and comparisons," *Renewable and sustainable energy reviews,* vol. 12, pp. 1221-1250, 2008.

[13] H. Chen, T. N. Cong, W. Yang, C. Tan, Y. Li, and Y. Ding, "Progress in electrical energy storage system: A critical review," *Progress in natural science,* vol. 19, pp. 291-312, 2009.

[14] F. Klumpp, "Comparison of pumped hydro, hydrogen storage and compressed air energy storage for integrating high shares of renewable energies—potential, cost-comparison and ranking," *Journal of Energy storage,* vol. 8, pp. 119-128, 2016.

[15] S. Rehman, L. M. Al-Hadhrami, and M. M. Alam, "Pumped hydro energy storage system: A technological review," *Renewable and Sustainable Energy Reviews,* vol. 44, pp. 586-598, 2015.

[16] D. Egré and J. C. Milewski, "The diversity of hydropower projects," *Energy Policy,* vol. 30, pp. 1225-1230, 2002.

[17] R. Stone, "Three Gorges Dam: into the unknown," ed: American Association for the Advancement of Science, 2008.

[18] P. M. Fearnside, "Dams in the Amazon: Belo Monte and Brazil's hydroelectric development of the Xingu River Basin," *Environmental management,* vol. 38, p. 16, 2006.

[19] Y. H. Bae, K. O. Kim, and B. H. Choi, "Lake Sihwa tidal power plant project," *Ocean Engineering,* vol. 37, pp. 454-463, 2010.

[20] D. Office of Electricity Delivery & Energy Reliability. (2016, Dec 20, 2018). *Castaic Pumped-Storage Plant, DOE Global Energy Storage Database*. Available: http://www.energystorageexchange.org/projects/440

[21] J. P. Deane, B. Ó. Gallachóir, and E. McKeogh, "Techno-economic review of existing and new pumped hydro energy storage plant," *Renewable and Sustainable Energy Reviews,* vol. 14, pp. 1293-1302, 2010.

[22] J.-M. Chapallaz, P. Eichenberger, and G. Fischer, *Manual on pumps used as turbines*: Vieweg Braunschweig, Germany, 1992.

[23] D. K. Okot, "Review of small hydropower technology," *Renewable and Sustainable Energy Reviews,* vol. 26, pp. 515-520, 2013.

[24] D. Office of Electricity Delivery & Energy Reliability. (2016, Dec 20, 2018). *San Luis (William R. Gianelli) Pumped Storage Hydroelectric Powerplant, DOE Global Energy Storage Database*. Available: http://www.energystorageexchange.org/projects/444

[25] N. Kishor, R. Saini, and S. Singh, "A review on hydropower plant models and control," *Renewable and Sustainable Energy Reviews,* vol. 11, pp. 776-796, 2007.

[26] L. N. Hannett, B. P. Lam, F. Prabhakara, Q. Guofu, D. Mincheng, and B. Beilei, "Modeling of a pumped storage hydro plant for power system stability studies," in *Power System Technology, 1998. Proceedings. POWERCON'98. 1998 International Conference on*, 1998, pp. 1300-1304.

[27] R. Jiang, J. Wang, and Y. Guan, "Robust unit commitment with wind power and pumped storage hydro," *IEEE Transactions on Power Systems,* vol. 27, p. 800, 2012.

[28] C. Bueno and J. Carta, "Technical–economic analysis of wind-powered pumped hydrostorage systems. Part II: model application to the island of El Hierro," *Solar energy,* vol. 78, pp. 396-405, 2005.

[29] C. Bueno and J. A. Carta, "Wind powered pumped hydro storage systems, a means of increasing the penetration of renewable energy in the Canary Islands," *Renewable and sustainable energy reviews,* vol. 10, pp. 312-340, 2006.

[30] T. Kuwabara, A. Shibuya, H. Furuta, E. Kita, and K. Mitsuhashi, "Design and dynamic response characteristics of 400 MW adjustable speed pumped storage unit for Ohkawachi power station," *IEEE Transactions on Energy Conversion,* vol. 11, pp. 376-384, 1996.

[31] E. Muljadi, M. Singh, V. Gevorgian, M. Mohanpurkar, R. Hovsapian, and V. Koritarov, "Dynamic modeling of adjustable-speed pumped storage hydropower plant," in *Power & Energy Society General Meeting, 2015 IEEE*, 2015, pp. 1-5.

[32] E. Camm, M. Behnke, O. Bolado, M. Bollen, M. Bradt, C. Brooks, *et al.*, "Wind power plant collector system design considerations: IEEE PES wind plant collector system design working group," in

Power & Energy Society General Meeting, 2009. PES'09. IEEE, 2009, pp. 1-7.

[33] S. Muller, M. Deicke, and R. W. De Doncker, "Doubly fed induction generator systems for wind turbines," *IEEE Industry applications magazine,* vol. 8, pp. 26-33, 2002.

[34] H. Li and Z. Chen, "Overview of different wind generator systems and their comparisons," *IET Renewable power generation,* vol. 2, p. 123, 2008.

[35] D. Office of Electricity Delivery & Energy Reliability. (2016, Dec 21, 2018). *Okikuyotsu (Okukiyotsu) No. 2 Pumped Hydro Storage Plant, DOE Global Energy Storage Database*. Available: http://www.energystorageexchange.org/projects/1683

[36] F. De Marco, A. Svalovs, and K. Chan, "Converter-connected power plant generic model for frequency stability studies," in *Power & Energy Society General Meeting, 2017 IEEE*, 2017, pp. 1-5.

[37] A. Joseph and T. R. Chelliah, "A Review of Power Electronic Converters for Variable Speed Pumped Storage Plants: Configurations, Operational Challenges, and Future Scopes," *IEEE Journal of Emerging and Selected Topics in Power Electronics,* vol. 6, pp. 103-119, 2018.

[38] J.-K. Lung, Y. Lu, W.-L. Hung, and W.-S. Kao, "Modeling and dynamic simulations of doubly fed adjustable-speed pumped storage units," *IEEE Transactions on Energy Conversion,* vol. 22, pp. 250-258, 2007.

[39] C. Xin, H. Minxiao, and Z. Chao, "Power control analysis for variable speed pumped storage with full-size converter," in *Industrial Electronics Society, IECON 2015-41st Annual Conference of the IEEE*, 2015, pp. 001327-001332.

[40] M. Dreidy, H. Mokhlis, and S. Mekhilef, "Inertia response and frequency control techniques for renewable energy sources: A review," *Renewable and Sustainable Energy Reviews,* vol. 69, pp. 144-155, 2017.

[41] J. Kim, V. Gevorgian, E. Muljadi, M. Nelms, A. Davis, and G. Li, "Coordinated Voltage Control Scheme of an Adjustable-Speed Pumped Storage Hydropower and a Wind Power Plant," in *IECON 2018-44th Annual Conference of the IEEE Industrial Electronics Society*, 2018, pp. 1741-1745.

[42] B. G. Teshager, H. Minxiao, S. Patrobers, Z. W. Khan, L. K. Tuan, and F. M. Shah, "Direct power control strategy based variable speed pumped storage system for the reduction of the wind power fluctuation impact on the grid stability," in *Compatibility, Power Electronics and Power Engineering (CPE-POWERENG), 2018 IEEE 12th International Conference on*, 2018, pp. 1-6.

[43] F. Petrakopoulou, A. Robinson, and M. Loizidou, "Simulation and analysis of a stand-alone solar-wind and pumped-storage hydropower plant," *Energy,* vol. 96, pp. 676-683, 2016.

[44] J. Feltes, Y. Kazachkov, B. Gong, B. Trouille, P. Donalek, V. Koritarov*, et al.*, "Modeling Ternary Pumped Storage Units," Argonne National Laboratory (ANL)2013.

[45] D. Office of Electricity Delivery & Energy Reliability. (2016, Dec 21, 2018). *Kops II Pumped Storage Power Station, DOE Global Energy Storage Database*. Available: http://www.energystorageexchange.org/projects/1645

[46] D. Office of Electricity Delivery & Energy Reliability. (2016, Dec 21, 2018). *Obervermuntwerk 2, DOE Global Energy Storage Database*. Available: http://www.energystorageexchange.org/projects/1345

[47] A. Puyo, "Hydraulic turbine development during the last few years," *La Houille Blanche,* pp. 3-

41, 1963.

[48] G. Pretro, "Main types of machine building arrangement on present day pumped-storage stations," *Hydrotechnical Construction,* vol. 6, pp. 328-335, 1972.

[49] G. Concorda, "PSLF user's manual, ver 18," ed, 2013.

[50] J. Weber, "Description of machine models GENROU, GENSAL, GENTPF and GENTPJ," *PowerWorld Corporation,* 2015.

[51] P. W. Sauer and M. A. Pai, "Power system dynamics and stability," *Urbana,* vol. 22, 1998.

[52] P. Kundur, N. J. Balu, and M. G. Lauby, *Power system stability and control* vol. 7: McGraw-hill New York, 1994.

[53] I. C. Report, "Computer representation of excitation systems," *IEEE Trans. Power Apparatus and Systems,* vol. 87, pp. pp. 1460-1464, 1968.

[54] D. Lee, "Ieee recommended practice for excitation system models for power system stability studies (ieee std 421.5-1992)," *Energy Development and Power Generating Committee of the Power Engineering Society,* vol. 95, p. 96, 1992.

[55] D. Lee, "IEEE recommended practice for excitation system models for power system stability studies (IEEE Std 421.5-2005)," *Energy Development and Power Generating Committee of the Power Engineering Society,* 2005.

[56] J. Feltes, V. Koritarov, L. Guzowski, Y. Kazachkov, B. Lam, C. Grande-Moran, *et al.*, "Review of existing hydroelectric turbine-governor simulation models," Argonne National Lab.(ANL), Argonne, IL (United States)2013.

[57] Z. Dong, R. Nelms, E. Muljadi, J. Tan, V. Gevorgian, and M. Jacobson, "Development of dynamic model of a ternary pumped storage hydropower plant," in *2018 13th IEEE Conference on Industrial Electronics and Applications (ICIEA)*, 2018, pp. 656-661.

[58] L. A. L. Tenorio, "Hydro turbine and governor modelling," *Norwegian University of Science and Technology,* 2010.

[59] E. De Jaeger, N. Janssens, B. Malfliet, and F. Van De Meulebroeke, "Hydro turbine model for system dynamic studies," *IEEE Transactions on Power Systems,* vol. 9, pp. 1709-1715, 1994.

[60] L. N. Hannett, J. W. Feltes, B. Fardanesh, and W. Crean, "Modeling and control tuning of a hydro station with units sharing a common penstock section," *IEEE Transactions on Power Systems,* vol. 14, pp. 1407-1414, 1999.

[61] L. N. Hannett, J. W. Feltes, and B. Fardanesh, "Field tests to validate hydro turbine-governor model structure and parameters," *IEEE Transactions on Power Systems,* vol. 9, pp. 1744-1751, 1994.

[62] M. Release, "The MathWorks," *Inc., Natick, Massachusetts, United States,* vol. 488, 2013.

[63] N. Schlag and C. Brancucci Martinez-Anido, "Western Interconnection Flexibility Assessment: Final Report," ed: NREL, 2015.

[64] W. E. C. Council, "2022 Common Case Reliability Assessment of Light Spring Condition," 2013.

[65] N. A. E. R. Corporation, "Interconnection Criteria for Frequency Response Requirements," 2011.

[66] D. Office of Electricity Delivery & Energy Reliability. (2016, Dec 28, 2018). *Helms Pumped Hydro Storage Project, DOE Global Energy Storage Database*. Available:

http://www.energystorageexchange.org/projects/442

[67] D. Office of Electricity Delivery & Energy Reliability. (2016, Dec 28, 2018). *Edward Hyatt (Oroville) Power Plant, DOE Global Energy Storage Database*. Available: http://www.energystorageexchange.org/projects/448

[68] D. Office of Electricity Delivery & Energy Reliability. (2016, Dec 28, 2018). *Big Creek (John S. Eastwood) Pumped Storage, DOE Global Energy Storage Database*. Available: http://www.energystorageexchange.org/projects/445

[69] J. Tan, Y. Zhang, S. You, Y. Liu, and Y. Liu, "Frequency Response Study of a US Western Interconnection under Extra-High Photovoltaic Generation Penetrations: Preprint," National Renewable Energy Lab.(NREL), Golden, CO (United States)2018.

[70] Y. Liu, S. You, J. Tan, Y. Zhang, and Y. Liu, "Frequency Response Assessment and Enhancement of the US Power Grids Toward Extra-High Photovoltaic Generation Penetrations—An Industry Perspective," *IEEE Transactions on Power Systems,* vol. 33, pp. 3438-3449, 2018.

[71] J. Tan, Y. Zhang, S. Veda, T. Elgindy, and Y. Liu, "Developing High PV Penetration Cases for Frequency Response Study of US Western Interconnection," in *Green Technologies Conference (GreenTech), 2017 Ninth Annual IEEE*, 2017, pp. 304-311.

[72] K. Clark, R. Walling, and N. Miller, "Solar photovoltaic (PV) plant models in PSLF," in *Power and Energy Society General Meeting, 2011 IEEE*, 2011, pp. 1-5.

[73] N. W. Miller, M. Shao, R. D'aquila, S. Pajic, and K. Clark, "Frequency response of the US eastern interconnection under conditions of high wind and solar generation," in *Green Technologies Conference (GreenTech), 2015 Seventh Annual IEEE*, 2015, pp. 21-28.